# Self-Assembled Monolayers for the Study of Biological Targets

Thesis by
Christie A. Canaria

In Partial Fulfillment of the Requirements
for the Degree of
Doctor of Philosophy

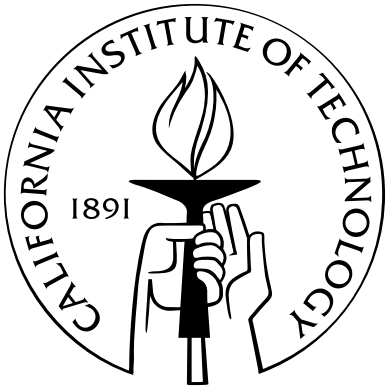


California Institute of Technology
Pasadena, California

2008
(Defended May 28, 2008)

# Acknowledgements

I am greatly indebted to my friends and colleagues in the Fraser lab. My advisor Scott Fraser has cultivated an environment that blends innovative thinking and interdisciplinary science, making my time as a graduate student memorable. Scott has been a fantastic motivator and truly supportive advisor, and I thank him for his brilliant insights and guidance. Rusty Lansford, equally, has served selflessly as my mentor, teacher, and advisor. His wisdom and encouragement made a significant impact on my success at Caltech. The members of our sub-group Jen Yang, Yuki Sato, Dave Huss, and Greg Poynter taught me a lot about biology and the beauty of embryos. Fraser lab houses a wealth of knowledge and talent, and I thank Larry Wade, David Koos, Helen McBride, Le Trinh, and C.J. Yu for their comments and suggestions over the years, which have aided me in becoming a better scientist. Special thanks go to Carole Lu, Sean Megason, and Bernadine Tsung-Megason; they made the time stuck in our office and out really enjoyable.

The resources at Caltech and abroad have also been invaluable to my research. Of note are Jessica Arlett, Blake Axelrod, and Woochang Lee from Michael Roukes' lab; Pamela Sontz and Natalie Muren from Jackie Barton's lab; and Joe Nemanick and Lauren Webb from Nate Lewis' lab. Prof. Charlie Little at the University of Kansas Medical Center shared his knowledge and thoughts on embryogenesis, vasculogenesis, and life with me. I am also grateful to the NSF, DARPA, and Grace Verberg and the P.E.O. Sisterhood for their financial support.

Wonderful times at Caltech began with my Lumberjacks: Brad Cenko, Robert Ward, and Dan Busby. The Sunday Nighters softball crew gave me great memories, too, and I note John Keith, Marie-Helene Rousseau, Andrew and Meredith Beyer, James Maloney, and Keiko Yoshida. My hunger for side projects on campus was fueled by Yvonne Banzali, Karen Carlson, and Angela Wood; the Bowling Club, Biotech Club, and Geek 2 Chic were delightful time sinks.

My parents Art and Ninette, and my sisters Amylin and Janice have been an ever-ready source of encouragement, faith, and motivation. My extended sisters Sheryll Mangahas, Danielle Hylton, and Olivia Ferrell remained close and supportive at all hours of the day. My personal growth during these graduate years has also been influenced by my association with Leela and her troupe LSJ. I began dancing with Leela the same time that I started at Caltech. Over the years, the women of LSJ provided a constant source of love and positive energy. The confidence, perspective, and strength I gained from them cannot be quantified.

# Abstract

Understanding the interactions of biological molecules with solid supports is vital for the development of detection systems and assay platforms. These relationships are frequently quite complex, involving hydrophobic interactions, electrostatic interactions, van der Waals forces, and covalent chemical bonds. We can exploit these interactions in a solid support device by modifying the surface substrate with thin films and monolayers. Self-assembled monolayers (SAMs) are powerful tools for functionalizing and imparting chemical character to surfaces. In this thesis, alkylthiol reagents are utilized to build SAMs on gold (Au) substrates. This work characterizes and studies monolayer formation. In addition, I use SAMs to generate surfaces specific for binding proteins, DNA, and cells. The popular biotin-streptavidin motif is used to demonstrate protein binding, as well as characterize monolayer composition as a result of solvent effects. Novel reagent syntheses are presented for both biotinylated alkylthiols and triethylene-glycol alkylthiols. Together, these two reagents generate substrates which bind specific proteins, while repelling non-specific ones. An additional reagent, "DMT-coated controlled porous glass (CPG)," was designed and synthesized for the generation of custom sequence oligonucleotides. Phosphoramidite syntheses using this modified CPG yield oligos with a 3' alkylthiol modification. SAMs generated with this reagent demonstrate specific binding of complement strands. Both electrochemical techniques and restriction enzymes (where appropriate) provide methods for releasing monolayer-bound species. Lastly, I employ SAMs to generate substrates amenable to cell capture and cell adhesion. Binding B- and T-cell lymphocytes is achieved,

demonstrating SAM-coated Au as a substrate for cell panning. Chemokine vascular endothelial growth factor (VEGF) is also bound to SAMs, generating surfaces amenable to cell adhesion and motility. Cells plated on higher surface concentrations of VEGF migrate faster, and I show the effect is specific to cells with VEGF receptors. Overall, this thesis explores the formation and utilization of SAMs for capturing and studying biological targets. The findings here may be transferred in the future into bio-sensing devices and arrays.

# Contents

# List of Figures

# List of Tables

# Chapter 1

# Introduction

## 1.1 A Preface to this Dissertation

In an effort to present this thesis in as clear a manner as possible, this synopsis provides the reader with a summary of the chapters and their contents.

- **Chapter 1** contains an introduction to the generation and analytical study of self-assembled monolayers and their recent applications towards generating sensing surfaces.
- **Chapter 2** reviews analytical techniques to study SAMs. General analytical characterizations of my substrates is presented here.
- **Chapter 3** explores the solvent effects on monolayer formation and the use of electrochemical techniques to generate recyclable substrates.
- **Chapter 4** focuses on using Watson-Crick based pairing to generate DNA substrates and subsequently protein- and cell-coated substrates.
- **Chapter 5** investigates protein-modified surfaces as growth substrates for cells and as tools to modulate cell behavior.
- **Chapter 6** is a conclusion of the thesis and presents an outline for possible future directions that would naturally follow this work.

## 1.2 Introduction

Interactions between biological molecules and solid supports are core for the development of both biological applications, such as DNA arrays and biosensors, and studies in basic biology. Proteins, for example, will adsorb to most non-natural surfaces. Adsorption is limited by diffusion of the biomolecule to the surface. However, once bound, desorption rates are very slow, making non-specific protein binding essentially irreversible. This process is not well controlled, and adsorbed proteins frequently denature on the surface, resulting in obscured or sterically hindered ligands. Resulting substrates are ill-defined and lack reproducibility in physical properties such as wettability, conductivity, and corrosion resistance. In order to properly study interactions between biological molecules and substrates, researchers require well-defined model substrates which repel non-specific proteins while binding proteins of interest.

To date, a number of model systems have been applied to study biomolecule interactions. They include substrate-bound polymers [1], self-assembled structures such as Langmuir-Blodgett films [2], suspended lipid bilayers [3], self-assembled monolayers (SAMs) of alkylsiloxanes on silicon [4], SAMs of alkyltrichlorosilanes on silicon [5], fatty acids on metal oxides [6, 7], alkyl phosphonate salts on zirconium [8], and SAMs of alkylthiolates on silver and gold (Au) [9–12]. The remainder of this chapter and thesis focus on the use of alkylthiolates on Au. This model system has the benefits of easy surface modification and stability in aqueous and biological conditions. Gold is quite stable and will not oxidize even at high temperatures [13]. Thiolate affinity for Au is very strong [14] and can be applied to Au by exposing Au to thiols or disulfides in almost any solvent or thiol vapor [15]. In addition, the conductive properties of Au make it properly suited for conducting electrochemical studies on SAMs.

## Self-assembly

Self-assembly is the spontaneous organization of components into higher-ordered patterns or structures [16]. The effects of self-assembly are evident on the cosmic level (dust particles into galaxies), in the world around us (atmospheric molecules into weather patterns), in the kitchen (detergent molecules into bubbles), and in our bodies (lipid bilayers in cell membranes). Component coordination typically does not rely on strong covalent chemical bonding, but instead depends on much weaker interactions such as van der Waals interactions, capillary action, gravity, or hydrophobic effects to reorganize individual elements into more thermodynamically stable, yet more ordered structures.

## SAM formation and features

The original SAM concept was made by Zisman in 1946 [17]. Initial studies on alkylthiols with Au were performed in the 1980s largely by Nuzzo and Allara [9–12]. From the 1990s and into present-day, the field has been dominated by the labs of Mrksich and Whitesides [18–22]. Alkylthiols are structurally comprised of an n-alkyl chain with a thiol group at one end and a functional group of choice at the other end (Figure 1.1a). Gold substrates may be nano- or micro-particulates in solution [23], but more commonly, they are prepared by thermally evaporating a thin adhesion layer of Cr followed by Au onto a 2-D substrate. Standard Au support substrates are glass coverslips or silicon wafers.

Upon immersion, alkylthiols spontaneously coordinate to the Au substrate and reduce to alkylthiolates (Equation 1.1) [24, 25].

$$\mathrm{RSH} + \mathrm{Au}(0)_n \rightarrow \mathrm{RS}^{-}\mathrm{Au}(\mathrm{I}) \bullet \mathrm{Au}(0)_n + \frac{1}{2}\mathrm{H}_2 \tag{1.1}$$

Disulfides, too, will adsorb onto gold to form monolayers and are believed to proceed

via S-S bond cleavage (Equation 1.2).

$$2\mathrm{Au} + \mathrm{RS} - \mathrm{SR} \rightarrow 2\mathrm{Au} - \mathrm{SR} \tag{1.2}$$

Thermally evaporated Au will often deposit in the Au(111) [26] crystal configuration, but may also form Au(110) [27], Au(100) [27], or Au(001) [28] lattices. Effects of monolayer packing have been explored between these configurations with only slight differences in SAM formation noted, so only Au(111) will be discussed here. In the hexagonal close packed configuration of Au(111), atoms are spaced 2.88 Å apart. The sulfur atoms coordinate into the threefold pockets of the underlying Au(111) surface with spacings of approximately 5 Å, and the aligned n-alkyl chains are tilted 30 ° from the surface normal (Figure 1.1b–c). The Au-S bond energy is approximately 40 kcal $\mathrm{mol}^{-1}$ [29], and each methylene unit in the chain has a van der Waals free energy of about 1 kcal $\mathrm{mol}^{-1}$ [30]. Collective methylene interactions result in longer n-alkylthiols yielding more stable and densely packed monolayers [12]. Although short chain alkylthiols adsorb faster, thermodynamically controlled competitive adsorption experiments show that long alkylthiols are preferentially adsorbed [31–33].

Depending on alkylchain length, final monolayer thickness ranges between 10–30 Å. SAM formation on Au substrates proceeds in distinct stages [33]. Briefly, alkylthiols adsorb from solution onto Au in a disordered fashion, resulting in 80–90% coverage of the substrate (Figure 1.2) [33]. The subsequent reorganization stage is slower as the alkylthiolates self-assemble into a more ordered and insulating film [34]. A number of STM studies suggest more complex processes for monolayer formation which include nucleation and growth of islands [35–37]. These islands are composed of tens of molecules, surrounded by other molecules lying flat on the Au surface. Above the critical coverage of flat laying thiols, dense well-packed islands continue to nucleate and grow until monolayer saturation is reached. Variables such as temper-

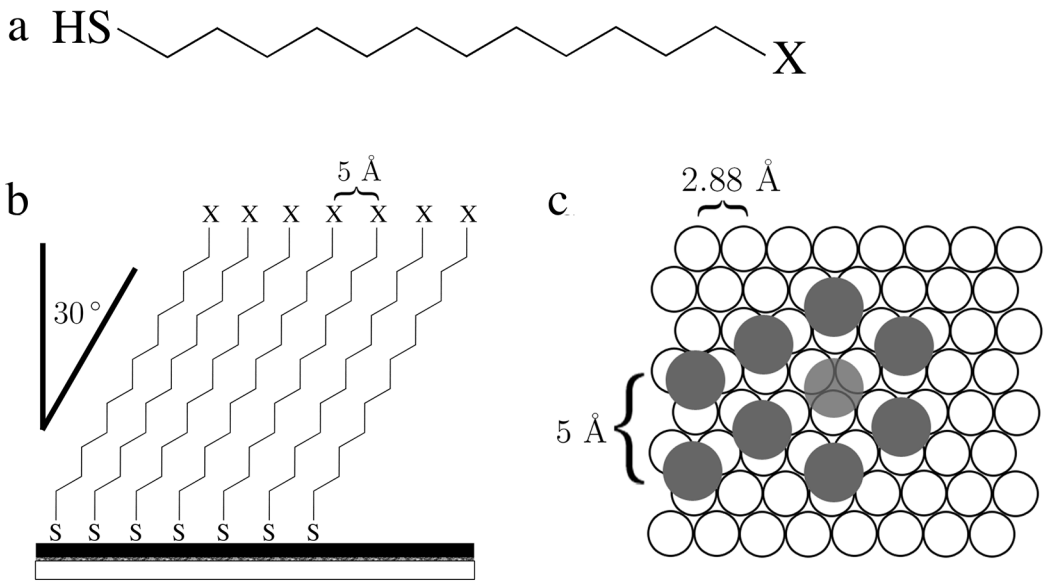


Figure 1.1 **Generic alkylthiol structure and coordination on Au(111) surfaces.** a) The basic alkylthiol molecule is comprised of an n-alkylchain with a thiol (-SH) group at one end and the functional moity of choice "X" at the other end. b) During self assembly, the thiol end of the molecule is oriented at the Au surface, and alkylchains are tilted 30° off normal axis. c) The Au(111) surface, the lowest energetic crystalline face of Au, is hexagonal close-packed with atoms spaced 2.88 Å apart (shown in white). Thiolate molecules are coordinated inside the trigonal pocket of Au atoms (shown in grey) and are spaced 5 Å apart.

ature, thiol concentration, terminating end group [38], and solvent composition [39] can affect alkylthiolate monolayer formation on Au. In practice, organic solvents such as ethanol, DMSO, or hexane are commonly used to solvate alkylthiols for adsorption onto Au substrates [40].

## SAM functionality

By varying the functional end "X" of the alkylthiol, SAMs can be engineered to exhibit a variety of chemical properties and reactivities, making them hydrophobic [14, 39, 41], repulsive [42, 43], or electrochemically active [21, 44–46]. Often, these functional "X" groups can be bulky, resulting in poorly formed monolayers (Figure 1.3). Functional group density on SAMs is controlled by varying the composition of the alkylthiol immersion solution.

In biological applications, SAMs which control protein adsorption are highly desireable. Hydrophobic SAMs promote non-specific protein adsorption. In contast, engineering a hydrophilic poly- or tri(etheylene glycol) (TEG) group into the SAM results in a monolayer which repels non-specific protein adsorption [42, 47, 48]. The mechanism for preventing protein adsorption is not fully understood, but it is believed that water coordination to the ethylene glycol groups creates an energetic penalty as proteins diffuse into the surface vicinity [49]. Alternatively, an alkylthiol with a biotin functional group (BAT) will specifically bind streptavidin proteins with high avidity. Used together, BAT and TEG create SAMs that specifically bind streptavdin while repelling the adsorption of non-specific proteins [47].

Once adsorbed, SAM properties may be characterized for properties such as wettability, chemical composition, and structural integrity. Common techniques include contact angle measurements, atomic force microscopy, scanning electron microscopy, X-ray photoelectron spectroscopy, and electrochemical techniques. An overview of

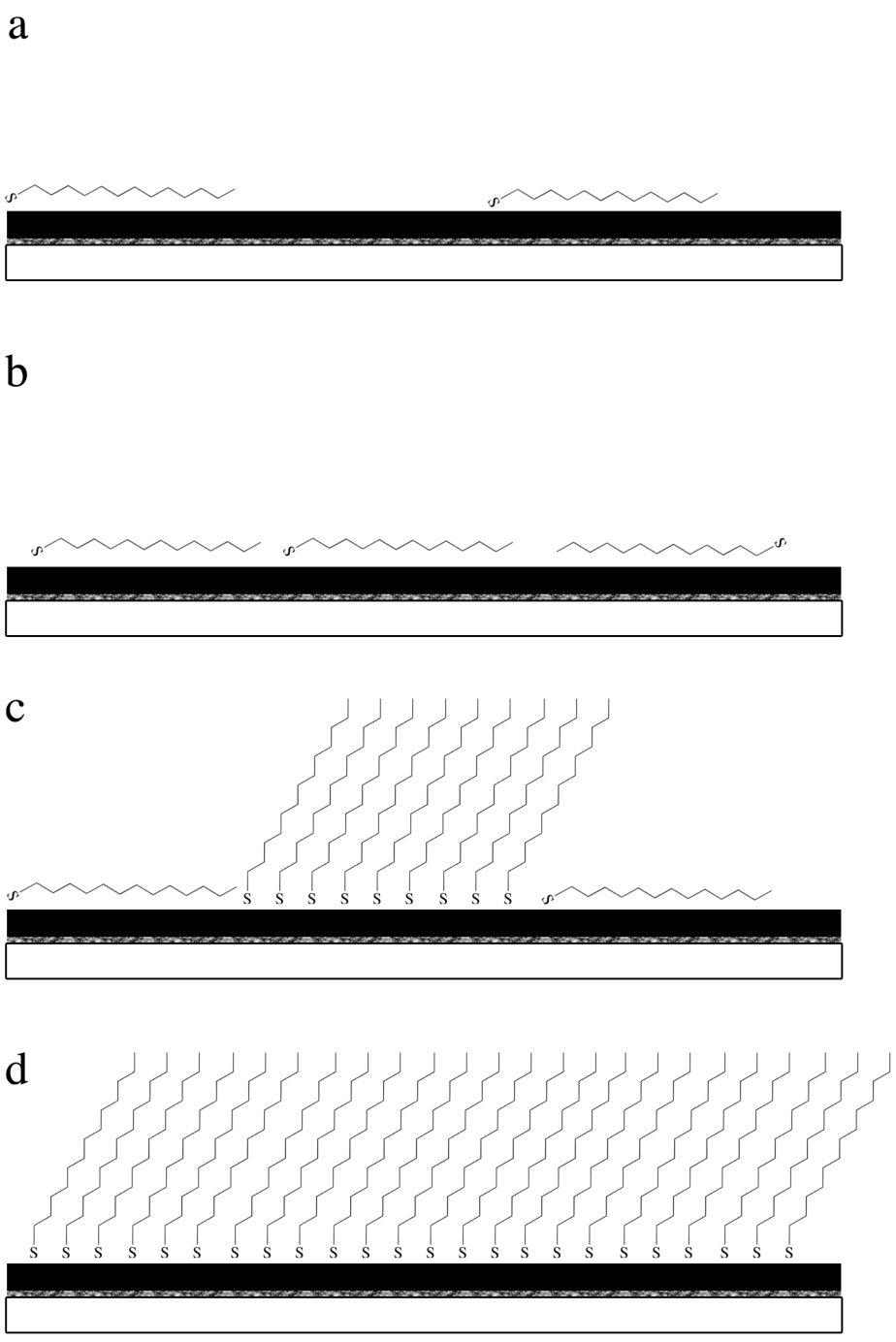


Figure 1.2 **Stages of alkylthiolate SAM formation on Au.** a) Thiol molecules intially adsorb onto the Au substrate laying down, b) and continue until they coat the surface. c) As more thiols adsorb, islands of well-packed monolayers begin to nucleate, d) and continue to grow until a complete monolayer forms.

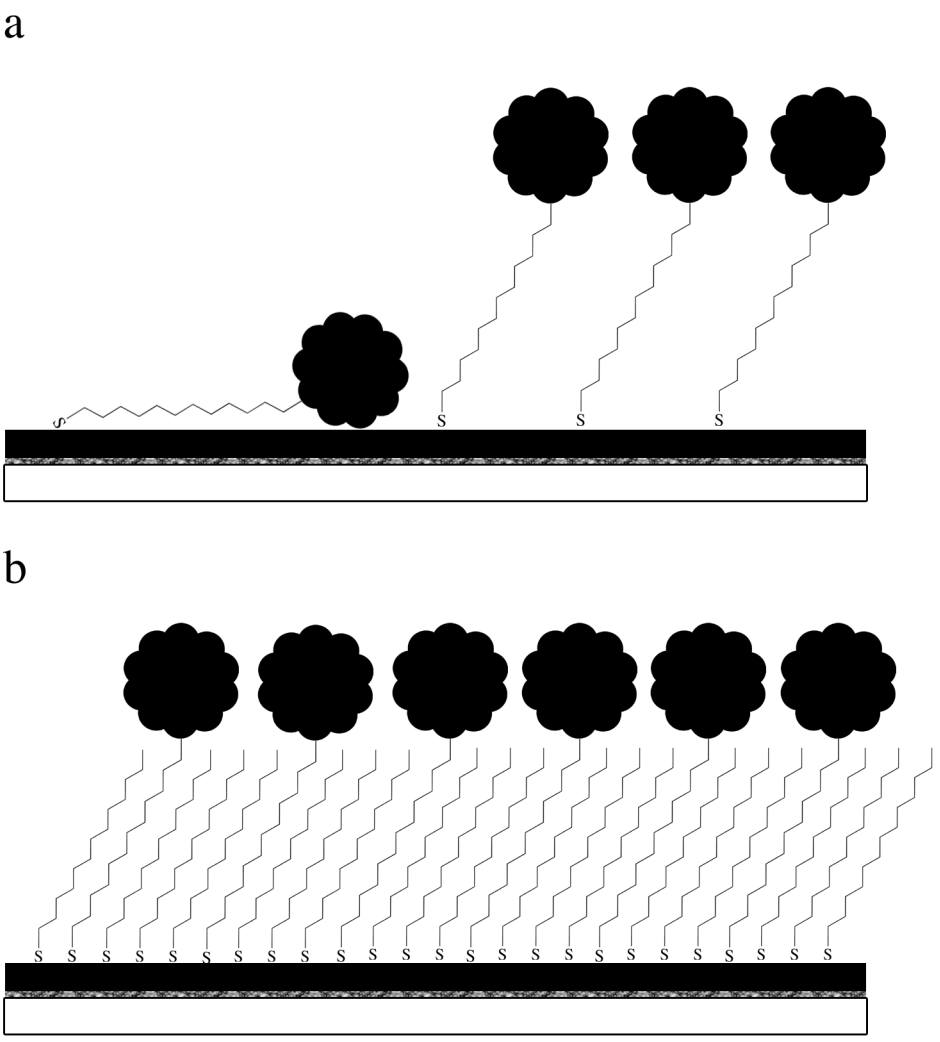


Figure 1.3 **Mixed SAMs on Au.** Schematics for mixed alkylthiol SAMs on Au. a) Adsorption of a bulky functionalized alkylthiol typically leads to poor, loosely-packed monolayer formation. b) Coadsorption of two alkylthiols leads to the formation of a mixed monolayer. Combining a bulky thiol with a shorter alkylthiol at or below the bulky group leads to a well-packed monolayer presenting bulky functional groups.

these anaytical techniques and analyses of substrates generated in this thesis are discussed in detail in Chapter 2.

## Biospecific recognition

Mixed monolayers presenting ligands with TEG groups yield surfaces capable of binding complement targets via specific ligand-receptor interactions, yet resistant to non-specific protein adsorption. Early work by Knoll et al. demonstrated by surface plasmon resonance (SPR) that mixed BAT/TEG monolayers could specifically bind streptavidin [50]. They continued by showing the specific and irreversible adsorption of biotinylated Fab fragments to the streptavidin surface. Conceivably, almost any biotinylated protein could be engineered to bind to a streptavidin-coated monolayer. For example, SAMs employing biotin have been studied in association with streptavidin conjugated to DNA, proteins, and nanoparticles [51–56]. Houseman et al. demonstrated the use of SAMs presenting quinone species. Peptides modified with cyclopentadiol covalently attach to create arrays for assaying tyrosine kinase c-Src [57]. SAMs have also been prepared to present maleimide groups. Thiol-modified carbohydrates covalently bind to create arrays for assaying lectin binding efficiency [58].

SAMs may be used for binding and culturing cells by displaying proteins and molecules which are amenable to cells [58–61]. Normally, polystyene substrates are used for tissue culture, but many alternative surfaces rely on the culture or implantation of cells within a polymeric matrix [62]. Ideally, these matrices and scaffolds are amenable to supporting engineered tissue as well as new tissue growth, but each cell type requires its own set of growth cues. SAM substrates are ideally suited for testing large arrays of potential growth factors and binding promoters. Controlled presentation of these ligands may help deduce their function and efficacy.

## Thesis work

The applications of SAMs to Au substrates provides us with tools to make advancements in biology and technology. As outlined above, SAMs can be manipulated to present small molecules, carbohydrates, and proteins. My work aims to better understand monolayer formation and create substrates for biological targets. Stem cells, specifically, are hugely important topic for study, as they are undifferentiated and capable of developing into any cell in the adult body. Stem cells hold the promise of treatment for degenerative, malignant, or genetic diseases; or injury due to inflammation, infection, and trauma. Successful proliferation of stem cells in culture is currently achieved using poorly controlled substrates and ill-defined media. Human stem cells are grown on mouse embryonic fibroblasts and in animal sera, which are a huge source of cross-species antigens. Continued development towards minimal media [63] and substrates [64–66] will be a great improvement. Next-generation experiments focused on stem cells are outlined in Chapter 6.

This thesis makes important first steps towards generating and optimizing substrates for studying cell growth and culture. SAMs with both biotinylated and oligo-modified proteins are utilized to specifically bind proteins, and subsequently cells. Together with light and fluorescence microscopy, we can quantify and qualitatively assess cell proliferation, health, and activity on controlled SAM substrates.

# Bibliography


[1] M. Livshits, A. Mirzabekov, *Biophys. J.* **71**, 2795 (1996).

[2] G. Roberts, *Contemporary Physics* **25**(2), 109 (1984).

[3] R. Zeineldin, et al., *Langmuir* **22**(19), 8163 (2006).

[4] R. Maoz, J. Sagiv, *J. Colloid Interface Sci.* **100**(2), 465 (1984).

[5] F. Maoz, L. Netzer, J. Gun, J. Sagiv, *J. Chim. Phys. (Paris)* **85**, 1059 (1988).

[6] D. Allara, R. Nuzzo, *Langmuir* **1**, 45 (1985).

[7] D. Allara, R. Nuzzo, *Langmuir* **1**, 52 (1985).

[8] H. Lee, L. Kepley, H. Hong, T. Mallouk, *J. Am. Chem. Soc.* **110**, 618 (1988).

[9] R. Nuzzo, D. Allara, *J. Am. Chem. Soc.* **105**(13), 4481 (1983).

[10] R. Nuzzo, F. Fusco, D. Allara, *J. Am. Chem. Soc.* **109**, 2358 (1987).

[11] R. Nuzzo, L. Dubois, D. Allara, *JACS* **112**, 558 (1990).

[12] M. D. Porter, T. Bright, D. Allara, C. Chidsey, *J. Am. Chem. Soc.* **109**, 3559 (1987).

[13] B. Johnson, R. Davis, *The Chemistry of Copper, Silver and Gold*. Pergamon Press, Oxford (1975).

[14] C. Bain, et al., *J. Am. Chem. Soc.* **111**(1), 321 (1989).

[15] G. Poirier, E. Pylant, *Science* **272**, 1145 (1996).

[16] G. Whitesides, *Science* **295**, 2418 (2002).

[17] W. Bigelow, D. Pickett, W. Zisman, *J. Colloid Interface Sci.* **1**, 513 (1946).

[18] C. Chen, M. Mrksich, S. Huang, G. Whitesides, D. Ingber, *Science* **276**(5317), 1425 (1997).

[19] X. Jiang, R. Ferrigno, M. Mrksich, G. Whitesides, *J. Am. Chem. Soc.* **125**, 2366 (2003).

[20] X. Jiang, D. Bruzewicz, A. Wong, M. Piel, G. Whitesides, *Proc. Nat. Acad. Sci.* **102**(4), 975 (2005).

[21] M. Mrksich, L. Dike, J. Tien, D. Ingber, G. Whitesides, *Experiment. Cell Research* **235**, 305 (1997).

[22] C. Roberts, et al., *J. Am. Chem. Soc.* **120**, 6548 (1998).

[23] M. Giersig, P. Mulvaney, *Langmuir* **9**(12), 3408 (1993).

[24] C. Widrig, C. Chung, M. Porter, *J. Electroanal. Chem* **310**(1–2), 335 (1991).

[25] M. Hasan, D. Bethell, M. Brust, *Journal of the American Chemical Society* **124**(7), 1132 (2002).

[26] P. Fentner, A. Eberhardt, P. Eisenberger, *Science* **266**, 1214 (1994).

[27] N. Camillone III, C. Chidsey, G. Liu, G. Scoles, *J. Chem. Phys.* **98**, 4234 (1993).

[28] J. Li, K. Liang, N. Camillone III, T. Leung, G. Scoles, *J. Chem. Phys.* **102**, 5012 (1995).

[29] R. Shaw, *The Chemistry of the Thiol Group*, chap. 3, p. 160. Wiley, London (1974).

[30] S. Wetterer, D. Lavrich, T. Cummings, G. Bernasek, S.L. nd Scoles, *J. Phys. Chem. B* **46**(9266-9275) (1998).

[31] T. Ishida, et al., *Japn. J. Appl. Phys.* **35**(12), L1710 (1996).

[32] K. Tamada, M. Hara, H. Sasabe, W. Knoll, *Langmuir* **13**, 1558 (1997).

[33] R. DeBono, G. Loucks, D. Manna, U. Krull, *Can. J. Chem.* **74**, 677 (1996).

[34] G. Hahner, C. Woll, M. Buck, M. Grunze, *Langmuir* **9**, 1955 (1993).

[35] J. Woodward, D. Schwartz, *J. Am. Chem. Soc.* **118**(33), 7861 (1996).

[36] K. Truong, P. Rowntree, *J. Phys. Chem.* **100**(51), 19917 (1996).

[37] R. Yamada, K. Uosaki, *Langmuir* **20**, 5218 (1997).

[38] G. Poirier, E. Plyant, J. White, *J. Chem. Phys.* **104**, 7325 (1996).

[39] C. Bain, J. Evall, G. Whitesides, *J. Am. Chem. Soc.* **111**, 7155 (1989).

[40] J. Love, L. Estroff, J. Kriebel, R. Nuzzo, G. Whitesides, *Chem. Rev.* **105**, 1103 (2005).

[41] C. Bain, G. Whitesides, *J. Am. Chem. Soc.* **111**, 7164 (1989).

[42] C. Golander, et al., in J. Harris (ed.), *Poly(ethylene glycol) chemistry, biotechnical and biomedical applications*, pp. 221–245. Plenum Press, New York (1992).

[43] J. Harris, *Poly(ethylene glycol) chemistry, biotechnical and biomedical applications*. Plenum Press, New York (1992).

[44] C. Hodneland, M. Mrksich, *Langmuir* **13**(23), 6001 (1997).

[45] M. Yousaf, M. Mrksich, *J. Am. Chem. Soc.* **121**, 4286 (1999).

[46] C. Hodneland, M. Mrksich, *J. Am. Chem. Soc.* **122**, 4235 (2000).

[47] M. Mrksich, G. Sigal, G. Whitesides, *Langmuir* **11**, 4348 (1995).

[48] G. Sigal, M. Mrksich, G. Whitesides, *J. Am. Chem. Soc.* **120**, 3464 (1998).

[49] P. Harder, M. Grunze, R. Dahint, G. Whitesides, P. Laibinis, *J. Phys. Chem. B* **102**, 426 (1998).

[50] J. Spinke, M. Liley, H.-J. Guder, L. Angermaier, W. Knoll, *Langmuir* **9**, 1821 (1993).

[51] K. Kukanskis, et al., *Anal. Biochemistry* **274**(1), 7 (1999).

[52] J. Schumaker-Parry, M. Zareie, R. Aebersold, C. Campbell, *Anal. Chem.* **76**, 918 (2004).

[53] M. Riepl, K. Enander, B. Liedberg, *Langmuir* **18**(18), 7016 (2002).

[54] A. Zybin, et al., *Anal. Chem.* **77**(8), 2393 (2005).

[55] G. Zhen, et al., *Langmuir* **20**, 10464 (2004).

[56] A. Arakaki, et al., *Biotechnology and Bioengineering* **88**(4), 543 (2004).

[57] B. Houseman, J. Huh, S. Kron, M. Mrksich, *Nature Biotech.* **20**, 270 (2002).

[58] B. Houseman, E. Gawalt, M. Mrksich, *Langmuir* **19**, 1522 (2003).

[59] Y. Feng, M. Mrksich, *Biochem.* **43**, 15811 (2004).

[60] B. Houseman, M. Mrksich, *J. Org. Chem.* **63**, 7552 (1998).

[61] W.-S. Yeo, M. Yousaf, M. Mrksich, *JACS* **125**, 14994 (2003).

[62] J. Langer, R; Vacanti, *Science* **260**, 920 (1993).

[63] M. Amit, C. Shariki, V. Margulets, J. Itskovitz-Eldor, *Biology of Reproduction* **70**, 837 (2004).

[64] C. Xu, M. Inokuma, J. Denham, K. Golds, P. Kundu, *Nature Biotech.* **19**, 971 (2001).

[65] M. Amit, V. Margulets, H. Segev, K. Shariki, I. Laevsky, *Biology of Reproduction* **68**, 2150 (2003).

[66] I. Klimanskaya, Y. Chung, L. Meisner, J. Johnson, *The Lancet* **365**, 1636 (2005).

# Chapter 2

# Analytical Methods for Characterizing Self Assembled Monolayers and Substrates

Chapter 1 discussed how self-assembly of alkylthiols onto gold substrates allows the control of surface properties such as electrostatic charge, polarity, hydrophobicity, and reactivity. These exceedingly thin films range in thicknesses between 10–30 Å. A number of analytical methods exist that allow us to quantitatively and qualitatively evaluate modified surfaces. A handful of these methods are highlighted and evaluated here.

## 2.1 Contact Angle Measurements

One of the easiest qualities to measure from a solid surface is wettability. When a drop of liquid is placed on a surface, it will either spread out to coat the surface as a thin film, or the liquid will remain relatively spherical (Figure 2.1). The final configuration of the liquid drop on the surface indicates the wettability of the surface by that liquid.

Consider the perimeter of a drop of water on a gold substrate in air. This intersection between water, gold, and air is referred to as the wetting line. The angle

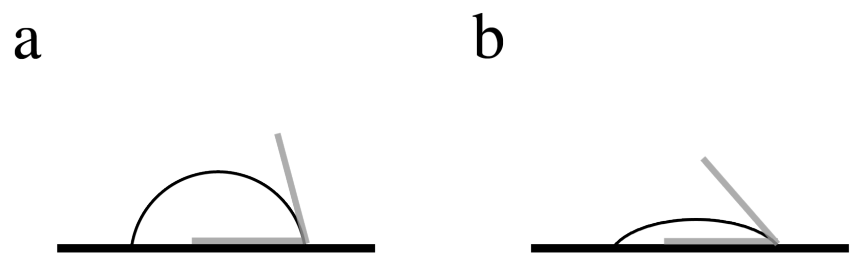


Figure 2.1 **Contact angle measurements by sessile water drop.** a) Sessile water drop on a hydrophobic surface forms a bead with a high contact angle. b) More hydrophilic surfaces give drops with lower contact angle.

between the plane of the gold and the tangent at the wetting line is defined as the contact angle. The contact angle of the drop can be considered a property of the material, provided that the solid surface is relatively smooth, and that humidity and liquid absorption are taken into consideration.

It should be noted, too, that contact angle measurements are dependent on whether or not a surface has had previous contact with liquid. Contact angle values for a drop moving across fresh substrates (advancing contact angles) are typically larger than for a drop moving across an already wetted surface (receding contact angles). This variability in contact angle measurements is known as hysteresis.

While contact angle measurements are easy to acquire, they must be collected under controlled conditions of humidity, time, temperature, and other parameters to be meaningful.

### 2.1.1 Methods

A 1000 Å Au layer was evaporated onto Si with a 30 Å Cr adhesion layer under high vacuum. Importantly, no photolithography features were added to the chips. Contact angle measurements can be skewed by features on the substrate surface. After rinsing samples in acetone, isopropanol, and methanol, and cleaning in ozone plasma, Au samples were treated in parallel under four different conditions: no SAM, TEG SAM,

hydroquinone (HQ) SAM, and oligonucleotide SAM (Figure 2.2). TEG alkylthiol was synthesized as described in Chapter 3.2.6. HQ was a gift from Dr. C. J. Yu, and a 26-mer oligo alkylthiol was synthesized as described in Chapter 4.3. Alkylthiol monolayers were adsorbed onto the samples from 1 mM ethanolic solutions overnight; the control sample (no SAM) was kept in ethanol. Samples were then removed from solution, washed in ethanol and water, and then dried under argon. Sessile drop contact angle measurements were acquired with a custom-made goniometer. Distilled, de-ionized water was added to the syringe, and water drops were gently added to the Au substrate. Advancing water drops were viewed against a protractor and the contact angle measured. At least three measurements were taken on various locations across each sample.

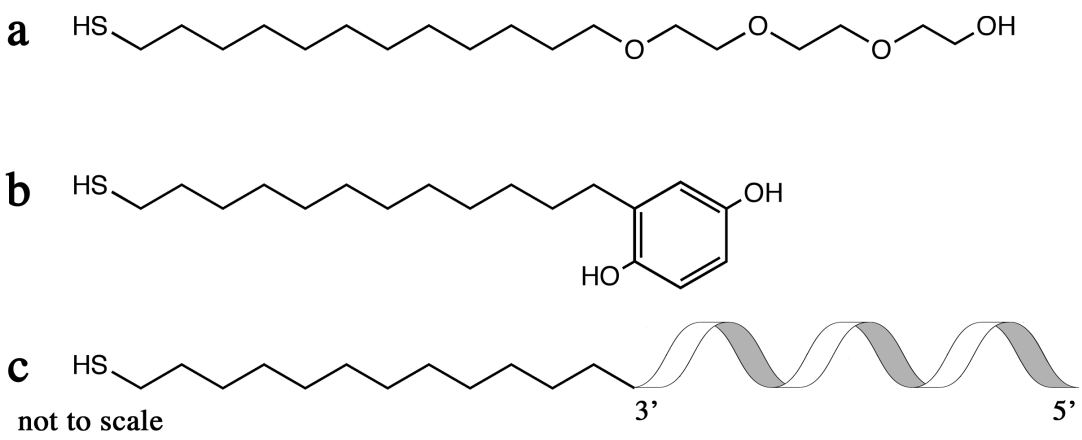


Figure 2.2 **TEG, hydroquinone, and oligo alkylthiol structures.** These figures are not to scale: a) TEG, b) hydroquinone alkylthiol (HQ), and c) oligo SAM

### 2.1.2 Results and Discussion

The resulting contact angles measured for various SAMs on Au substrates are given below in Table 2.1. Fresh gold substrate is hydrophobic in nature, but its wettability is prone to change as contaminants adsorb from the atmosphere. TEG is hydrophilic,

Table 2.1. Contact angle measurements for water on Au

| Sample | Contact angle |
|---|---|
| no SAM | $55.1 \pm 5.8\,^\circ$ |
| TEG SAM | $33.3 \pm 1.3\,^\circ$ |
| HQ SAM | $65.4 \pm 1.7\,^\circ$ |
| oligo SAM | $49.5 \pm 1.2\,^\circ$ |

and water coordinates very easily with ethylene glycol groups [1–3]. Likewise, an oligo SAM is hydrophilic. In contrast, the HQ SAM is more hydrophobic. These characteristics are reflected in the contact angles measured for water on the SAMs. The "no SAM" sample has an average contact angle of $55.1 \pm 5.8\,^\circ$. The standard deviation for these samples is indicative of a more variable substrate. This is not surprising since the "no SAM" surface composition is not well controlled. The other samples have lower standard deviations, as expected with controlled surface functionalization. TEG and oligo SAM samples have lower contact angles, $33.3 \pm 1.3\,^\circ$ and $49.5 \pm 1.2\,^\circ$, respectively. These hydrophilic substrates hold water drops with low surface tension, yielding drops with lower contact angles. Despite the hydroxy groups, HQ SAMs are still more hydrophobic. Water is repelled from the surface and the resulting water drops have a higher contact angle.

In general, contact angle measurements are informative for determining the wettability of chips on the macro-scale, but only provide qualitative insight. Surface characterization of substrates on the micro- or nano-scale is not possible, however, as the user is limited by the size of water droplets which are on the order of millimeters.

## 2.2 Scanning Electron Microscopy

Electron microscopy is capable of generating images with spatial resolution as detailed as 10 nm, an order of magnitude beyond what optical microscopy can produce.

The first scanning electron microscope (SEM) was used to generate images of solid substrates in 1942 [4]. Since then, SEM has been employed to study and analyze surfaces of cells, pollen, insects, and other biological specimens [5].

Though similar to reflectance microscopy, the technique of SEM does not directly capture optical light with image-forming lenses. Instead of employing a light source, an electron beam is focused and manipulated with lenses, apertures, and magnetic coils onto a sample. Application of an electron beam causes emission of secondary electrons, backscattered electrons, X-rays, light, and heat. Secondary electrons yield information about sample topography. Backscattered electrons give insight into the elemental make-up of the sample, and X-rays can indicate crystallinity.

In classic SEM, the electron beam is scanned across the sample substrate, and secondary electrons are emitted and collected in real time. Data is displayed on a monitor in terms of contrast and brightness of electrons. Samples which emit more electrons appear brighter; less electron-rich samples appear darker in comparison. Accordingly, heavier atoms wealthy in electrons emit more secondary electrons and yield better images. In contrast, organic elements such as hydrogen, carbon, oxygen, and nitrogen emit many fewer electrons. Non-conducting samples must also be grounded to avoid build up of electron charge which will ultimately decrease image quality. Consequently, biological samples such as cells need to be preserved with harsh fixatives and coated with a metal layer prior to imaging. Environmental SEM could overcome this difficulty, but this topic is beyond the present scope and is not discussed at this time. Here, I evaluate SEM as a technique for analyzing SAMs on Au substrates.

### 2.2.1 Methods

Gold substrate samples were produced by thermal evaporation as described above. Briefly, samples were cleaned by ozone plasma treatment, then incubated in either

ethanol or 1 mM TEG in ethanol for 2 hours to generate a control and SAM-coated sample, respectively. Substrate samples were then rinsed in ethanol, dried under an argon stream, and mounted onto an SEM chuck. The SEM chucks and sample substrates were both electrically grounded using copper tape. An FEI Qanta SEM was employed to generate images of substrate topography. Images were generated with auto-contrast and auto-brightness settings.

### 2.2.2 Results and Discussion

Samples of thermally evaporated Au on silicon wafers were imaged by SEM. Two samples were analyzed: a bare Au sample and an Au sample with an adsorbed alkanethiol SAM (Figure 2.3). Comparing the two samples, no discernible differences can be identified.

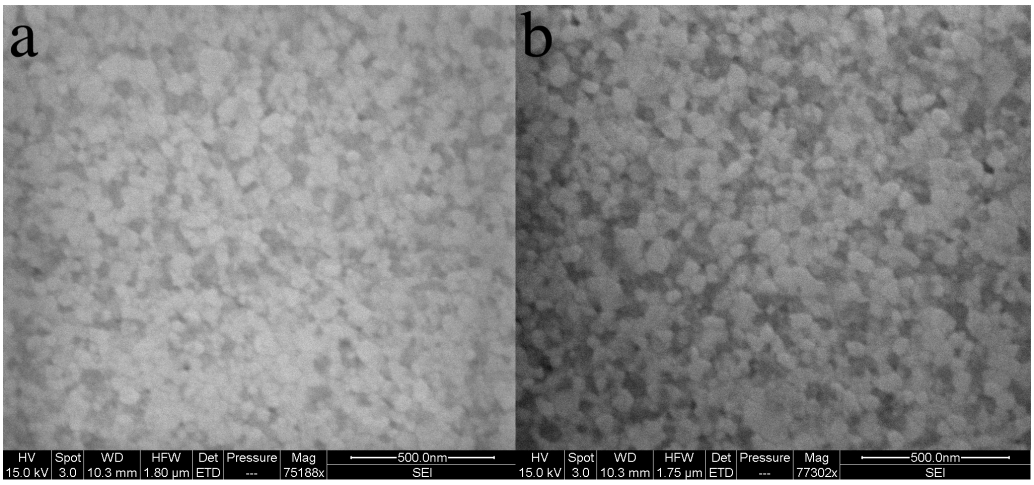


Figure 2.3 **SEM images of Au substrates.** Images of a) bare Au and b) Au coated with an alkylthiol monolayer. Samples were prepared by thermal evaporation of Au onto the silicon substrate, and Au is visible as colloidal islands. Island features range from 60–100 nm in diameter.

Previously, Whitesides et al. demonstrated that SAMs comprised of two different alkanethiols could be spatially controlled by using microcontact printing methods [6]. Alkanthiol squares with 20 $\mu$m features were printed on Au substrate and imaged. At

the highest magnification used, individual Au colloid islands are visible, and even the boundary between the two alkanethiols is visible, but individual molecules cannot be resolved.

At present, the best spatial resolution attained by SEM is 10 nm [7]. While the SEM technique succeeds at producing high-resolution topographical images for substrates, it is inadequate for imaging single proteins or molecules.

## 2.3 X-Ray Photoelectron Microscopy

X-ray photoelectron spectroscopy (XPS), also known as electron spectroscopy for chemical analysis (ESCA), is a powerful method for characterizing the chemical content of SAMs on gold substrates. The technique is based on the photoelectron effect which was originally discovered by Heinrich Hertz in 1887. Radiation from high-frequency, low-intensity light was observed to eject electrons from metal foils. Einstein explained this phenomenon [8] with the equation

$$h\nu = \frac{1}{2}mv_e^2 + E_b + q\Phi \tag{2.1}$$

where $h$ is Planck's constant, $\nu$ is the frequency of incident light, and $\frac{1}{2}mv_e^2$ is the kinetic energy of the ejected photoelectron of mass $m$ and velocity $v_e$. $E_b$ is the electron binding energy, $q$ is a reference charge, and $\Phi$ is the work function of the emitting material, or the minimum energy required to remove a delocalised electron from the metal surface.

From Equation 2.1, note that in order for a photoelectron to be emitted ($\frac{1}{2}mv_e^2 > 0$), $h\nu$ must exceed some critical value specific to the material ($E_b + q\Phi$). Photoelectrons from atoms in more electropositive states are emitted with less kinetic energy (greater $E_b$) and vice versa. Chemical and oxidation states for electrons can therefore be inferred from ESCA.

While metal films are ideal materials to study, core electrons of adsorbed elements will also emit photoelectrons. A conductive substrate is ideal, however, to reduce charging effects of X-ray radiation. Conventional commercial ESCA employs either $Al_{\kappa\alpha}$ (1486 eV) or $Mg_{\kappa\alpha}$ (1254 eV) X-ray sources. Core electrons of atoms near the surface can become energized and emitted as photoelectrons. Electrons buried under the surface lose energy in transit to the surface and emit with increased $E_b$, whereas electrons deep in the surface do not escape at all.

Efficiency in photoelectron ejection also varies between core electron levels and elements. In an effort to make ESCA quantitative, researchers have empirically measured the atomic sensitivity for various elements [9]. By convention, atomic sensitivity values are normalized to fluorine core electrons (F1s) and unitless. Quantitative comparison of ESCA peaks are accomplished by dividing the spectrum peak area by the sensitivity factor. Since sensitivity factors are empirically derived, this method of analysis is semi-quantitative.

### 2.3.1 Methods

The M-Probe Surface Spectrometer ESCA instrument by Surface Science with an $Al_{\kappa\alpha}$ X-ray source was used to acquire these spectra. Gold samples were thermally evaporated onto silicon wafers and functionalized with various alkylthiol monolayers. Samples were mounted onto chucks, loaded into the instrument loading arm, and set under vacuum for 1–2 hours before transportation into the analysis chamber. Scans were acquired under the following settings: averaged over 4 scans, resolution setting 4, and spot size 4.

### 2.3.2 Results and Discussion

Various samples were prepared and analyzed with XPS. Representative spectra are given in Figure 2.4. Binding energies for photoelectrons of interest are also provided

in Table 2.2. Briefly, a bare gold sample is compared with samples adsorbed with a TEG monolayer and an oligo/TEG mixed monolayer, as well as a silicon sample.

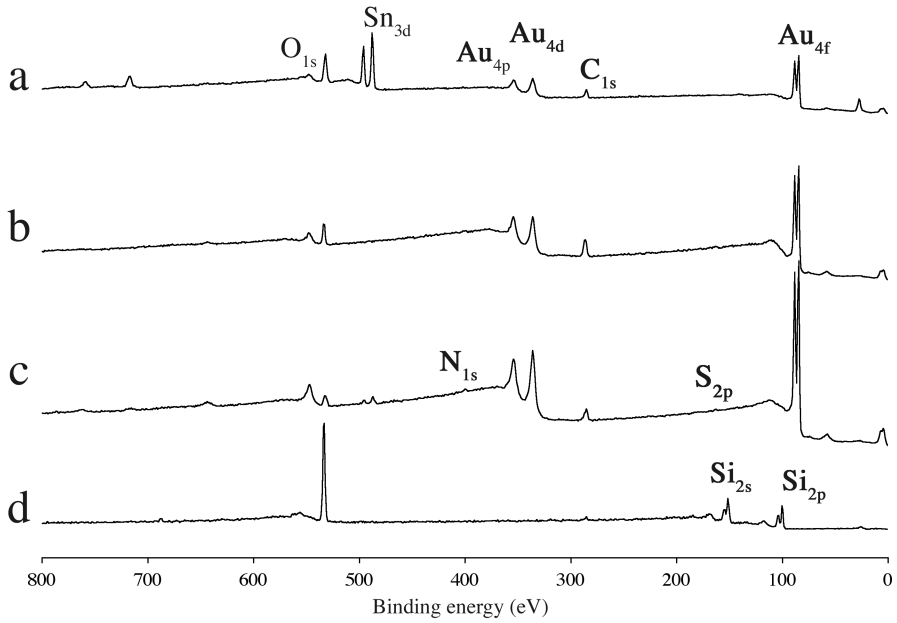


Figure 2.4 **ESCA spectra for Au and Si surfaces.** Binding energy spectra for a) bare gold sample, b) TEG SAM on gold, c) oligo/TEG SAM on gold, and d) silicon substrate

As discussed in Chapter 3, freshly prepared gold samples quickly become contaminated upon contact with air [22–25]. The most prevalent contaminants are hydrocarbons. In Figure 2.4a, the XPS spectrum contains peaks for Au, O, C, and Sn. Au is plentiful with electrons in varying energy orbitals, giving rise to the multiple peaks seen at 84, 87, 335, and 353 eV. The C peak at 284 eV and O peak at 533 eV arise from contaminants physisorbed on the sample surface. The Sn peaks at 485 and 593 eV are trace contaminants incorporated into the gold during the thermal evaporation process. These peaks are not visible in the spectra for SAM-coated samples (Figure 2.4b–c). The alkylthiol monolayer shields the trace Sn photoelectrons

Table 2.2. ESCA/XPS elemental binding energies and atomic sensitivity

| Energy (eV) | Element Core Electron | Chemical Binding | Atomic sensitivity[a] | Reference |
|---|---|---|---|---|
| 83.9 | Au4f7/2 | Au | 2.8 | [10] |
| 88.5 | Au4f5/2 | NdAuGe | 2.05 | [11] |
| 334.9 | Au4d5/2 | Au | 2.05 | [10] |
| 353.8 | Au4p3/2 | NdAuGe | | [11] |
| 531.9 | O1s | OH | 0.66 | [12] |
| 283.93 | C1s | C-H | 0.25 | [13] |
| 400.2 | N1s | N-H or N-O | 0.42 | [14] |
| 132 | P2p | $K_2HPO_4$ | 0.39 | [15] |
| 192.6 | P2s | $P_2O_5$ | 0.29 | [16] |
| 163.8 | S2p3/2 | RSH | 0.54 | [17] |
| 99.5 | Si2p3/2 | Si | 0.27 | [10] |
| 103.3 | Si2p3/2 | SiO | 0.27 | [18] |
| 153 | Si2s | Si | 0.26 | [19] |
| 484.9 | Sn3d5/2 | AuSn | 4.3 | [20] |
| 493.1 | Sn3d3/2 | Sn in oxide films | 1.77 | [21] |

[a]All atomic sensitivity data come from Wagner et al. [9]

from the detector, however the underlying Au is abundant and Au photoelectrons are recorded.

The TEG alkylthiol reagent used (Figure 2.2a) is elementally comprised of carbon, oxygen, and sulfur. The XPS spectrum for TEG SAM sample displays peaks for Au, C, and O. Photoelectrons for S are not visible and are likely not detected due to the thiol's position underneath the monolayer. Likewise, the XPS spectrum for the oligo SAM sample displays peaks for Au, C, O, and N, but not S or P. This is due to variation in atomic sensitivity to X-rays. The low ionization potential of Au makes the atomic sensitivity factor for Au relatively high, 2.08–2.8 (Table 2.2). Non-metals with higher ionization potentials have lower sensitivity factors indicating low signal.

ESCA/XPS is a powerful tool for chemical identification. This technique is sensitive enough to differentiate between electrons in varied core levels within a given element and provides information on element oxidation states and surrounding electrochemical environment. Unfortunately, this technique provides semi-quantitative

compositional analysis, at best.

## 2.4 Electrochemisty

The conductive properties of Au make it an amenable substrate for performing electroanalytical measurements. Generally, these methods vary electrode potential over time while the current response of adjacent chemical species is monitored. By Faraday's law, charge measured is directly proportional to the quantity of chemical species undergoing a loss (oxidation) or gain (reduction) of electrons.

$$Q = n\Im e \tag{2.2}$$

In Equation 2.2, $Q$ is the charge generated in Coulombs (C); $n$ is number of chemical species undergoing oxidation/reduction (in moles); $\Im$ is Faraday's constant (96,487 $\mathrm{C\,mol^{-1}}$); and $e$ is the number of electrons lost/gained per molecule. Tracking the change in charge as a function of time yields the current ($I$), allowing us to track changes in the chemical species of interest (Equation 2.3).

$$I = \frac{dQ}{dt} \tag{2.3}$$

The electrochemical techniques discussed here are performed using a 3-electrode cell. The cell is comprised of a working electrode, usually a conductive material such as Au or glassy carbon; a counter, or auxillary electrode, usually in Pt or another conductive, non-reactive material; a reference electrode; an electrolyte solution; and a redox reactive species (Figure 2.5). Potential is measured between the working electrode and the reference electrode, and current is measured between the working electrode and counter electrode.

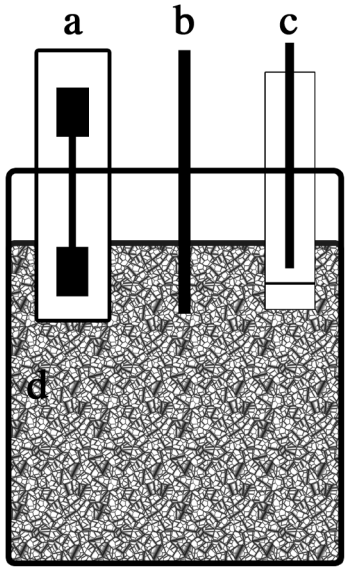


Figure 2.5 **Electrochemical cell setup.** The cell is comprised of a) a working electrode, Au patterned on a Si chip; b) Pt wire-mesh counter electrode; c) Ag/AgCl (saturated KCl) reference electrode; and d) PBS electrolyte solution with 30 mM $K_3Fe(CN)_6$.

Cyclic voltammetry (CV) is an electrochemical technique in which Faradaic response to applied potentials is studied. A pre-determined range of potentials is measured, starting at an initial point and varying linearly over time up to a pre-defined potential value, the switching potential. At this point, the direction of the potential scan is reversed until the initial potential value is reached (Figure 2.6). During the forward scan of the waveform, cathodic potential increases and current increases as active species in solution become reduced. After reaching the switching potential, the reverse scan moves the potential in the anodic direction and reactive species at the working electrode are oxidized. Anodic current is plotted as a dip in the current vs. potential (I-E) curve.

It should be noted that the convention used here measures the cathodic potential at the working electrode as the more negative potential value. In Figure 2.6 and the remaining CV traces given here, the X-axis runs from positive to negative. This

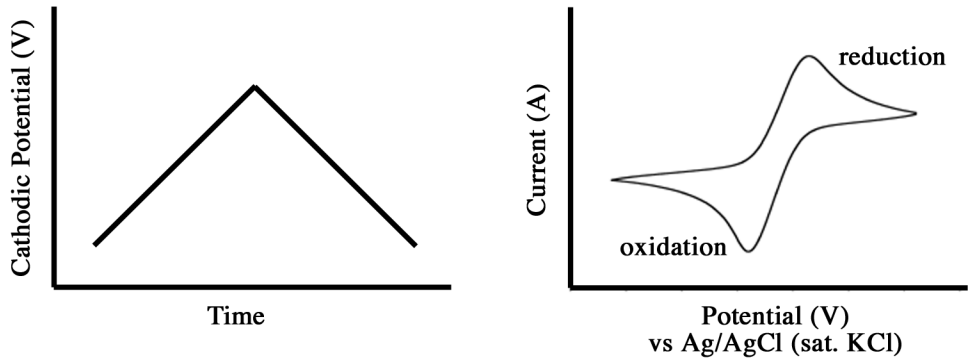


Figure 2.6 **Cyclic voltammetry curves.** An idealized schematic of applied potential sweep and measured current response

can be rationalized when considering application of an oxidative potential to Au working electrodes. Positive charge builds up on the electrode and the Fermi levels are *decreased*. Applying reductive potentials builds up negative electron charge on the electrode and the Fermi energy levels are *increased*. The reader may encounter other publications in which the cathodic potential are diagrammed to the left. In either case, the more positive potentials indicate cathodic direction.

CV is typically used to probe the reactivity of redox active species in solution or bound to the electrode. In this thesis, I utilize the sensitivity of the working electrode instead to probe SAM coverage on the Au working electrode. Bare, clean Au working electrodes give I-E curves as seen in Figure 2.6. SAMs on a Au substrate act as an insulating layer and change the shape of the I-E curve. Even SAMs in their intermediary formation stages can be characterized using CV; tiny pinholes in the monolayers provide sites for redox reactions and sources for current rise.

### 2.4.1 Methods

A CH Instruments potentiostat acquired CV measurements. As illustrated above (Figure 2.5), the 3-electrode cell was comprised of Au-coated Si as the working elec-

trode, a Pt counter electrode, and a Ag/AgCl reference electrode. PBS and 30 mM potassium ferrocyanide III ($K_3Fe(CN)_6$, Aldrich) served as the electrolyte and redox active species, respectively. A short cathodic scan preceded the full cyclic voltammogram to ensure that the $Fe(CN)_6$ (II) species was present at the working electrode surface. This short pre-scan is not included in these I-E curves. I-E curves were acquired at a scan rate of 100 $mV\,sec^{-1}$.

Mercaptohexanol, mercaptohexane, and mercaptoundecanol were all purchased from Sigma. TEG-disulfide is the disulfide form of TEG (Figure 2.2) and was a gift from Dr. C. J. Yu. BAT was synthesized as shown in Chapter 3.2.6. Total thiol concentrations for mixed ethanlic solutions was 1 mM. SAM formation was quenched by rinsing in ethanol before analysis by CV. Temperature experiments were conducted using incubation ovens.

### 2.4.2 Results and Discussion

A variety of alkylthiols were applied to Au substrates and assessed for the quality of SAMs adsorbed. CV traces for a variety of SAMs on Au are given in Figure 2.7. The symmetric trace given in Figure 2.7a is indicative of a bare Au substrate. The redox species $Fe^{2+/3+}$ easily converts between the reduced and oxidized forms at an uncoated electrode. The shape of the CV trace varies as the electrode surface becomes modified by SAMs.

Similarly shaped traces are given in Figures 2.7b–c for mercaptohexane- and mercaptohexanol- coated samples, respectively. The peak heights, however, are diminished compared to bare Au control. This signifies that the uncoated Au area has decreased. Mercaptohexyl chains will coordinate on Au, but previously studies noted that these shorter chains form incomplete SAMs which are less stable [26–28]. This is apparent in the CV traces; $Fe^{2+/3+}$ continues to undergo redox reactions at the electrode, likely at sites of pinholes, or uncovered patches of Au.

In contrast, SAMs formed from undecylthiols result in more tightly packed monolayers. TEG-disulfide, TEG, and mercaptoundecanol treated samples yield CV traces with very different shapes (Figure 2.7d–f). The lack of cathodic current indicates that redox activity of $Fe^{2+/3+}$ has been diminished. The tail at the anodic region is not due to Fe oxidation, but rather to slight oxidation of the Au/thiolate and reconstruction of the electrode/monolayer interface [29].

The BAT SAM sample has an asymmetric CV trace, though similar in shape to the bare Au control (Figure 2.7g). The diminished cathodic peak indicates reduction of the Fe species and sub-monolayer coverage of the electrode. Hydrophobic properties of the biotin species result in biotin burial into the hydrophobic alkyl chain region [30] and monolayer imperfections. Co-adsorbing TEG or mercaptoundecanol, however, aids in forming a more complete SAM. TEG, in particular, reduces biotin burial into the alkyl chain monolayer by promoting ethylene glycol orientation in both BAT and TEG towards the solvent interface. Presumably, the hydroxyl group in mercaptoundecanol promotes the same orientation. A greater discussion of this phenomenon is provided in Chapter 3.3.2.

SAM formation on Au electrodes was also tracked by CV. Samples were incubated with 1 mM ethanolic solutions of BAT for time scales ranging from 6 minutes to over 16 hours (Figure 2.8). From previous experiments, we know that BAT reagent does not form a complete SAM even after long periods. After 48 minutes, we observe a slight decrease CV trace peak current compared to the bare Au control. At this point, a SAM begins to form on the Au electrode, but it is incomplete and full of imperfections. Even after 16 hours, a full monolayer is still not observed.

A short time course for samples incubated in TEG demonstrates SAM formation as a function of concentration and time (Figure 2.9). TEG is capable of forming very well ordered, insulating monolayers. Au incubation in high ethanolic concentration of

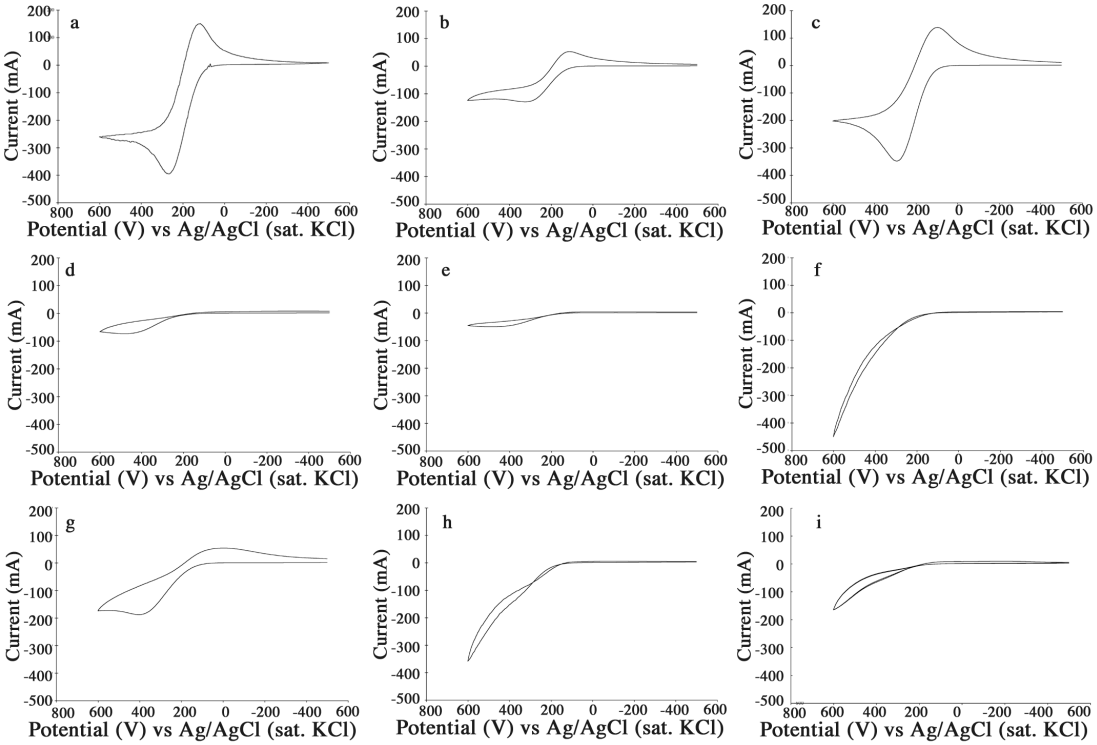


Figure 2.7 **CV traces of various SAMs on Au.** Au samples were incubated in 1 mM ethanolic solution of alkylthiols overnight. a) Bare Au, b) mercaptohexane, c) mercaptohexanol, d) TEG-disulfide, e) TEG thiol, f) mercaptoundecanol, g) BAT, h) mixed SAM—1 BAT: 10 TEG, i) mixed SAM—1 BAT: 10 mercaptoundecanol

TEG (10 mM, Figure 2.9a) indicates that almost complete monolayers are achieved after 6 minutes, a relatively short time. As the alkylthiol concentration is lowered, longer time scales are necessary to reach comparable electrode coverage (Figure 2.9b–c). Overnight incubations at these lower alkylthiol concentrations yield fully insulated electrodes.

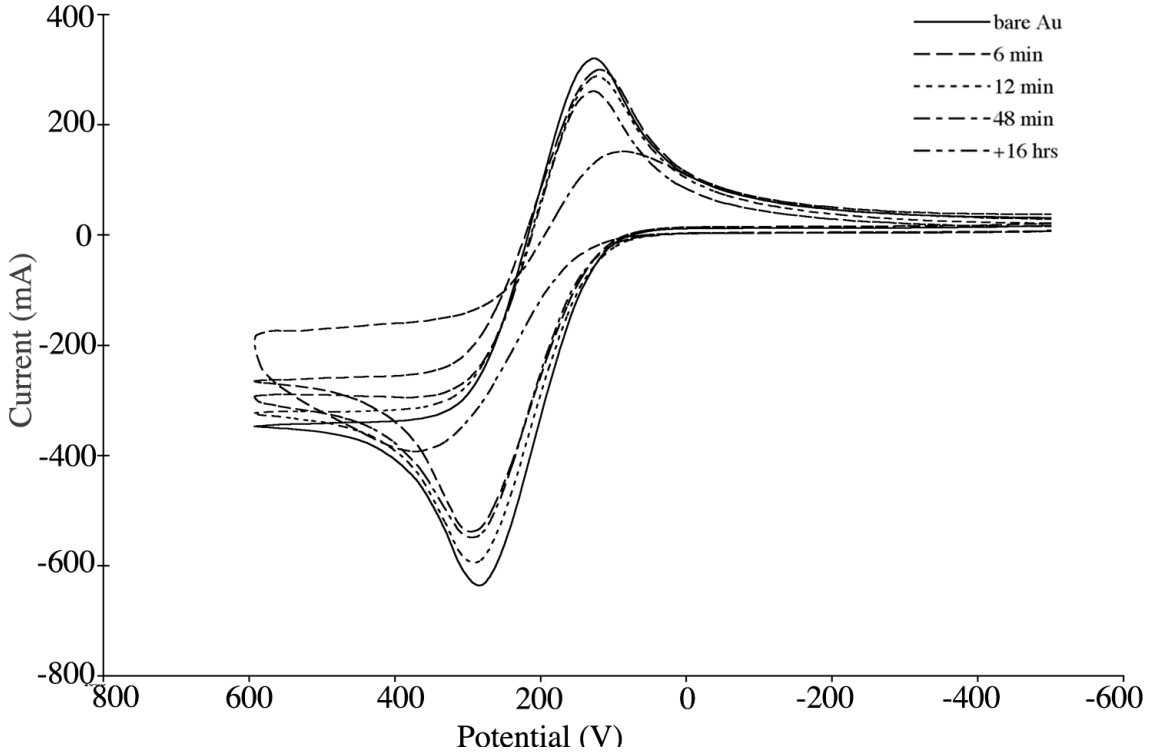


Figure 2.8 **CV trace time course for BAT SAM formation.** CV traces for Au sample were acquired after incubating in 1 mM BAT at various times.

In an effort to determine SAM stability, coated electrodes were incubated at various temperatures and monitored by CV. Data for conditions at room temperature and 120 °C are given here. From Figure 2.10, we find that SAMs are stable on electrodes after sitting in air overnight at room temperature. At 120 °C in air overnight, alkylthiol monolayers are easily oxidized and degrade. In the presence of air, the thiolate moity will oxidize to the sulphate species, which does not bind to Au. Additional

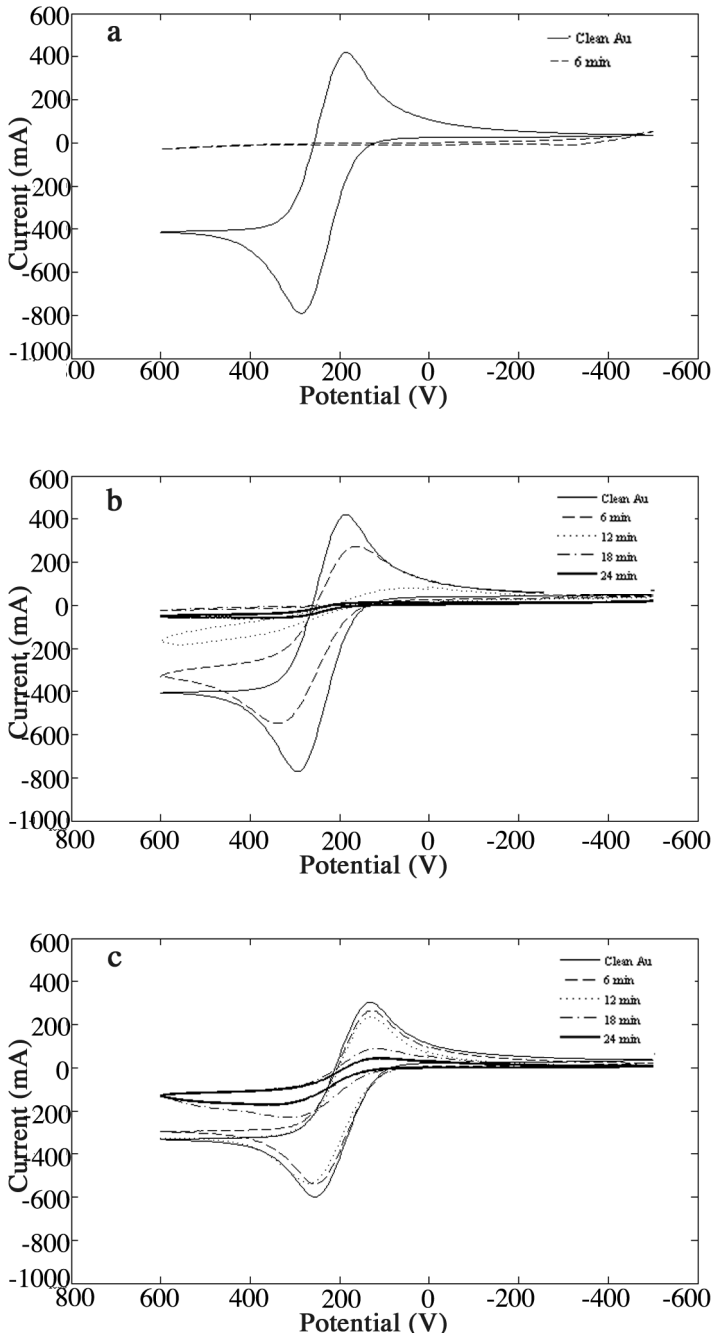


Figure 2.9 **TEG concentration effects on SAM formation.** CV traces for Au samples were acquired after incubating a) 10 mM TEG, b) 1 mM TEG, and c) 0.1 mM TEG at various time periods.

studies (data not shown) demonstrate that SAMs are stable up to 80 °C and partial degradation is seen at 110 °C.

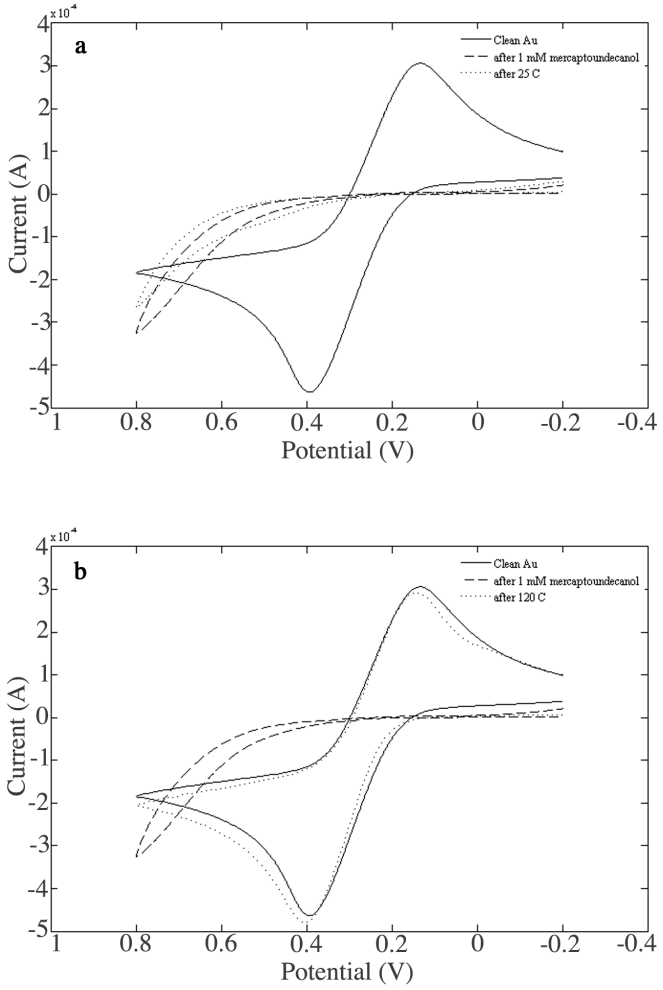


Figure 2.10 **Temperature effects on SAM stability.** Au electrodes were immersed in 1 mM mercaptoundecanol overnight. SAM stability at a) 25 °C and b) 120 °C was monitored by CV.

## 2.5 Fluorescence Microscopy

Fluorescence microscopy is a popular and useful method for assaying DNA hybridization events and microarrays [31]. Dyes are easily conjugated to small molecules and

proteins, allowing them to be tracked. In fluorescence, a photon ($h\nu$) is absorbed by the fluorophore, exciting an electron to a higher-energy state. As the electron relaxes back to the ground state, it releases a photon (less energtic than the excitation photon). In fluorescence microscopy, an excitation source such as a mercury arc lamp or a laser produces energetic photons. Filters, mirrors, and lenses direct excitation wavelength light to the sample specimen where the fluorophores are excited. The emitted photons are collected and detected by eye or camera (Figure 2.11).

Fluorescent quenching of dye molecules in close proximity to gold films and nanoparticles has been well documented. Singlet excited state lifetimes are greatly reduced as a result of energy transfer from the excited dye molecule to the bulk metal [32–34]. Fluorescence microscopy is used as a detection method for biological interactions in this thesis, so it is worthwhile to address the issue of fluorophore quenching.

An elegant experiment by Dubretret et al. demonstrated distance-dependent dye quenching by Au nanoparticles [35]. Fluorescent beacons were tethered to Au via a 25-base-pair-long single strand- (ss-)oligo probe with a hairpin structure in which the $5'$ and $3'$ ends are self-complementary. In the hairpin configuration, the dye is in close proximity to Au and upon excitation, fluorescence is deeply quenched. Addition of the complement target strand breaks the hairpin formation and the fluorophore is extended away from the Au surface approximately 80 Å. Fluorescence levels in this scenario are increased 600-fold. Another experiment by Schneider et al. examined distance-dependent fluorescence quenching by controlling dye-Au separation [36]. Au nanoparticles were coated in multi-layers of polymer and fluorophore. Dye-Au distances were quantified by TEM, and monitored by UV-Vis spectroscopy. Au-dependent quenching was measured by recording emission intensities before and after dissolving away the Au with cyanide, leaving the fluorophore and polymer shells intact. Their study found that a dye-Au separation of 80 Å was still close enough for

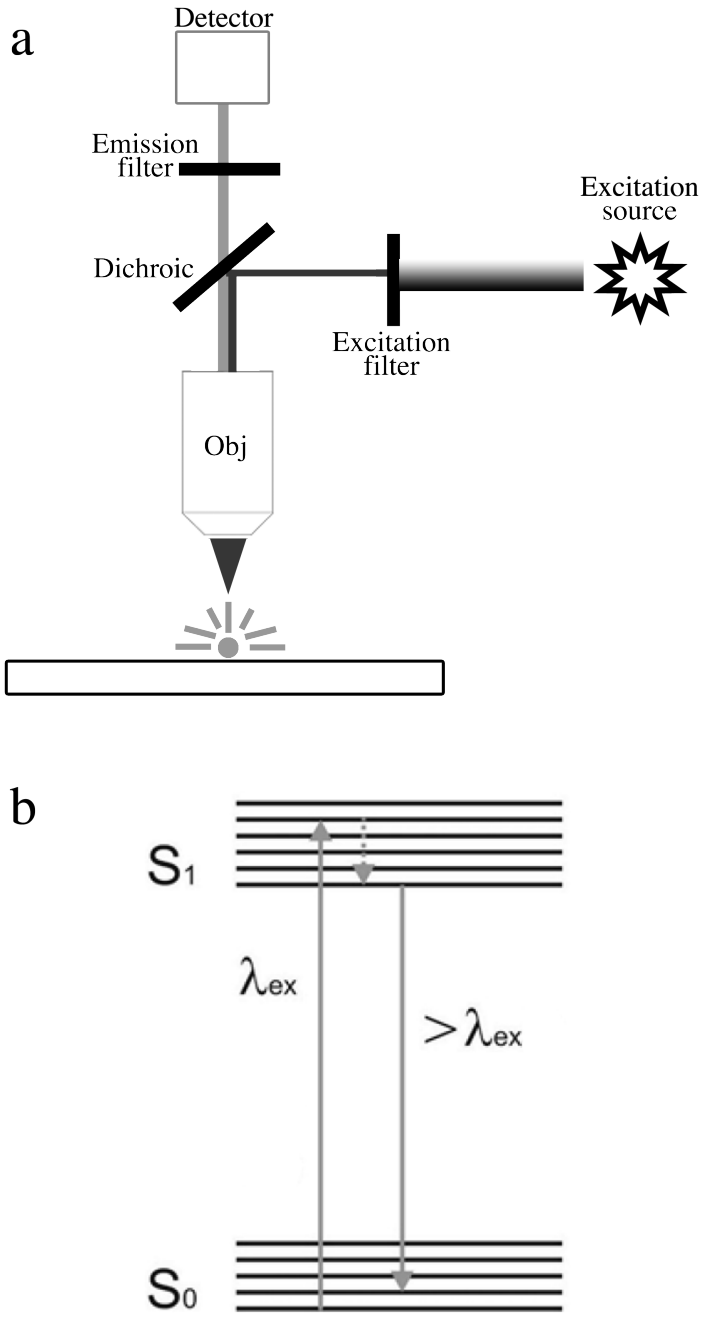


Figure 2.11 **Sample fluorescent microscope setup.** a) An excitation source emits photons which are absorbed by the fluorescent specimen. As the electron relaxes back to ground state, it emits a photon which is collected by a detector. b) Jablonski diagram depicting electronic states and fluorescence process

Au to cause some fluorophore quenching. However, fluorescent intensities remained "sufficiently bright for potential applications as diagnostic or sensing devices [36]."

Fluorescence measurements taken in this thesis work arise from either Cy3-labeled cells, beads, proteins, or oligos. In the case of beads and cells, the fluorophores are plentiful and distanced far enough from the Au that signals remain easily detected. Labels on proteins and oligos are separated by more than 80 Å from the Au surface. Fluorescent signals from labeled streptavidin and oligos may still experience some quenching (16%), but are still detectable [37]. For this reason, fluorescence intensity readings from chromophores on SAMs are semi-quantitative.

## 2.6 Conclusions

Throughout this thesis, a number of analytical techniques were successfully employed for the investigation of SAMs on Au substrates. Contact angle measurements and electrochemistry give insight into monolayer hydrophobicity and structural integrity, respectively. ESCA/XPS provides element identification for adsorbed monolayers and molecules. SEM is less informative for studying SAM structures, but it does produce nice images of the underlying gold substrate. Electrochemical methods remain the most qualitatively informative techiques for analyzing SAM structures.

Additional techniques may provide insight into monolayer formation, composition, and reactivity. For lack of resources, we were unable to employ them here. Scanning tunneling microscopy (STM) has yielded impressive topography images of SAMs and adsorbed proteins [38]. An alternative to ESCA for elemental analyses may be reflective mode Fourier-transform infrared spectroscopy (FTIR) [39, 40]. ESCA/XPS requires lengthy instrument pump-down times, whereas FTIR can be performed in ambient environment. Lastly, one promising technique is surface plasmon spectroscopy (SPR). With this method, real-time data can be acquired to track

SAM formation and subsequent protein adsorption to thin gold substrates [41–44].

## Acknowledgements

C. A. C. graciously thanks Prof. Nate Lewis and the Beckman Institute's Molecular Materials Resource Center facility for assistance and access to XPS/ESCA facility and goniometer. Special thanks go to Bruce Brunschwig, Joe Nemanick, and Lauren Webb for training me on equipment.

# Bibliography

[1] J. Andrade, V. Hlady, S. Jeon, *Adv. Chem. Ser.* **248**, 51 (1996).

[2] R. Wang, H. Kreuzer, M. Grunze, *J. Phys. Chem. B* **101**, 9767 (1997).

[3] K. Feldman, G. Hahner, N. Spencer, P. Harder, M. Grunze, *Journal of the American Chemical Society* **121**(43), 10134 (1999).

[4] V. Zworykin, J. Hillier, S. R.L., *ATSM Bulletin* **117**, 15 (1942).

[5] J. Bozzola, *Electron Microscopy—Methods and Protocols*, vol. 369 of *Methods in Molecular Biology*. Humana Press, Inc., Totowa, NJ, second edn. (2007).

[6] L. Yan, X. Zhao, G. Whitesides, *J. Am. Chem. Soc.* **120**, 6179 (1998).

[7] D. Joy, *Future Fab Intl.* **9** (2000).

[8] A. Einstein, *An. Phys.* **17**, 132 (1905).

[9] C. Wagner, et al., *Surface and Interface Analysis* **3**(5), 211 (1981).

[10] D. Briggs, M. Seah, *Practical surface analysis*, vol. 1. John Wiley & Sons, Inc., second edn. (1993).

[11] A. Jezierski, A. Szytula, B. Penc, D. Fus, *Journal of Alloys and Compounds* **317–318**, 340 (2001).

[12] A. Atrens, A. Lim, *Applied Physics A* **51**, 411 (1990).

[13] C. Bichler, H. Langowski, M. Bischoff, U. Moosheimer, in *39th Annual Technical Conference of the Society of Vacuum Coasters* (1996).

[14] A. Sadough-Vanini, J. Audouard, P. Marcus, *Corrosion Science* **36**(11), 1825 (1994).

[15] P. Bertrand, *J. Vac. Sci. Technol.* **18**(1), 28 (1981).

[16] A. Al-Harthi, D. Thompson, G. Khattak, L. Wenger, M. Salim, *Journal of Non-Crystalline Solids* **212**, 180 (1997).

[17] R. Holm, *Analysis of Organic and Biological Surfaces*, chap. 2, p. 37. John Wiley & Sons, Inc. (1984).

[18] A. Oya, F. Beguin, K. Fujita, R. Benoit, *Journal of Materials Science* **31**, 4609 (1996).

[19] B. Lowenberg, B. Callen, J. Davies, R. Sodhi, S. Lugowski, *Journal of Biomedical Materials Research* **29**, 279 (1995).

[20] J. Moulder, W. Stickle, P. Sobol, K. Bomben, *Handbook of X Ray Photoelectron Spectroscopy: A Reference Book of Standard Spectra for Identification and Interpretation of XPS Data*. Physical Electronics, Zurich, Switzerland (1995).

[21] T. Tateishi, Y. Ito, Y. Okazaki, *Materials Transactions, JIM* **38**(1), 78 (1997).

[22] C. Bain, G. Whitesides, *J. Am. Chem. Soc.* **111**, 7164 (1989).

[23] R. Nuzzo, L. Dubois, D. Allara, *JACS* **112**, 558 (1990).

[24] K. Peterlinz, R. Georgiadis, *Langmuir* **12**, 4731 (1996).

[25] S. Xu, et al., *J. Chem. Phys.* **108**, 5002 (1998).

[26] T. Ishida, et al., *Japn. J. Appl. Phys.* **35**(12), L1710 (1996).

[27] K. Tamada, M. Hara, H. Sasabe, W. Knoll, *Langmuir* **13**, 1558 (1997).

[28] R. DeBono, G. Loucks, D. Manna, U. Krull, *Can. J. Chem.* **74**, 677 (1996).

[29] S. Strbac, O. Magnussen, R.-J. Behm, *J. Serb. Chem. Soc.* **66**(4), 281 (2001).

[30] K. Nelson, et al., *Langmuir* **17**, 2807 (2001).

[31] P. Park, et al., *Journal of Biotechnology* **112**, 225 (2004).

[32] A. Ishida, Y. Sakata, *J. Chem. Soc., Chem. Comm.* **1**, 57 (1998).

[33] K. Saito, *J. Phys. Chem. B* **103**, 6579 (1999).

[34] T. Pagnot, D. Barchiesi, G. Tribillon, *App. Phys. Lett.* **75**, 4207 (1999).

[35] B. Dubertret, M. Calame, A. Libchaber, *Nature Biotech.* **19**, 365 (2001).

[36] G. Schneider, G. Decher, *Nano Letters* **6**(3), 530 (2006).

[37] C. Yun, et al., *JACS* **127**, 3115 (2005).

[38] R. Yamada, H. Sakai, K. Uosaki, *Chem. Lett.* **7**, 667 (1999).

[39] M. D. Porter, T. Bright, D. Allara, C. Chidsey, *J. Am. Chem. Soc.* **109**, 3559 (1987).

[40] D. Yan, J. Jordan, V. Burapatana, G. Jennings, *Langmuir* **19**, 3357 (2003).

[41] R. Georgiadis, K. P. Peterlinz, A. W. Peterson, *J. Am. Chem. Soc.* **122**(13), 3166 (2000).

[42] J. Ladd, et al., *Langmuir* **20**, 8090 (2004).

[43] C. Boozer, et al., *Anal. Chem.* **76**, 6967 (2004).

[44] C. Boozer, J. Ladd, S. Chen, S. Jiang, *Anal. Chem.* **78**, 1515 (2006).

# Chapter 3

# Controlling Adsorption and Desorption of Alkylthiols on Gold Substrates

In this chapter, I report the novel synthesis of alkylthiol reagents and approaches for generating recyclable biosensors. The use of aqueous media for the formation of protein binding alkylthiolate monolayers on Au surfaces results in accelerated alkylthiolate monolayer formation and improvement in monolayer integrity as visualized by fluorescence microscopy and CV techniques. I have also developed an electrocleaning protocol that is compatible with microfluidic devices, and this technique serves as an on-chip method for cleaning Au substrates both before and after monolayer formation. The techniques for the formation and dissociation of biotinylated SAMs from aqueous solvents reported here may be applied towards the development of Au-based sensor devices and microfluidic chips in the future. A potential use of these devices includes the specific capture and triggered release of target cells, proteins, or small molecules from liquid samples.

## 3.1 Background

The ability to tailor interactions between biological molecules and solid supports is vital for the development of detection systems and assay platforms. These relation-

ships are frequently quite complex and involve hydrophobic interactions, electrostatic interactions, van der Waals forces and covalent chemical bonds. We can exploit these interactions in a solid support device by modifying the surface substrate with thin films and monolayers [1]. Self-assembled monolayers (SAMs) can be engineered to exhibit a variety of chemical properties and reactivities making them hydrophobic [2–4], repulsive [5, 6], or electrochemically active [7–10]. In practice, SAMs employing biotin have been studied in association with streptavidin conjugated to DNA, proteins, and nanoparticles [11–16]. Such SAMs are vital for bioassay technologies such as DNA chips, protein chips, and small molecule biosensors.

Alkylthiols form SAMs on Au substrates in distinct stages [17]. An n-alkylthiol, such as the ones used in this paper, is structurally comprised of an n-alkyl chain with a thiol group at one end and a functional group of choice at the other end. We employ triethylene glycol and biotin in the alkylthiols studied here. Upon adsorption, alkylthiols are reduced to alkylthiolates [18, 19] that initially adsorb onto a Au surface in a disordered fashion, resulting in 80–90% coverage of the substrate [17]. The subsequent adsorption stage is slower as the alkylthiolates self-assemble into a more organized and insulated film [20]. Variables such as temperature, thiol concentration, terminating end group [21], and solvent composition [3] can affect alkylthiolate monolayer formation on Au.

The organic solvents ethanol, DMSO, or hexane are often used to solvate hydrophobic alkylthiols [22], but they are not compatible with polydimethylsiloxane (PDMS), one of the most common materials used for making microfluidic devices (GE Silicones, Electronic Materials Handbook). Depending on the volume of liquid and thickness of the PDMS microfluidics layer, these organic solvents may swell the PDMS [23] causing polymer delamination from the Au surface. Evaporation of solvents via the PDMS can also occur and deleteriously affect formation of well-assembled alkylthiol monolayers. Alkylthiols with large hydrophilic groups, such as

an oligoethylene glycol or an oligonucleotide, are soluble in aqueous solvents [13] that are compatible with PDMS.

SAMs on Au have been successfully made and stored in aqueous solvents [24]. Monolayers of hydrophobic alkylthiol monolayers may be formed in aqueous solutions by the aid of surfactants [24]. In water, hydrophobic alkylthiols spontaneously coordinate to the water-air interface. The addition of surfactants results in micelle formation around alkylthiols and aids in their diffusion to the gold surface [24]. Studies by Yang et al. indicate that alkylthiol-based SAMs desorb more slowly when stored in water (5% DMF or DMSO) compared to butan-2-ol or hexane [25]. The dilute amphiphilic DMF or DMSO are thought to coordinate to small defect sites to prevent both oxidation and re-solvation of alkylthiolates. Samples undergoing a short thiolate adsorption time followed by incubation in water have also been shown to exhibit more crystalline packing of alkylthiolate chains [26]. The long alkyl chains associate via van der Waals and hydrophobic interactions in aqueous solutions that promote organization of the stable SAMs on the Au surface [26].

An essential requirement for high-quality alkylthiolate monolayers is a clean Au substrate [27]. Clean Au substrates exposed to ambient conditions will quickly collect impurities from the environment and atmosphere that can impact SAM growth [4, 28–30]. These contaminants are typically hydrocarbon pollutants which can be cleaned off the Au substrates using agents such as aqua regia solution, piranha solution, and ozone plasma [22]. While each of these methods yields clean Au surfaces that permit quality SAM formation, they each present major drawbacks for cleaning integrated biosensors. The thin Au components within a device, including the test substrates and the electrical leads, are quickly dissolved upon exposure to acid-based cleaning reagents. Ozone plasma effectively oxidizes and degrades Au-bound contaminants, but it is difficult to ozone clean the Au surfaces packaged under PDMS layers.

Other methods such as ozone laser ablation, plasma treatment, and electrochem-

ical cleaning were also considered as options for cleaning Au pads. However, as test substrates become more densely populated on a chip, laser cleaning of chips becomes limited by wavelength diffraction. As biosensing surfaces shrink to the nano-scale, the small features will need to be addressed using different techniques. The use of nanoelectrodes may be the solution. Electrochemical techniques have been previously reported to clean Au chip surfaces of contaminants effectively enough for alkylthiol attachment and subsequent SAM formation [18, 31–35]. Application of sufficiently oxidative (+0.85 V vs. SCE in 0.1 M $H_2SO_4$) or reductive (-1.03 V vs. SCE in 0.1 M NaOH) potentials on gold induces desorption of surface species, including the alkylthiolates used to make specific monolayers [36]. This technique has the additional positive attribute for our studies in that it permits Au pads at the tips of our cantilevers to be cleaned individually or as a group. Another advantage of electrocleaning is that we can specifically target desired Au pads located at the ends of cantilevers with nanometer resolution, which is essential for the longterm goal of addressing individual cantilevers on a BioNEMS chip.

Here I report the development of a reusable biosensor system by the formation of functionalized alkylthiolate monolayers on addressable Au surfaces. The techniques are developed with future applications in microfluidic systems in mind. Two ethylene glycol modified alkylthiolates TEG and BAT (Figure 3.1) were adsorbed

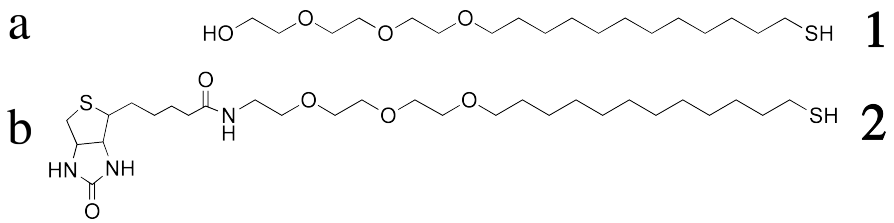


Figure 3.1 **Chemical structures for TEG and BAT.** a) Tri(ethylene glycol) dodecylthiol (TEG), b) Biotinylated tri(ethylene glycol) dodecylthiol (BAT)

onto Au surfaces in order to bind specific analytes while repelling non-specific ones. Alkylthiolates containing ethylene glycol reduce the non-specific binding of proteins, bacteria, and cells to Au and Si surfaces [37–46]. I show that insulating TEG and BAT monolayers on Au surfaces were adsorbed from water at faster rates and with fewer monolayer pinholes than SAMs adsorbed from ethanol. Finally, electrochemical techniques efficiently remove contaminants from Au surfaces to enhance alkylthiolate monolayer formation in a manner that is addressable on a nanometer scale and does not damage the Au surfaces during repeated cleaning.

## 3.2 Materials and Methods

### 3.2.1 Reagents

Silicon wafers were purchased from Wafer World. Chromium was purchased from R.D. Mathis Company and gold shots from Refining Systems, Inc. Phosphate buffered saline (PBS) was prepared as 0.139 M NaCl, 2.68 mM KCl, 8.1 mM $Na_2HPO_4$, and 1.1 mM $K_2HPO_4$ (Mallinckrodt) in Nanopure water. Potassium ferrocyanide and potassium ferricyanide were purchased from Aldrich. Absolute ethanol was purchased from Aaper Alcohol and Chemical Company. Cy3-labeled streptavidin was purchased from Zymed, Inc. Reagents BAT and TEG were synthesized in house using techniques described both below and in literature [47].

### 3.2.2 Preparation of Substrates and Monolayers

Silicon wafers were photo-patterned using dark field transparency masks (Figure 3.2) and positive photoresist. A 3 nm chromium adhesion layer and 100 nm Au layer were then thermally evaporated. Diced Au substrates were then plasma cleaned at an oxygen flow rate of 0.8 $\mathrm{L\,min^{-1}}$ in an UV ozone cleaner (SAMCO UV & Ozone Dry

Stripper, Model UV-1) at 100 °C for 30 min followed by a 2 min nitrogen purge. Au substrates used in electrochemical experiments underwent a pre-cleaning treatment by CV scans out to 1.2 V (vs. Ag/AgCl, saturated KCl), at a scan rate of 100 $mV\,s^{-1}$ in 30 mM ferrocyanide/PBS. These electrocleaned samples were then rinsed in copious amounts of water and ethanol, dried under a stream of argon, and immediately placed in thiol solution. Reagent compositions (BAT and TEG stock solutions of 10 mM in ethanol) were varied for a total thiol concentration of 0.1 mM. Diluting the ethanolic stock solution of thiols in absolute ethanol and Nanopure water gave aqueous solvent compositions of 50% and 1% ethanol. For brevity, we refer to 1% ethanol in the context of thiol solvent as "water." Upon removal, samples were rinsed in ethanol and dried under argon.

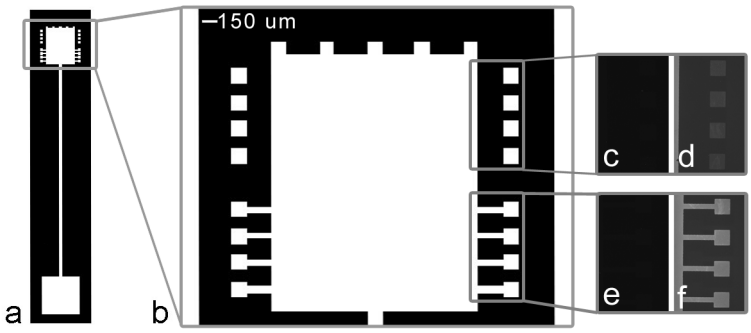


Figure 3.2 **Photolithography mask for Au samples.** a) The bottom square provides ohmic contact for the electrode and the top detailed half serves as the working electrode surface. b) A magnified view of the working electrode area. Both electrically addressable and isolated Au pads are presented. Control substrates without SAMs do not bind Cy3-streptavidin; electrochemically untreated sample is c) and treated is e). Biotinylated SAMs on electrochemically precleaned Au bind Cy3-streptavidin; electrochemically untreated sample is d) and treated is f). The relative fluorescence intensities (mean and standard deviation) for Au pads are as follows (4 samples): 2c) 7.8 ± 0.3, 2d) 59.7 ± 1.9, 2e) 8.0 ± 0.1, 2f) 120 ± 4

### 3.2.3 Electrochemical Methods

The structural integrity of the adsorbed monolayer is characterized using CV method [48]. During a CV scan, a tightly assembled monolayer insulates the Au surface against electron transfer with a redox-active molecule in solution. Any defects in the monolayer film are detected by CV and characterized by current flow. CV measurements were carried out with a CH Instruments Model 600B potentiostat (CH Instruments, Austin, TX). A conventional three-electrode electrochemical cell was constructed with a platinum wire/mesh counter electrode and Ag/AgCl reference electrode in saturated KCl. The Au substrate served as the working electrode. Measurements were taken in an electrolyte solution of 30 mM potassium ferrocyanide in PBS at a scan rate of 100 mV $\text{sec}^{-1}$. CV potentials were scanned from 0.2 V to 0.8 V. Electrocleaning of samples was accomplished by a CV scan from 0.2 V to 1.2 V at 100 mV $\text{sec}^{-1}$ in the same electrolyte solution. Oxidative desorption of SAMs from Au was accomplished by the application of a 30 second DC pulse at 1.4 V in an electrolyte solution of PBS. A more detailed theory of CV is given in Chapter 2.4.

To qualitatively compare different samples, we calculated peak current densities (PCD) acquired by CV. PCD values for a given sample were determined as the average value for cathodic and anodic current magnitudes for the sample divided by average value for cathodic and anodic current magnitudes for an untreated, clean gold sample. For clarity, the determination of PCD is given below in Equation 3.1, where $I_{pa}$ and $I_{pc}$ are the current peak heights at the anodic and cathodic curves, respectively.

$$\text{PCD} = \frac{\frac{I_{pa,sample}+I_{pc,sample}}{2}}{\frac{I_{pa,clean}+I_{pc,clean}}{2}} \tag{3.1}$$

A PCD value of 1 would indicate no monolayer coverage across the Au surface, whereas a PCD value of 0 would indicate complete monolayer coverage across the Au surface. The peak current densities for CV traces are calculated for each sample

condition and are given in Table 3.1.

### 3.2.4 Protein-Binding Assays

The Au samples with adsorbed BAT/TEG SAMs were submersed in a 60 nM solution of Cy3-labeled streptavidin in PBS for 30 minutes at room temperature. The samples were removed and washed five times with 1 ml of PBS, then stored in PBS for immediate analysis by fluorescence microscopy.

### 3.2.5 Fluorescence Microscopy

Images were acquired on an upright Zeiss Axioplan 2 infinity corrected microscope (Zeiss, Germany) and acquired with a monochrome CCD Zeiss Axiocam HRm camera. Zeiss Plan-Neofluar objectives 10x/0.3, 20x/NA 0.5, and 40x/NA 0.75 were used in conjunction with a Chroma (Rockingham, VT) Cy3 filter set. A mercury arc lamp served as the excitation source. Images were acquired in 8-bit monochrome resolution and 1030 x 1300 pixel resolution.

### 3.2.6 Synthetic Methods

Literature reports the use of radical chemistry initiated by photolysis to achieve the synthesis of TEG compound **1** in decent yield [49, 50]. The results in our lab, however, were inconsistent. Instead, we developed the synthesis shown in Figure 3.3 to produce the same compound.

In the first step, triethylene glycol is deprotonated in anhydrous DMF by NaH, then reacted to large excess with 1,11-dibromoundecane to yield 11-(bromoundecyl)-triethylene glycol (41% yield). The introduction of thioacetate was achieved by reacting 11-(bromoundecyl)triethylene glycol to sodium thioacetate, prepared by a reaction of sodium methoxide and thioacetic acid, giving the desired product, 11-

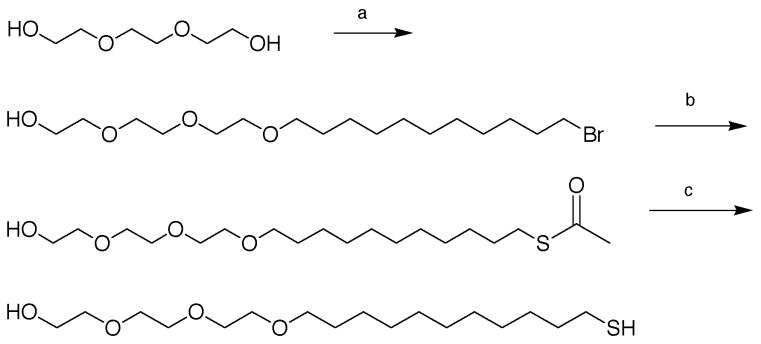


Figure 3.3 **Synthesis of poly(ethylene glycol) dodecylthiol (TEG).** (a) (i) NaH/DMF, (ii) 1,11-dibromoundecane; (b) (i) NaH/$CH_3OH$, (ii) $CH_3COSH$; (c) $NH_4OH/CH_3OH$, 40 °C.

(thioacetylundecyl)triethylene glycol, in excellent yield (93%). The deprotection of thiol ester was straightforward, via ammonia hydrolysis in methanol as a solvent (54% yield).

A biotinylated alkylthiol reagent in the literature is depicted in Figure 3.4 [50, 51]. The body of the compound consists of three sections: biotin, TEG, and alkyl chain. In compound **3**, an amide bond connects the dodecyl chain and the ethylene glycol groups. Compound (**2**) presented here has an ether bond connecting the alkyl chain to the ethylene glycol group, more closely mimicking the structure of TEG. The synthesis of compound **2** ( Figure 3.5) is favored over that of **3** because the intermediate **10** may be reacted with any activated carboxyl group to generate novel alkylthiol reagents. Synthesis of **3**, however, proceeds by appending the PEG group to biotin, followed by multi-step attachment of the alkyl chain [50].

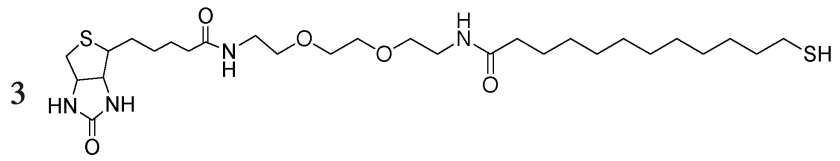


Figure 3.4 **Biotinylated alkylthiol molecule.** Biotinylated alkane thiol described by Knoll and Nelson et al.

The selective tosylation of triethylene glycol in two steps using NaH and *p*-toluenesulfonyl chloride in anhydrous DMF led to the formation of **5** (73% yield). The azide **6** was prepared in almost quantitative yield (99%) by stirring **5** in large excess of $NaN_3$ in DMF/ $H_2O$. Reaction of this compound to excess amount of 1,12 dibromododecane resulted in the attachment of the azotriethylene glycol to the alkyl chain to yield 12-(azotriethyleneoxy)-1-bromododecane (**7**) in low yield (24% yield). The resulting bromoalkane **7** was refluxed with thiourea in ethanol, followed by hydrolysis by NaOH solution, affording the diazodo disulfide **8** (46% yield). The reduction of the azo group by triphenylphosphine in THF provided the corresponding amine; after protection by tert-butoxycarbonate, **9** was obtained in excellent yield (82% yield). The removal of the tert-butoxycarbonate group by trifluoroacetic acid (TFA) in $CH_2Cl_2$ gave ammoniumtriethyleneoxydodecane disulfide **10** (80% yield). The introduction of biotin to the linker through a reaction of the corresponding amine to the activated biotin derivative **4** was straightforward. The benefit of this reaction is its application for the attachment of a carboxylated molecule of choice [52]. The final compound **12** can be prepared by a simple reduction of the disulfide **11** by dithiothreitol (DTT) in basic medium.

In summary, we have designed and synthesized two biofunctionalized alkyl thiols. The synthesis of 11-(mercaptoundecyl) triethylene glycol in three steps has provided a feasible alternative method. Furthermore, mercaptododecyltriethyleneoxy biotin

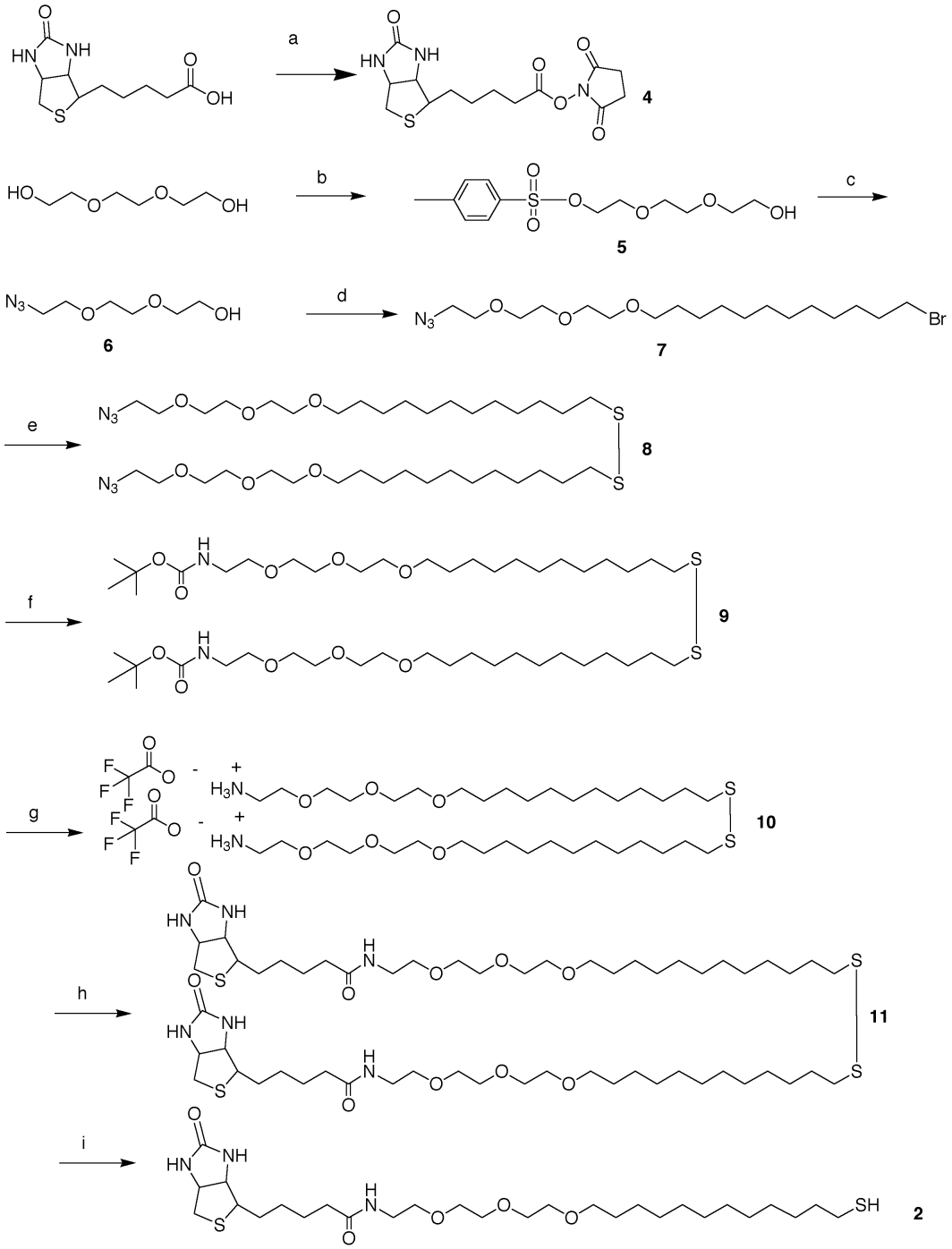


Figure 3.5 **Synthesis of biotinylated alkylthiol.** a) N-hydroxysuccinimide/DCC/DMF; b) (i) NaH/DMF, (ii) p-toluenesulfonyl chloride; c) $NaN_3$/DMF/$H_2O$, 58 °C; d) (i) NaH/DMF, (ii) 1,12-dibromododecane; e) (i) thiourea/EtOH/$H_2O$, 88 °C (ii) NaOH; f) (i) $Ph_3P$/THF/$H_2O$, (ii) ditertbutyl dicarbonate/THF/TEA; g) TFA/ $CH_2Cl_2$/triisopropyl silane; h) **7**/DMF/TEA; i) DTT/THF/MeOH/TEA

amide **2** is novel and viable for the formation of SAMs. The intermediate aminotriethyleneoxydodecanethiol **10** will be very useful for attachment of any activated carboxyl groups in order to make novel receptors for biosensor development.

## 3.3 Results and Discussion

### 3.3.1 Electrochemical Cleaning of Au Surfaces Improves Monolayer Coverage

The cleanliness of substrates and method of cleaning directly influence the quality of alkylthiolate monolayer formation [27]; the presence of contaminants impedes alkylthiolate monolayer formation [2]. Contaminants such as hydrocarbons may arise from the air and adsorb non-specifically to Au surfaces [53] making cleaning a necessary step prior to alkylthiolate monolayer formation.

To determine cleanliness of an Au substrate, we use the conductive properties of Au to allow cyclic voltammetry (CV) inspection of the quality of the alkylthiolate monolayer coverage on Au surface. CV analysis detects defects in alkylthiolate monolayers, such as pinholes, gaps, islands, and disordered packing in general, which can expose the Au substrate to the surrounding solvents [54]. Current flow occurs when $Fe^{2+/3+}$ ions are able to exchange electrons with the bare Au substrate, or one coated in a defective alkylthiolate monolayer. Adsorption of 0.1 mM TEG in ethanol reagents onto cleaned Au substrates after 12 hours at room temperature results in complete monolayer coverage and thus Au insulation from the $Fe^{2+/3+}$ ions in solution (Table 3.1).

Au/Si based chips in a nanofabrication room are initially cleaned with ozone plasma. The Au and Si surfaces of these biosensor chips are receptive to quality alkylthiolate monolayer formation if used immediately (data not shown). However,

Table 3.1. Calculated peak current density for gold electrodes insulated with BAT and/or TEG alkylthiolates (0.1 mM final concentration after 1 h)[a]

| Alkylthiolate percentage | | Solvent | | |
|---|---|---|---|---|
| BAT | TEG | $H_2O$ | $H_2O$/EtOH (1:1) | EtOH |
| 0 | 0 | 1 | 1 | 1 |
| 0 | 100 | 0.00 | 0.43 | 0.31 |
| 100 | 0 | 0.90 | 0.51 | 0.54 |
| 50 | 50 | 0.00 | 0.64 | 0.75 |
| 25 | 75 | 0.02 | 0.49 | 0.78 |
| 12.5 | 87.5 | 0.00 | 0.45 | 0.78 |
| 6.25 | 93.75 | 0.00 | 0.32 | 0.73 |

[a]PCD values have been normalized against 0% BAT, 0% TEG conditions.

we regularly make numerous potential biosensor chips at a time and then store them under $N_2$ conditions for periods of days to weeks before use. During this storage time, it is common for unidentified contaminants to absorb onto the Au surfaces which can deleteriously effect alkylthiolate monolayer formation as determined by CV analysis. We observe similar Au surface contamination when biosensor chips are stored overnight in air, 100% ethanol, 100% methanol, or dd$H_20$ (data not shown). Contamination of the Au surfaces severely limits our ability to consistently generate quality alkylthiolate monolayers.

We attempted numerous procedures to clean the Au surfaces of stored chips with rinses in ethanol, methanol, isopropanol, or acetone, but CV analysis indicated that the ensuing alkylthiolate monolayer coverage was substandard, suggesting contaminants remained on the Au substrates. More stringent cleaning protocols such as piranha or aqua regis treatments effectively reconditioned the chips to their pre-stored quality. However, the strong acid treatments are highly corrosive to our chips. Specifically, piranha treatment often causes delamination of the Au from the Si substrate and destroys the small photo-patterned Au surface features on our chips (data not shown). We also considered using ozone plasma treatment to recondition the stored

chip Au surfaces as previously mentioned. However, ozone plasma, piranha and aqua regis treatments are not amenable for use with PDMS covered chips due to polymer compatibility issues or lack of Au surface accessibility, nor can they be used to clean individual substrate elements within an array.

Another process, electrocleaning, can remove bound contaminants without destroying the underlying Au surfaces [55]. Electrocleaning also permits the sequential or simultaneous cleaning of the numerous Au substrates located throughout our biosensor chips. The efficacy of electrochemical treatments on Au electrodes and subsequent SAM formation were tested by comparing electrically connected Au substrates against electrically isolated Au substrates on a single chip (Figure 3.2a). Au regions that were electrically connected were cleaned during the anodic potential sweep to +1.2V (100 mV $sec^{-1}$), whereas electrically isolated Au regions were not. The entire chip was then immersed in a BAT:TEG containing ethanol solution in order to form a BAT:TEG monolayer. The chips were then incubated with Cy3-streptavidin in order to indirectly assay the quality of alkylthiolate monolayer formation, since CV analysis was not feasible on the electrically isolated Au substrates. The relative fluorescent intensity of the streptavidin-Cy3 protein binding to the BAT:TEG monolayer was determined using fluorescent microscopy. For these samples, the electrically isolated regions consistently exhibited half the fluorescence intensity compared to the electrically connected regions (Figure 3.2c–f). These data are interpreted to suggest that pre-cleaned Au substrates are able to specifically bind more protein since they can bind more biotin on the higher quality BAT:TEG mixed monolayers on cleaned Au substrates compared to the inferior BAT:TEG absorption on dirty Au substrates.

### 3.3.2 Effect of Adsorption Solvent on SAM Formation

Certain organic solvents (i.e., DMSO, DMF, hexane) that are used to generate alkylthiolate monolayers are not compatible with PDMS or biological agents [23] (GE Sil-

icones, Electronic Materials Handbook). We explored the possibility of generating alkylthiolate monolayers using the solvents ethanol and/or water. We first tested the solubility of BAT and TEG ethanol and water-based solvents and then determined their ability to form quality alkylthiolate monolayers. We used CV to evaluate the quality of the alkylthiolate monolayer coverage of Au substrates and protein binding to evaluate the biological functionality of the formed alkylthiolate monolayers.

The solubility of TEG, BAT, and BAT:TEG mixtures in water and ethanol solutions varies. At 0.1 mM thiol concentrations, TEG dissolves completely in both water and ethanol. However, BAT and BAT:TEG solutions (1:4) yield a white precipitate in solvent compositions lower than 30% ethanol. At higher ethanol concentrations, no precipitate was observed. We chose 50% ethanol as the intermediate solvent composition in our study because the effects of equivalent amounts of water and ethanol could be observed, and there would be no interference in SAM formation due to insoluble thiol molecules. Solubility of the thiol molecule in a given solvent plays a key role in the formation of SAMs [56–58]. Based on our combined observations of thiol solubility, our CV measurements, and fluorescence microscopy data we can infer the composition and extent of SAM formation on Au substrates in our aqueous solutions.

Of all the thiol compositions tested here, pure TEG is the most soluble in ethanolic and aqueous solvents. Solutions of pure TEG form the most insulating SAMs and form SAMs at the fastest rate. The TEG molecule has two distinct parts: a twelve carbon hydrophobic alkyl chain and a hydrophilic triethylene glycol chain (Figure 3.1). From Table 3.1, the peak current density value for TEG-coated electrodes was lowest when SAMs were adsorbed from water ($< 0.001$), indicating a highly insulating monolayer. In comparison, TEG SAMs formed in 50% ethanol and ethanol have higher PCD values, 0.432 and 0.308, respectively. There exist unfavorable interactions between water and the alkylthiol chain of TEG and attractive hydrophobic interactions between the alkylthiol chains [59]. An energetic penalty would be imposed for any

SAM defect that increases the amount of the hydrophobic alkyl chains exposed to water. Therefore, SAMs prepared in aqueous solutions are likely more well ordered, with fewer defects, than those prepared from ethanol solutions [24]. Over the course of 24 hours, the TEG SAMs in 50% ethanol and ethanol also form highly insulating monolayers, but that time scale is an order of magnitude larger than for TEG SAMs formed in water.

BAT is soluble in ethanol, but is only partially soluble in aqueous solvents. BAT is similar to TEG, but also includes a hydrophobic biotin group (Figure 3.1). At 0.1 mM, BAT forms a white precipitate when diluted in water or in ethanolic solvents of 30% ethanol and lower. We observe from Table 3.1 PCD values that BAT forms SAMs with fewer defects when adsorbed from ethanolic solutions than when adsorbed from water. In water, the insoluble nature of BAT likely makes delivery of the molecule to the liquid/Au interface more difficult. Only after longer incubation times ($>$ 24 hrs) do BAT molecules adsorbed from water make insulating monolayers (data not shown). The pure BAT SAMs formed from ethanolic solutions only provide partial coverage and insulation across the Au surface after a 1 hour incubation at RT (Table 3.1).

The lack of full electrode insulation may be due to steric interference of the BAT biotin end groups. The triethylene glycol group between the alkyl chain and the biotin group is long enough to allow the hydrophobic biotin to wrap around and bury into the hydrophobic alkyl chains [50]. This likely prevents the tight association of the alkyl regions of the alkylthiolates required for the formation of tightly packed, defect-free monolayers. In a previous study, angle-resolved X-ray photoelectron spectroscopy revealed that biotin head groups of BAT molecules were buried within the alkyl chain monolayer [50]. In contrast to pure TEG solutions that form higher-quality SAMs in water, pure BAT solutions form higher-quality SAMs in ethanolic solvents.

Similar to pure BAT solutions, mixed BAT:TEG solutions exhibited partial sol-

ubility in ethanolic solvents of 30% and below. The mixed SAMs tested had BAT percentage compositions ranging from 50% to 6.25%. From Table 3.1, the general trend of PCD values measured for these mixed monolayers indicates a decrease in PCD, or increase in monolayer quality, as aqueous composition of solvent increases and as TEG composition of the thiol mixture increases. We postulated above that TEG monolayer formation is greatly influenced by the presence of water. It would appear that the hydrophobic interactions of the alkyl chains in both BAT and TEG, coupled with an energetic penalty of defects within a monolayer, are also a dominant force in the formation of mixed monolayers. Mixed monolayers formed from ethanol also indicate that SAM quality increases as TEG composition increases. We show that incorporation of TEG into a BAT monolayer can increase the order of the alkyl chains within the monolayer. The ethylene glycol groups of TEG can coordinate with the ethylene glycol groups of BAT, reducing the likelihood of biotin groups burying into the alkyl chains of the monolayer. Biotin groups that might otherwise be buried within the monolayer are presented to the solvent interface and thus accessible for binding events.

### 3.3.3 Specific Binding of Fluorescent Proteins to SAMs

In order to assay the composition and functionality of the BAT:TEG mixed alkylthiolate monolayers, we used fluorescence microscopy and CV on the same Au substrates to correlate the relative fluorescence intensities of Cy3-labeled streptavidin with the amount of accessible BAT molecules on the Au substrates. Au chip substrates were immersed in mixed thiol solutions ([BAT] + [TEG] = 0.1 mM) of 3 different solvent compositions ($\sim$ 100% ethanol, $\sim$ 50% ethanol, and $\sim$ 100% water) for 60 minutes at room temperature and subsequently incubated with 200 mM Cy3-labeled streptavidin in PBS for 30 minutes at room temperature. Based on the protein-binding assay, fluorescence levels for Au samples linearly increased as the BAT concentration

of the thiol solutions increased (Figure 3.6). However, thiol composition in solution

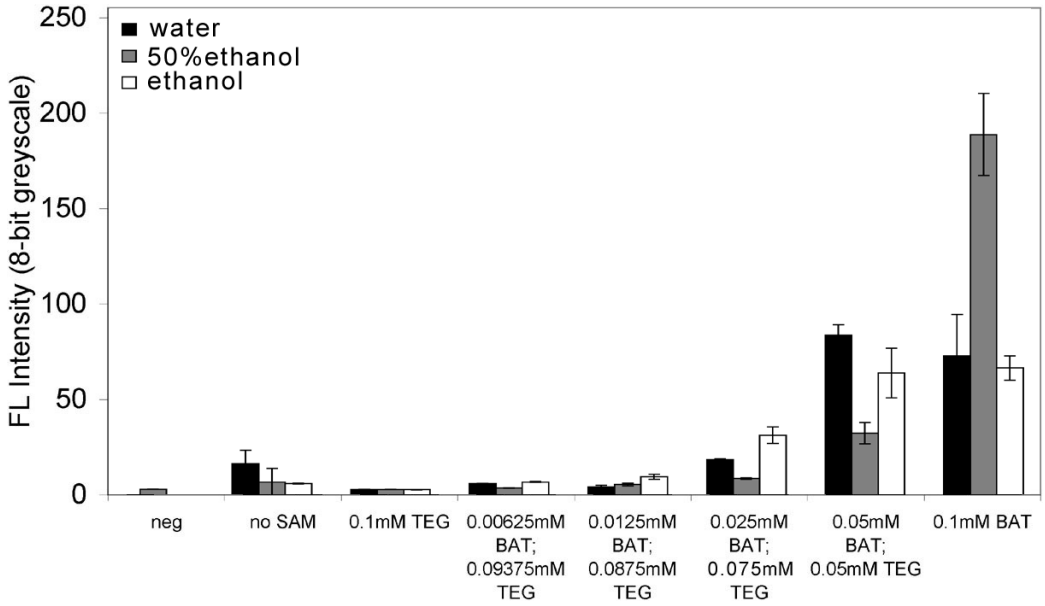


Figure 3.6 **Relative FL intensities for SAMs on Au.** Relative fluorescence intensities plotted in a bar graph displaying signal for Au samples incubated in Cy3-streptavidin under each thiol adsorption condition. Thiols were adsorbed for 1 hour prior to Cy3- streptavidin incubation. Each graph represents the average of 16 independent samples.

does not necessarily correlate with the thiol composition of the adsorbed SAM [50]. For a given mixed thiol composition, mixed monolayers adsorbed from water have more thiol molecules on Au than monolayers adsorbed from ethanol, as indicated by CV data; however, the number of BAT molecules adsorbed are comparable, as indicated by fluorescence measurement. From this, we deduce that the TEG composition of monolayers adsorbed from water is higher vs. monolayers adsorbed from ethanol. Formation of mixed SAMs from 50% ethanol is governed by the solubility of TEG and BAT in the solvent. PCD values for SAMs formed from 50% ethanol indicate intermediate monolayer coverage compared to water and ethanol conditions. Solubility of BAT 50% ethanol is assisted by the presence of TEG. We expect the surface ratio of BAT/TEG to be lower compared monolayers formed from ethanol,

since multiple TEG can coordinate around a single BAT. As the thiols approach the Au surface, there is a higher local concentration of TEG to BAT. This results in fewer BAT incorporated into the monolayer and lower levels of Cy3-protein adsorption. The decrease in protein binding by monolayers adsorbed from aqueous ethanol solution may be attributed in part to the observed solubility properties of the BAT and TEG reagents.

### 3.3.4 Electrocleaning to Recycle Au Substrates

We have explored the utility of using electrochemical methods for the directed or triggered release of alkylthiolate monolayers from Au in order to regenerate the Au surface for the subsequent and repeated formation of new alkylthiolate monolayers. We chose to focus on electrochemical methods of alkylthiolate monolayer desorption because of the control, speed, and amenability of the protocol to arrays of electrodes in microfluidic devices. Thermal desorption, displacement of short chain alkylthiolates by longer chain alkylthiolates, piranha solutions, and plasma oxidation are all applications that work well for cleaning bulk samples, but not for addressing single Au samples within a sensor array. Metal polishing and piranha solution are damaging to small metal features.

Electrochemical desorption of alkylthiolate monolayers, however, allows us to control individual electrodes, is compatible with PDMS-based microfluidics systems and has the added advantage of being rapid. The application of both reductive [34, 60, 61] and oxidative [36, 61] potentials for the desorption of alkylthiolate monolayers from Au have been reported.

Our attempts to reductively desorb alkylthiolate monolayers from Au (-1.0 V vs. Ag/AgCl) resulted in the desorption of alkylthiolate monolayers along with the delamination of the Au from the Si substrate, which is consistent with previous reports [55]. We tested the application of DC and AC anodic potentials (0.8 V to 1.4

V) at various time pulses (2–60 sec) to determine an optimized alkylthiolate monolayer removal protocol. AC anodic potentials were additionally tested at frequencies ranging from 10 Hz–10 kHz. CV measurements were taken to characterize the surface coverage of alkylthiolate monolayers on Au surfaces treated under the different cleaning protocols (data not shown). We found that the shortest, most effective DC cleaning protocol was a 30 second pulse at 1.4 V. The most effective AC treatment was an AC potential of 1.2 V with an amplitude of 0.2 V at a frequency of 1 kHz for 30 seconds.

We next investigated whether the chip Au substrates could withstand multiple alkylthiolate monolayer formation-and-desorption cycles. Using both CV and fluorescence microscopy, Au substrates were characterized throughout the process, which included the following steps (Figure 3.7): 1) Au surface electrocleaning (anodic sweep

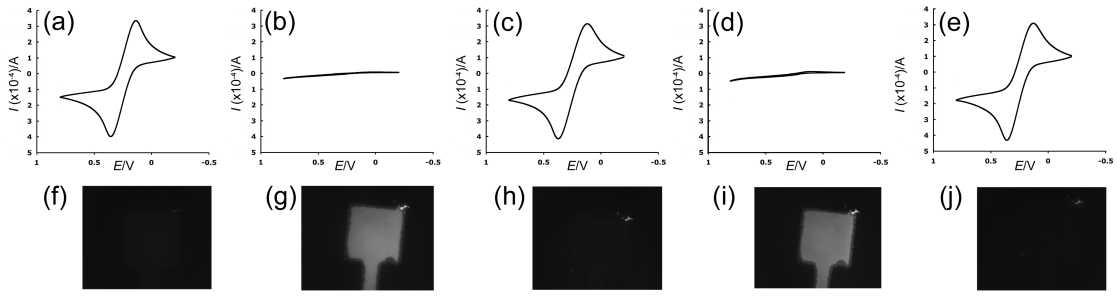


Figure 3.7 **CV traces and corresponding fluorescence microscopy images for Au electrode as it undergoes recycling treatments.** Two cycles are shown. a), f) Bare Au electrode b), g) After 1 h of BAT:TEG (1:4) SAM formation c), h) After 30 sec DC pulse at 1.4 V (vs. Ag/AgCl, saturated KCl) d), i) After second BAT:TEG (1:4) SAM formation e) After 30 s DC pulse at 1.4 V (vs. Ag/AgCl, saturated KCl)

to 1.2 V); 2) formation of BAT:TEG monolayer (1:4 thiol ratio; 0.1 mM in water for 60 minutes, RT), 3) adsorption of Cy3-strp (30 min, RT), and 4) repeat cycle. For a given chip, CV traces for the pre-cleaned electrode overlap very well with the CV traces for the chip after oxidative desorption of the alkylthiolate monolayer. Traces for the BAT:TEG monolayer yield very low current, indicating quality monolayer

formation. Fluorescent images of the pre-cleaned Au (Figure 3.7c) and post-SAM cleaned Au (Figure 3.7e and 3.7g) yielded background fluorescence intensities. The biotinylated SAMs bound Cy3-strp, yielding FL images of Au pads with positive signal. The electrocleaning protocols could be repeated at least ten times without any noticeable blemishes to the Au substrates.

We demonstrate the ability to repeatedly form and remove alkylthiolate monolayers on Au surfaces using a method that is compatible with a packaged microfluidics device. The accelerated formation of BAT and TEG alkylthiolate monolayers from water results in low-defect monolayers. These functionalized substrates have potential applications in biosensor devices and for metal substrate passivation [62]. Additionally, the ability to electrochemically remove alkylthiolates monolayers from the Au surface permits us to recycle our devices at least 10 times, allowing capture as well as release of cells or proteins bound via specific monolayers. A complete cycle of Au substrate cleaning, alkylthiolate monolayer formation and alkylthiolate monolayer removal requires 30 minutes, which will likely be important for making fluidic-based chips for assaying multiple analytes. This reduction in monolayer formation and cleaning times speeds up the process of creating recyclable biological sensors for lab-on-a-chip experiments.

# Acknowledgements

This research was funded under DARPA grant MLR.00018-3-AFOSR.000019 and RDL.NASA.000143. C.A.C. thanks Blake Axelrod, Jessica Arlett, and Melaku Muluneh for their assistance in materials fabrication; and John Keith and Brad Cenko for helpful discussions.

# Bibliography

[1] M. Mrksich, *Chem. Soc. Rev.* **29**, 267 (2000).

[2] C. Bain, et al., *J. Am. Chem. Soc.* **111**(1), 321 (1989).

[3] C. Bain, J. Evall, G. Whitesides, *J. Am. Chem. Soc.* **111**, 7155 (1989).

[4] C. Bain, G. Whitesides, *J. Am. Chem. Soc.* **111**, 7164 (1989).

[5] C. Golander, et al., in J. Harris (ed.), *Poly(ethylene glycol) chemistry, biotechnical and biomedical applications*, pp. 221–245. Plenum Press, New York (1992).

[6] J. Harris, *Poly(ethylene glycol) chemistry, biotechnical and biomedical applications*. Plenum Press, New York (1992).

[7] M. Mrksich, L. Dike, J. Tien, D. Ingber, G. Whitesides, *Experiment. Cell Research* **235**, 305 (1997).

[8] C. Hodneland, M. Mrksich, *Langmuir* **13**(23), 6001 (1997).

[9] M. Yousaf, M. Mrksich, *J. Am. Chem. Soc.* **121**, 4286 (1999).

[10] C. Hodneland, M. Mrksich, *J. Am. Chem. Soc.* **122**, 4235 (2000).

[11] K. Kukanskis, et al., *Anal. Biochemistry* **274**(1), 7 (1999).

[12] J. Schumaker-Parry, M. Zareie, R. Aebersold, C. Campbell, *Anal. Chem.* **76**, 918 (2004).

[13] M. Riepl, K. Enander, B. Liedberg, *Langmuir* **18**(18), 7016 (2002).

[14] A. Zybin, et al., *Anal. Chem.* **77**(8), 2393 (2005).

[15] G. Zhen, et al., *Langmuir* **20**, 10464 (2004).

[16] A. Arakaki, et al., *Biotechnology and Bioengineering* **88**(4), 543 (2004).

[17] R. DeBono, G. Loucks, D. Manna, U. Krull, *Can. J. Chem.* **74**, 677 (1996).

[18] C. Widrig, C. Chung, M. Porter, *J. Electroanal. Chem* **310**(1–2), 335 (1991).

[19] M. Hasan, D. Bethell, M. Brust, *Journal of the American Chemical Society* **124**(7), 1132 (2002).

[20] G. Hahner, C. Woll, M. Buck, M. Grunze, *Langmuir* **9**, 1955 (1993).

[21] G. Poirier, E. Plyant, J. White, *J. Chem. Phys.* **104**, 7325 (1996).

[22] J. Love, L. Estroff, J. Kriebel, R. Nuzzo, G. Whitesides, *Chem. Rev.* **105**, 1103 (2005).

[23] J. Lee, C. Park, G. Whitesides, *Anal. Chem.* **75**, 6544 (2003).

[24] D. Yan, J. Jordan, V. Burapatana, G. Jennings, *Langmuir* **19**, 3357 (2003).

[25] G. Yang, N. Amro, Z. Starkewolfe, G.-Y. Lui, *Langmuir* **20**, 3995 (2004).

[26] U. Sur, V. Lakshminarayanan, *J. Electroanal. Chem* **565**, 343 (2004).

[27] Z. Yang, et al., *Biosensors and Bioelectronics* **10**(9-10), 789 (1995).

[28] R. Nuzzo, L. Dubois, D. Allara, *JACS* **112**, 558 (1990).

[29] K. Peterlinz, R. Georgiadis, *Langmuir* **12**, 4731 (1996).

[30] S. Xu, et al., *J. Chem. Phys.* **108**, 5002 (1998).

[31] C. Zhong, J. Zak, M. Porter, *J. Electroanal. Chem* **421**, 9 (1997).

[32] T. Kakiuchi, H. Usui, D. Hobara, M. Yamamoto, *Langmuir* **18**, 5231 (2002).

[33] D. Yang, C. Wilde, M. Morin, *Langmuir* **12**, 6570 (1996).

[34] X. Jiang, R. Ferrigno, M. Mrksich, G. Whitesides, *J. Am. Chem. Soc.* **125**, 2366 (2003).

[35] J. Shepherd, et al., *JACS* **126**, 8329 (2004).

[36] F. Loglio, M. Schweizer, D. Kolb, *Langmuir* **19**, 830 (2003).

[37] P. Harder, M. Grunze, R. Dahint, G. M. Whitesides, P. E. Laibinis, *J. Phys. Chem. B* **102**(2), 426 (1998).

[38] R. Valiokas, S. Svedhem, S. Svensson, B. Liedberg, *Langmuir* **15**(10), 3390 (1999).

[39] N. Alcantar, E. Aydil, J. Israelachvili, *Journal of Biomedical Materials Research Part B: Applied Biomaterials* **51**(3), 343 (2000).

[40] Y. Chan, R. Schweiss, C. Werner, M. Grunze, *Langmuir* **19**(18), 7380 (2003).

[41] R. Wang, H. Kreuzer, M. Grunze, A. Pertsin, *Physical Chemistry Chemical Physics* **2**(8), 1721 (2000).

[42] K. Feldman, G. Hahner, N. Spencer, P. Harder, M. Grunze, *Journal of the American Chemical Society* **121**(43), 10134 (1999).

[43] D. Schwartz, *Annu. Rev. Phys. Chem.* **52**, 107 (2001).

[44] S. Herrwerth, W. Eck, S. Reinhardt, M. Grunze, *Journal of the American Chemical Society* **125**(31), 9359 (2003).

[45] S. Herrwerth, et al., *Langmuir* **19**(5), 1880 (2003).

[46] A. Pertsin, M. Grunze, I. Garbuzova, *J. Phys. Chem. B* **102**(25), 4918 (1998).

[47] C. Canaria, J. Smith, C. Yu, S. Fraser, R. Lansford, *Tetrahedron Lett.* **46**(28), 4813 (2005).

[48] M. D. Porter, T. Bright, D. Allara, C. Chidsey, *J. Am. Chem. Soc.* **109**, 3559 (1987).

[49] C. Pale-Grosdemange, E. Simon, K. Prime, G. Whitesides, *J. Am. Chem. Soc.* **113**(1), 12 (1991).

[50] K. Nelson, et al., *Langmuir* **17**, 2807 (2001).

[51] W. Knoll, F. Schmitt, C. Klein, *International Patent Application WO 92/10757*, Boehringer Mannheim BmbH, BRD.

[52] G. Hermanson, in *Bioconjugate Techniques*, pp. 169–181. Academic Press, Inc., San Diego (1996).

[53] M. Amrein, D. Muller, *Nanobiology* **4**, 229 (1999).

[54] F. Schreiber, *Progress in Surface Science* **65**, 151 (2000).

[55] C. Hodneland, *The Design of Methods for Controlling the Interactions of Proteins and Cells with Surfaces*, doctoral thesis, University of Chicago (2001).

[56] T. Ishida, et al., *Langmuir* **17**(24), 7459 (2001).

[57] T. Schneider, D. Buttry, *J. Am. Chem. Soc.* **115**, 12391 (1993).

[58] R. Yamada, H. Sakai, K. Uosaki, *Chem. Lett.* **7**, 667 (1999).

[59] D. Hatchett, R. Uibel, K. Stevenson, J. Harris, H. White, *J. Am. Chem. Soc.* **120**(5), 1062 (1998).

[60] M. Walczak, et al., *Langmuir* **7**, 2687 (1991).

[61] D. Yang, H. Al-Maznai, M. Morin, *J. Phys. Chem. B* **101**, 1158 (1997).

[62] C. Whelan, M. Kinsella, H. Ho, K. Maex, *J. Electronic Materials* **33**(9), 1005 (2004).

# Chapter 4

# Oligonucleotide-Mediated Capture and Release of Biological Targets

Here, we move beyond the biotin-streptavidin motif and focus on utilizing Watson-Crick based pairing to create substrates which bind and release biological targets. I manufacture short single strand- (ss-) oligonucleotides (oligos) with a $3'$ alkyldisulfide modification to generate oligo-presenting SAMs. Briefly, I have designed the synthesis as a modification of coarse porous glass (CPG) with terminal dimethoxy trityl (DMT) alkyldisulfide groups. Phosphoramidite oligo synthesis with my customized CPG yields oligos with a $3'$ dodecylthiol modification. Fluorescently labeled complement strands combined with fluorescence microscopy allow me to track oligo-mediated binding events. The oligo sequence is also designed with an internal *Bam*HI binding site. Utilizing restriction enzymes, I show the specific release of bound targets from oligo SAMs.

## 4.1 Background

DNA arrays were born from the Southern blotting techniques developed by E. M. Southern et al. [1]. In these assays, DNA is immobilized from a gel onto a nitrocellulose membrane substrate and visualized using labeled complement strands (fluorophore, radioisotope, redox active species). Since then, arrays of DNA have been

developed as high-throughput screening tools to perform single nucleotide polymorphism (SNP) genotyping [2], profile cell gene expression [3], and study protein-DNA interactions [4].

This chapter focuses on characterization of chemisorbed alkylthiol-modified oligos on Au surfaces. Researchers in the lab utilize a variety of methods for oligo attachment including the following: hexylthiol-modified oligos adsorbed directly onto gold [5–7], biotinylated oligo onto streptavidin-coated surfaces [8–10], covalent attachment of amine-modified oligos to aldehyde-terminated surfaces [11], and attachment of thiol-modified oligos to maleimide-terminated surfaces [12]. The alkylthiol-modified oligos are only available commercially in propyl- and hexyl-modifications. From previous research, we know that SAMs made with these shorter $n$-alkylthiol chains are less stable and prone to substitution by longer chains ($n \geq 11$) [13–15]. In response, I have synthesized dodecyl-modified oligos for adsorption directly onto Au substrates. In addition, these dodecylthiol-modified oligos are similar in alkylchain length to TEG. Mixed monolayers of dodecylthiol-modified oligos and TEG are therefore more stable and well formed. Target binding of fluorescent oligos is detected by fluorescence microscopy.

In principle, DNA array platforms are designed with short oligomers physically constrained on a solid substrate. Arranging oligo sequences densely on the substrate allows for high-throughput arrays. Chemical methods for attaching amino-, acrydite-, and thiol-modified oligos onto silicate and other substrates have been documented [16]. A number of biotechnology companies have embraced and applied these methods. Affmetrix (Santa Clara, CA), one of the first commercial DNA array companies, uses technology in which oligonucleotides are sythesized directly on the silicon chip. A surface is coated with photo-removable protecting groups. Photolithography techniques are used to deprotect the substrate in an array pattern, and oligonucleotides are built up serially [17]. Another company Illumina (San Diego, CA)

synthesizes full sequence oligos, then covalently binds them to silica beads. Subsequently, the beads are arranged onto a silicon chips in a high-density array. Nanogen utilizes a gel polymer array and infuses oligos into the gel [18–20]. A positive potential is applied to the array and accelerates hybridization of the negatively charged complement strand, similar to electrophoresis. This increases sensitivity of the array, as diffusion limited transport of oligos to the array is overcome by electrostatic forces. Clinical Micro Sensors (Pasadena, CA) built an array of Au electrodes, each with thiol-modified oligo. Ferrocene-modified complement strand hybridization is detected as redox activity with electrochemical techniques. Alkylthiol modified oligos were adsorbed onto Au electrodes. Affymetrix, Illumina, and Nanogen detect hybridization events with fluorophore-tagged complement strand.

While tagged oligos are the natural target for capture on DNA arrays, proteins and cell arrays may be built theoretically upon DNA arrays [21, 22]. Antibodies are easily modified with oligos by either covalent attachment [23, 24] or biotin-streptavidin interactions. Once a layer of cell-specific antibodies is bound, cells may be panned out of solution onto the 2-D array. In addition, once oligos are hybridized onto an array, they may be further modified and manipulated by enzymes such as Klenow [4], T4 DNA ligase [7], and restriction enzymes [4, 7]. In this chapter, I show capture of biological targets, modeled as polyvalent beads utilizing Watson-Crick base pairing interactions, and enzymatic release of targets.

## 4.2 Materials and Methods

### 4.2.1 Reagents

Gold substrates were prepared as previously described. Phosphate buffered saline (PBS) was prepared as 0.139 M NaCl, 2.68 mM KCl, 8.1 mM $Na_2HPO_4$, and 1.1 mM $K_2HPO_4$ (Mallinckrodt) in Nanopure water. Oligos modified by Cy3, biotin, and

thiol at the 3′ end were purchased from Integrated DNA Technologies (IDT) with the following sequence: 5′ > CAC CAG CGC TAA GGA TCC ACC GGT CG < 3′.

Polystyrene beads (250 nm, Cy3-labeled, streptavidin modified) were purchased from Sigma. Tg30 antibody against human embryonic stem (hES) cells and hES cells were both provided by Shelley Hough and Dr. Martin Pera. 4 (4-N-maleimidophenyl) butyric acid hydrazide (MPBH) was purchased from Pierce. Desalting columns (3000 MW and 50,000 MW cut-off) were purchased from Centricon.

### 4.2.2 Oligo Labeling Antibody

Briefly, antibody Fc carbohydrates are oxidized to aldehydes/ketones, and thiol-modified oligos are activated with MPBH. Primed antibody and oligos are subsequently conjugated together.

A stock solution of NaOAc buffer (0.1 M, pH 5.5) is prepared in DI water. Fresh batches of $NaIO_4$ (4.3 mg in 1 ml NaOAc buffer) and MPBH (0.6 mg in 43 $\mu$l DMSO, 40 mM) are made for each reaction. Desalting columns are equilibrated by spinning twice with 100 $\mu$l PBS at 13,000 g. Oligo is diluted to give 30 nmol in 150 $\mu$l PBS. To the oligo was added 7.5 $\mu$l (300 nmol) MBPH. This reaction was allowed to proceed for 2 hours at room temperature. During this time, 3 nmol antibody was diluted to 150 $\mu$l (4 mg $ml^{-1}$). To the antibody was added 150 $\mu$l $NaIO_4$, and this reaction was allowed to proceed 30 minutes on ice, in the dark. Activated oligo was purified and collected by a 3,000 MW column, and oxidized antibody was purified and collected by a 50,000 MW column. Antibody and oligo were quantified by NanoDrop UV-VIS spectrometer. Oligo and antibody were added together in a 5:1 molar ratio and incubated for 2 hours at room temperature. Unreacted oligo was washed away and labeled antibody was recovered using a 50,000 MW column.

### 4.2.3 Oligo Hybridization and Cleavage

Total alkylthiol concentrations of TEG and oligo-alkylthiol (**10**) solutions were prepped in PBS in the range of 40–400 $\mu$M. At these low concentrations, SAM adsorption was allowed to proceed overnight. Complement strands (purchased from IDT) were hybridized at 500 nM for 30–120 minutes against the oligo-modified SAM. Samples were washed in PBS prior to imaging. Where applied, Cy3-streptavidin was prepared as 200 nM in PBS and incubated for 30 minutes.

For enzymatic cleavage experiments, *Bam*HI was used in Roche Buffer B. DNAse I was used in a $Mg^{2+}$ buffer (40 mM Tris-HCl, 10 mM NaCl, 1 mM $CaCl_2$, 6 mM $MgCl_2$, pH 7.9) or a $Mn^{2+}$ buffer (40 mM Tris-HCl, 10 mM NaCl, 1 mM $CaCl_2$, 1 mM $MnCl_2$, pH 7.9)

## 4.3 Synthesis of Dimethoxy Trityl-Modified Coarse Porous Glass

Controlled porous glass (CPG) is the standard solid substrate utilized in automated phosphoramidite sythesis of oligos. Alkylthiol modified oligos are only available commercially in either propyl or hexyl forms, neither of which can be effectively utilized with my current set of dodecylthiol molecules BAT and TEG. Thus, I set out to synthesize my own dimethoxytrityl-(DMT)-modified CPG to generate oligos with a 3' disulfide modification. This asymmetric disulfide is comprised of the oligo and a propanol group. We expect that the propyl group will be quickly displaced by long-chain reagent TEG during SAM formation, and thus calculate the oligo reagent sulfur contribution as a thiolate. The synthesis scheme is given in Figure 4.1.

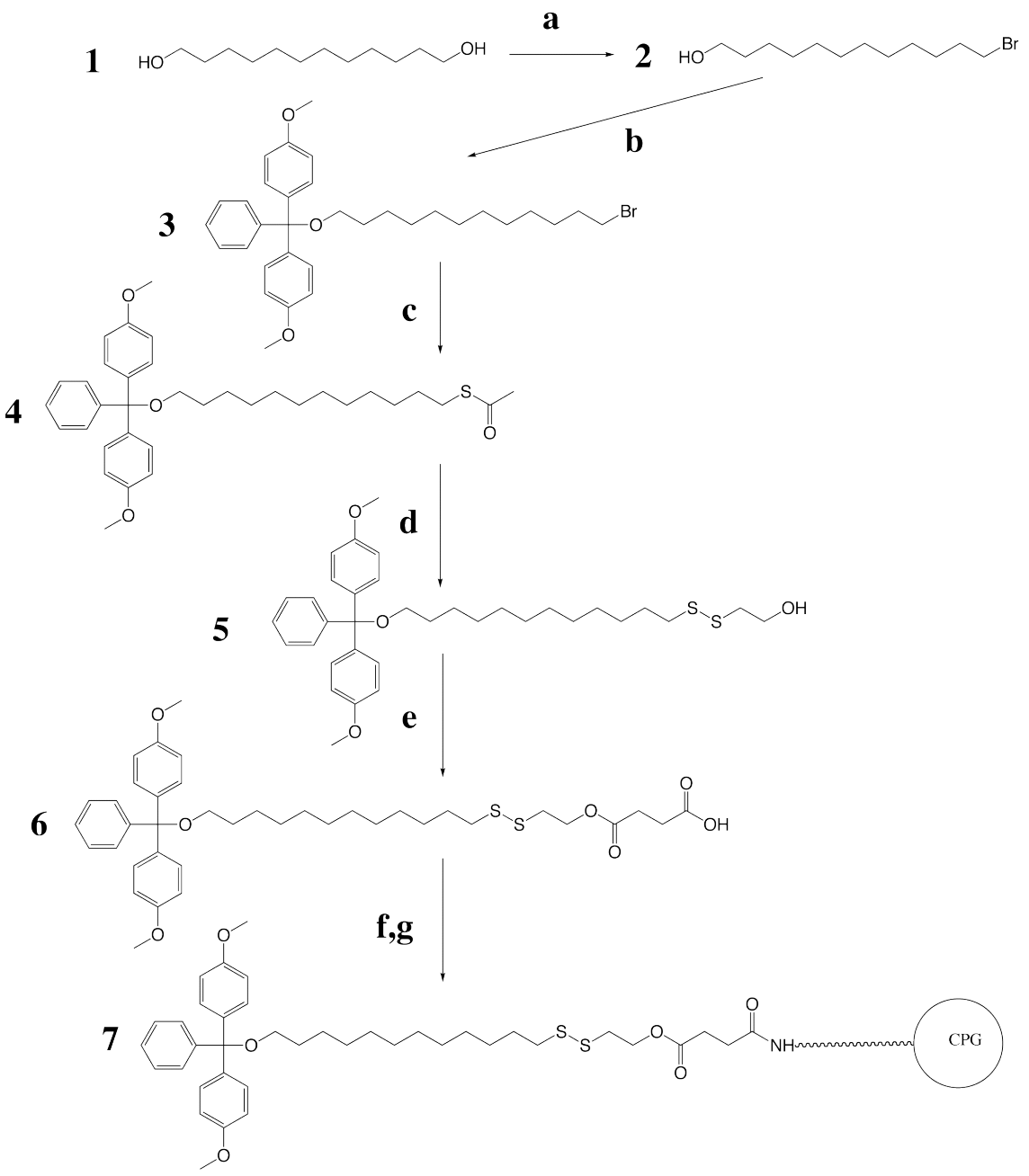


Figure 4.1 **Synthesis scheme of DMT-modified CPG.** a) HBr, cyclohexane. Reflux for 6 hrs, argon. b) DMT-Cl, TEA, $CH_2Cl_2$. Stir overnight at RT. c) $C_2H_3OSK$, DMF. Stir overnight at RT. d) Mercaptoethanol, NaOH, ACN. Stir in air overnight at RT. e) succinic anhydride, pyridine. Stir overnight at RT in air. f) BOP, DIPEA in $CH_2Cl_2$, amino-modified coarse porous glass. Swirl for 2 hrs at RT. g) Quench unreacted amine. TEA, acetic anhydride. Swirl 30 min.

### 4.3.1 Synthetic Methods

**2. 12-bromododecan-1-ol**

To a round bottom flask of 10.2 g (50.4 mmol) 1,12 dodecanediol (**1**) in 150 ml of cyclohexane was added 150 ml HBr (48%) and stirred under reflux for 6 hours. The mixture was extracted three times wtih hexane (50 ml), washed with saturated $NaHCO_3$, then washed with brine, and dried with $Na_2SO_4$. The solution was then concentrated to a yellow oil which was loaded onto a silica gel in hexane. The column was run with hexane:ethyl acetate (90:10 to 80:20). The product fraction was collected and concentrated to give white crystals. Yield 8.65 g (32.6 mmol); 64.7% yield. TLC Rf=0.33; 60% hexane: 40% ethyl acetate. $^1$H-NMR (DMSO-$d_6$, 300 MHz): $\delta$1.22-1.37 (m, 18H), $\delta$1.73 (q, 2H), $\delta$3.45 (t, 2H), $\delta$3.49 (t, 2H), $\delta$4.09 (bs, 1H). Mass spec. m/z $[M+H]^+$: 265.2

**3. 4,4'-((12-bromododecyloxy)(phenyl)methylene)bis(methoxybenzene)**

To 1.1 g (4.15 mmol) of **2** in a round bottom flask was added 15 ml chloroform solvent, 14.05 g (41 mmol) DMT-Cl, and 0.87 ml (6.26 mmol) triethylamine. The mixture was stirred overnight at room temperature, then extracted with hexane two times. The organic fraction was then washed with $NaHCO_3$ and brine, then dried with $Na_2SO_4$, and concentrated to give a dark brown oil which was loaded onto a silica column in hexane. The column was run with hexane:ethyl acetate (90:10 to 80:20). The product fraction was collected and concentrated to give white crystals in high yield. TLC Rf=0.7; 6 hexane: 1 ethyl acetate. $^1$H-NMR (DMSO-$d_6$, 300 MHz): $\delta$1.19 (m, 16H), $\delta$1.51 (q, 2H), $\delta$1.75 (q, 2H), $\delta$2.91 (t, 2H), $\delta$3.49 (t, 2H), $\delta$3.7 (s, 6H), $\delta$6.8-7.3 (m, 13H)

**4. S-12-(bis(4-methoxyphenyl)(phenyl)methoxy)dodecyl ethanethioate**

To 4.71 g (8.47 mmol) **3** in a round bottom flask was added 50 ml DMF and 2.9 g (25 mmol) potassium thioacetate to give a brown solution. The reaction was stirred overnight at room temperature and took on a black color. The organic phase was extracted out of DMF by adding ethyl acetate and water, then it was washed with brine, dried with $Na_2SO_4$, and concentrated to give a dark oil which was loaded onto a silica gel in hexane. The column was run with hexane:ethyl acetate (95:5 to 85:15). The product fraction was collected and concentrated to give a brown oil. Yield 4.03 g (7.17 mmol); 85% yield. $^1$H-NMR (DMSO-$d_6$, 300 MHz): $\delta$1.19 (m, 16H), $\delta$1.48 (m, 4H), $\delta$2.28 (s, 3H), $\delta$2.79 (t, 2H), $\delta$2.92 (t, 2H), $\delta$3.7 (s, 6H), $\delta$6.8-7.3 (m, 13H). Mass spec. m/z $[M+Na]^+$: 585.4

**5. 2-((12-(bis(4-methoxyphenyl)(phenyl)methoxy)dodecyl)disulfanyl)ethanol**

In a round bottom flask, 0.89 g (1.58 mmol) of **4** was dissolved completely with ACN (40 ml) and 2.2 ml (32 mmol) mercaptoethanol and stirred very well. To this mixture was added 0.7 g (5.07 mmol) $K_2CO_3$ and stirred overnight. The reaction was concentrated to an oil and redissolved in $CH_2Cl_2$. This organic phase was washed with brine, dried with $Na_2SO_4$, and concentrated to give a pale pink oil which was loaded onto a silica column in hexane. The column was run with hexane:ethyl acetate (90:10 to 80:20). $^1$H-NMR (DMSO-$d_6$, 300 MHz): $\delta$1.19 (m, 16H), $\delta$1.53 (m, 4H), $\delta$2.67 (t, 2H), $\delta$2.74 (t, 2H), $\delta$2.91 (t, 2H), $\delta$3.6 (q, 2H), $\delta$3.71 (s, 6H), $\delta$4.89 (t, 1H) $\delta$6.8-7.3 (m, 13H). Mass spec. m/z $[M+Na]^+$: 619.4

**6. 4-(2-((12-(bis(4-methoxyphenyl)(phenyl)methoxy)dodecyl)disulfanyl)-ethoxy)-4-oxobutanoic acid**

To a 10 ml round-bottom flask was added 0.47g (.0788 mmol) **5** dissolved in pyridine (5 ml) with 0.157 g (1.57 mol) succinic anhydride and a catalytic amount of 0.19 g

(1.57 mmol) DMAP. The reaction was stirred overnight in air. The pyridine was co-evaporated with toluene three times to give a white power. This solid was redissolved in $CH_2Cl_2$ (10 ml), washed twice with ice cold citric acid and water, then dried with $Na_2SO_4$. The product was concentrated to give a white powder and loaded onto a silicon column in hexane. The column was run with hexane:ethyl acetate (90:10 to 80:20). The product fraction was collected and concentrated to give a white powder. $^1$H-NMR (DMSO-$d_6$, 300 MHz): $\delta$1.19 (m, 16H), $\delta$1.58 (m, 4H), $\delta$2.43 (s, 2H), $\delta$2.54 (t, 2H), $\delta$2.68 (t, 2H), $\delta$2.89 (t, 2H), $\delta$2.9 (t, 2H), $\delta$3.71 (s, 6H), $\delta$4.2 (t, 2H), $\delta$6.8-7.3 (m, 13H). Mass spec. m/z $[M+Na]^+$: 695.5

### 7. 3-((16-(bis(4-methoxyphenyl)(phenyl)methoxy)hexadecyl)disulfanyl)propyl 4-(CPG-amino)-4-oxobutanoate

To 0.03 g (43 $\mu$mol) of **6** was added $CH_2Cl_2$ (5 ml) with 1 g of amino-modified coarse porous glass (Sigma, 130 $\mu$mol $g^{-1}$ capacity) and swirled gently by hand. With gentle swirling, 0.02 g (43 $\mu$mol) BOP was added first, followed by 0.02 ml (129 $\mu$mol) DIPEA. The reaction was swirled gently on an elliptical rotator for 2 hours. The CPG was then collected by vacuum filtration and soaked in $CH_2Cl_2$. To quench unreacted amines, to this slurry was added TEA (0.2 ml) and acetic anhydride (0.2 ml), and it was gently swirled for another 30 minutes. The slurry was collected again by vacuum filtration and washed with methanol three times. DMT loading on CPG was quantitated by adding $\mu$l of trichloroacetic acid to 2 mg of **7**. The solvent turns orange once DMT deprotection is achieved and is quantified by UV-Vis spectrometry. Quantitation reveals 1 $\mu$mol DMT per 25 mg CPG.

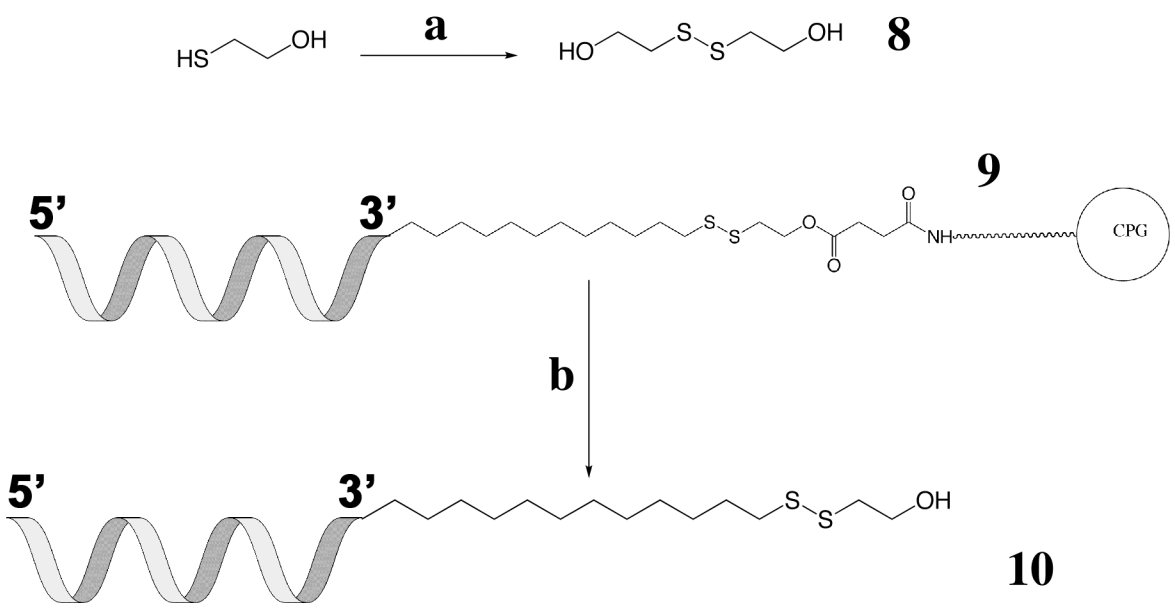


Figure 4.2 **Synthesis scheme of oligo-modified alkylthiols.** a) Mercaptoethanol, ethanol, excess ammonia. Stirred overnight at RT. b) CPG-bound oligo (**9**), $NH_4OH$, **8**. Incubated overnight at 65 °C, then HPLC purified.

## 4.4 Synthesis of Oligo-Modified Disulfide

**8. 2,2'-disulfanediyldiethanol**

To 2 ml (28 mmol) of 2-mercaptoethanol was added methanol (20 ml) and 8.4 ml (84 mmol) trichloronitromethane. The solution was allowed to stir at room temperature overnight. The mixture was then then co-evaporated under reduced pressure and product **8** was collected as a yellow oil. $^1$H-NMR ($CDCl_3$, 300 MHz): $\delta$1.38 (t, 1H), $\delta$3.72 (t, 2H), $\delta$3.91 (t, 2H)

**9. Oligo-modified CPG**

25 mg of **7** was poured into a column and loaded onto a AB 3400 DNA Synthesizer. A 27-mer sequence was synthesized with the final DMT-off and kept the oligo on the column. The *Bam*HI strand is synthesized as follows: 5′ > CGA CCG CT**G GAT CC**T TAG CGC TGG TGT < 3′

**10. 2-((12-oligododecyl)disulfanyl)ethanol**

The column with **9** is removed from the DNA synthesizer and residual solvents are removed by lyophilizer. The CPG is transferred to an eppendorf tube to which is added 900 $\mu$l $NH_4OH$ and 30 $\mu$l **8**. The tube is clamped shut and allowed to incubate at 65 °C overnight. The mixture is filtered to collect the supernatant and lyophilized to dryness to yield crude oligo. The crude is resuspended in 600 $\mu$l of 50 mM $NH_4OAc$ and filtered by HPLC fraction collection. The product fraction **10** is lyophilized and resuspended in PBS. Mass spec. m/z: 8046

## 4.5 Results and Discussion

### 4.5.1 Titrating Oligo Hybridization on Au Substrates

Various mixed-component alkylthiol solutions were prepared in PBS. Aqueous buffer is chosen over ethanol solvent due to DNA precipitation in alcohol. Au samples were immersed in oligo-alkylthiols and TEG concentrations ranging from 100% DNA to 0.1% DNA in TEG. The SAM-coated substrates were assessed by hybridizing them with Cy3-labeled complement strands. Control samples were prepped without SAMs; with a TEG sam; and as a negative control, without exposure to Cy3-oligo (Figure 4.3). On an 8-bit relative fluorescence scale, we measured very low background levels: negative control = 1.9, no SAM control = 3.7 $\pm$0.3, TEG control = 2.4 $\pm$0.2 (n=16). All concentration levels of oligo-alkylthiol tested yielded fluorescence intensities above background. Samples incubated with 10% oligo bound the highest levels of Cy3-labeled complement. Decreased oligo-alkylthiol composition (0.1% and 1%) in the SAM yields lower complement binding, but lower intensities were also observed on samples with higher oligo-alkylthiol content (25%–100%).

SPR studies reported by Peterson et al. show that both hybridization kinetics and

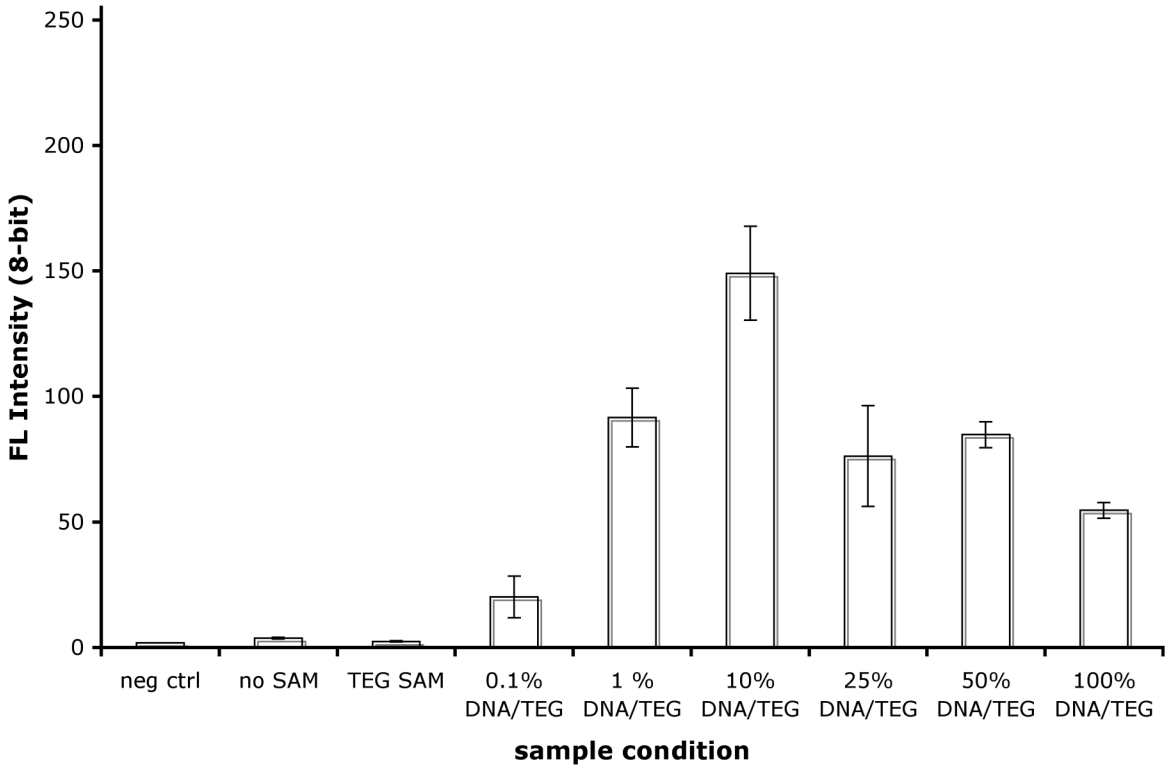


Figure 4.3 **FL intensities for Cy3-oligo SAMs on Au.** Mixed ss-oligo/TEG SAMs on Au bind Cy3-labeled complement strands. Total thiol concentrations for SAM adsorption are 400 $\mu$M in PBS. (Error bars represent standard deviation. n=16)

hybridization efficiencies are reduced for high levels of oligo-hexylthoils adsorbed to Au [25]. In their studies, they quantify oligo coverage by fitting SPR reflectance data to a multi-layer Fresnel model to extract DNA monolayer thickness and dielectric values. These parameters are then converted to DNA coverage (in molecules $\mathrm{cm}^{-2}$) [26, 27]. According to their calculations, maximum hybridization efficiency is reached at ss-oligo probe densities of $2.0 \times 10^{12}\,\mathrm{cm}^{-2}$.

We already demonstrated in Chapter 3 that mixed alkylthiol solution compositions do not literally translate into mixed SAM compositions. In the case of oligo-alkylthiols, molecule flexibility and conformation may play a role in both oligo incorporation into the SAM and complement hybridization. If we theorize a 5 Å spacing for high-density packed oligo-alkylthiols and a 20 Å diameter for double stranded-(ds)-oligos, that leaves very little room for 1:1 hybridization events. It is possible that a single Cy3-labeled complement strand might bind to two surface-bound oligos, leading to reduced hybridization capacity, or some surface-bound oligos simply remain inaccessible to complement strands due to molecular crowding. Based on our titration experiments, we chose to continue our studies under 1% and 0.1% DNA in TEG working conditions.

### 4.5.2 Temperature Effects and Enzyme Reactivity

Next, we explore enzymatic cleavage of the 1% ds-oligo SAMs. A *Bam*HI site (GGATCC) is located in the middle of the oligomer strand. Changes in fluorescence intensities for samples before and after 30 minute incubation in various temperatures and enzyme solutions is given in Table 4.1. The fluorescence is presented as a percentage drop after incubation.

From the table, samples treated with either plain buffer or *Eco*RI spiked buffer retained near-initial fluorescence intensity evels, *Eco*RI recognizes a different 6-bp

Table 4.1. Oligo-SAM fluorescence percentage after enzyme incubation

| Temperature | no enzyme | *Eco*RI | *Bam*HI |
|---|---|---|---|
| 21 °C | 91.9 | 93.7 | 53.5 |
| 37 °C | 98.8 | 95.9 | 67.7 |
| 40 °C | 95.4 | 89.0 | 61.8 |

binding site (GAATTC) and does not result in oligo cleavage. *Bam*HI, however, does result in ds-oligo cleavage. *Bam*HI is a robust enzyme, so it is not surprising that the cleavage is observed at the range of temperatures tested.

We track intensity levels for samples (10% oligo) incubated with 4 units of *Bam*HI over time (Figure 4.4) and observe greater signal losses for longer incubation times. However, failure to cleave 100% ds-oligos after 60 minutes of incubation is notable. Equivalent units of enzyme are capable of cleaving comparable amounts of oligo in solution (data not shown). Enzyme efficiency appears to be diminished at a 2-D substrate. In order to address steric hindrance as a source for diminished activity, SAMs generated from 0.1% oligo-alkylthiol solutions were incubated with *Bam*HI for 60 minutes. The resulting fluorescence intensities dropped to background levels, suggesting that all ds-oligos present were cleaved (Figure 4.5). Next, we tested the ability of *Bam*HI to cleave slightly larger targets: oligo-tethered proteins. Au substrates were treated with 0.1% oligo-alkylthiol in TEG, then hybridized with biotinylated complement strands, and subsequently with Cy3-labeled streptavidin. These fluorescent samples were incubated in enzyme and buffer and monitored for changes in flurescence (Figure 4.6). The changes in fluorescence were analyzed by unpaired t-test (Instat by GraphPad). Signal intensities for samples before and after buffer incubation were considered not significant (n=22). However, signal intensities for samples before and after *Bam*HI incubation were considered very significant (n=23).

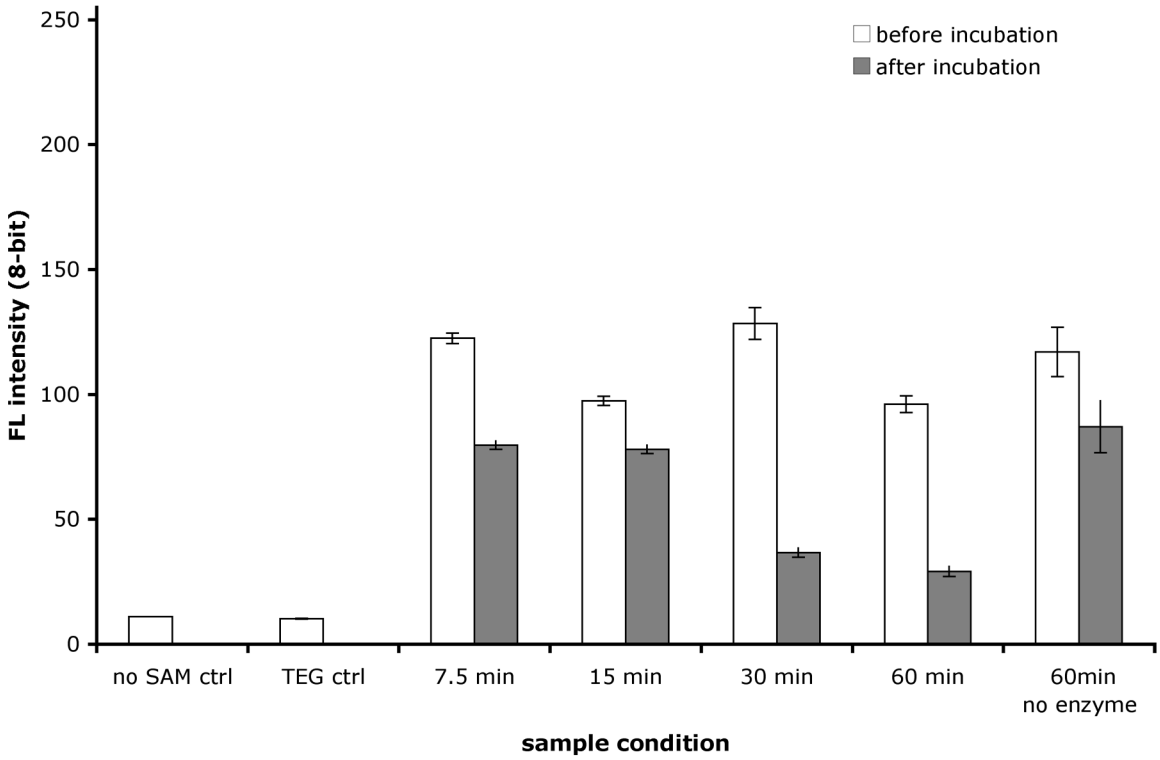


Figure 4.4 **Temporal tracking of ds-oligo cleavage by *Bam*HI.** Fluorescent intensities for oligo SAMs hybridized with Cy3-labeled complement strands. Measurements are taken and observed to drop over 60 minutes of incubation in 4U *Bam*HI at room temperature. (n=16)

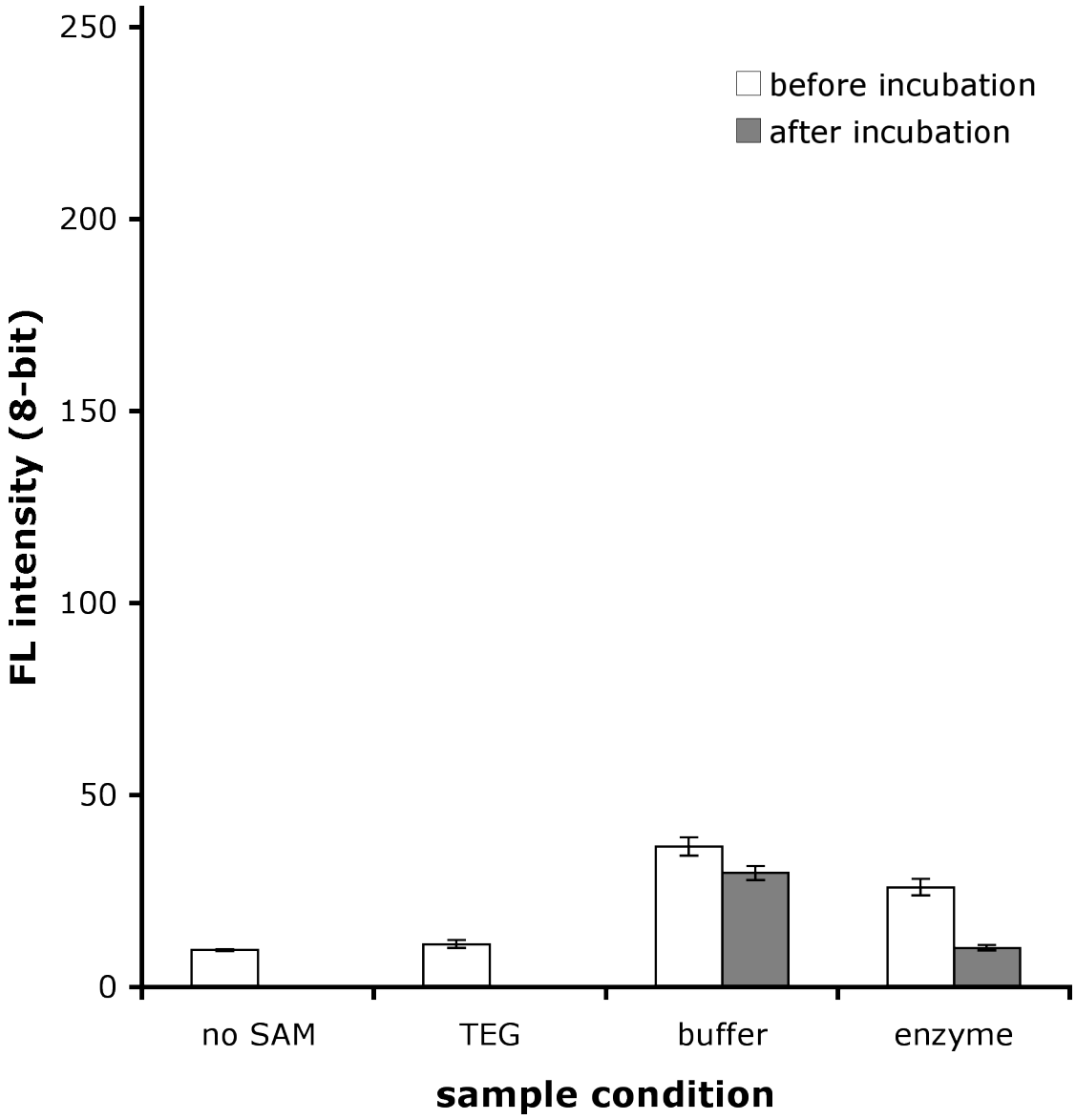


Figure 4.5 **Low density ds-oligo cleavage by *Bam*HI.** Fluorescent intensities for SAMs generated from 0.1% oligo-thiol in TEG hybridized with Cy3-labeled complement strands. Signal drops to background levels after 60 minutes of incubation in enzyme. Control samples in buffer retain fluorescence signal. (n=16)

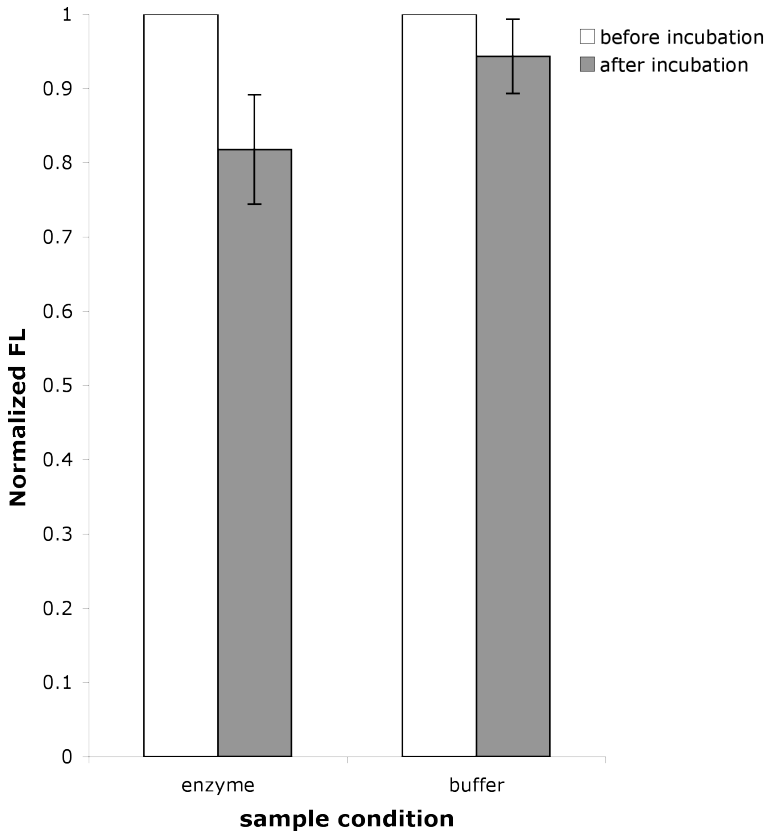


Figure 4.6 **Enzymatic cleavage of proteins from SAMs.** SAMs generated from 0.1% oligo-thiol in TEG hybridized with biotin-labeled complement strands bind Cy3-labeled streptavidin. Control samples in buffer retained fluorescence signal. Samples exposed to *Bam*HI lost partial fluorescence intensity. Drop in fluorescence intensity is normalized to initial intensity. (n=22)

The next trial was to bind polyvalent targets to SAMs. Oligo-modified SAMs were hybridized with biotin-modified complement strands, and then incubated with streptavidin-coated polystyrene beads. These beads bound specifically to SAM substrates. Samples were exposed to DNase I, an enzyme which cuts both ss- and ds-DNA. After 2 hours of enzyme incubation, some 23.7% of the beads were cleaved.

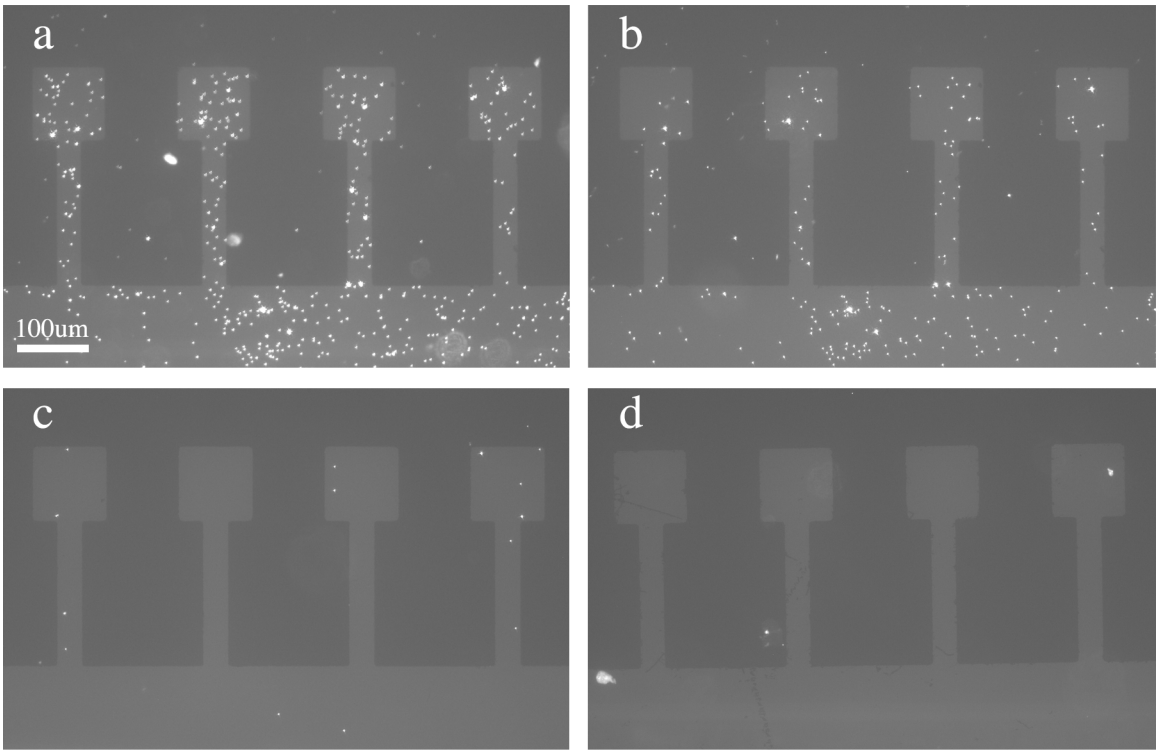


Figure 4.7 **Oligo-mediated adhesion of beads on Au.** Oligo-modifed SAMs are hybridized with 3′ biotin-modified complementary oligos. a) Streptavidin coated fluorescent beads are bound onto the biotin-modified ds-oligo SAM. b) After 2 hrs of incubation in DNAse I at 37 °C, 23.7% of the beads were cleaved and removed. c) TEG sample and d) no SAM sample do not bind beads.

Protein and molecule dimensions are considered as a source of steric hindrance. A double-stranded 26-mer oligo is approximately 88 Å in length, assuming a 3.4 Å rise per base pair. *Bam*HI protein associated to DNA spans 12 base pairs and is

approximately 66 Å× 44 Å× 41 Å (Figure 4.8) [28]. The *Bam*HI binding site is located in the middle of the 26-mer, leaving 5 bp (17 Å) space on the solvent side of the oligo monolayer and 10 bp (34 Å) space on the Au side of the oligo monolayer. A small molecule like Cy3 would produce negligible steric hindrance for a *Bam*HI enzyme as it diffuses to the oligo. Streptavidin, however, is approximately 100 Å in dimension [29], even larger than *Bam*HI. The polystyrene beads used in these experiments are 250 nm in diameter, an order of magnitude larger than these proteins. It is certainly conceivable that enzymes' diffusion to the interstitial space is may be low at these tight dimensions. The SAM surface is coated in TEG, but the polystyrene bead is not. *Bam*HI may desorb onto the bead before it can perform, or the ds-oligo might lie against the bead, restricting access to the enzyme. To address these issues, future experiments to vary the oligo length and a restriction enzyme site position will be designed.

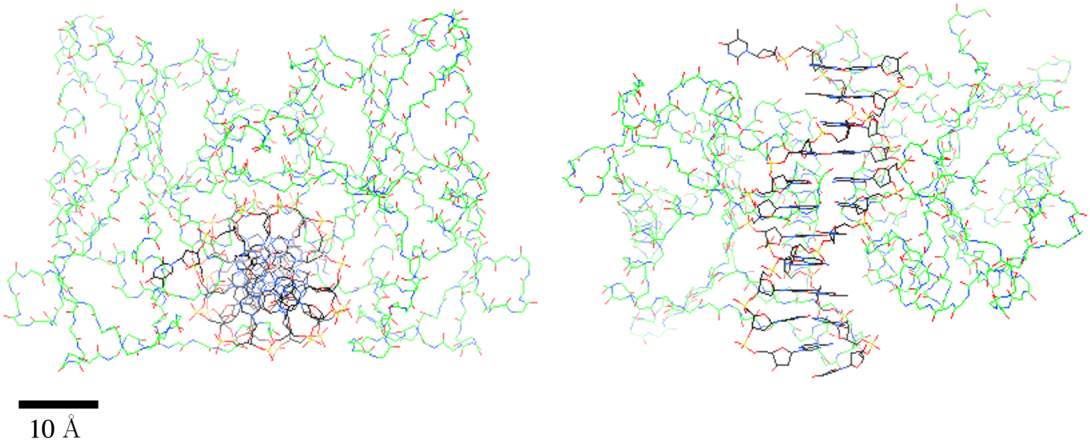


Figure 4.8 **Structure of *Bam*HI protein coordinate to DNA.** Protein structure of *Bam*HI based on X-ray crystallography [28]. The enzyme wraps around 12 base pairs when coordinated to the proper sequence GGA TCC. Structure is accurate to 2 Å.

## 4.6 Conclusions

In conclusion, we've demonstrated the ability to bind biological targets via oligo-mediated interactions. Small molecules, proteins, and beads bound with target oligo strands have all been specifically bound to DNA probes on SAM substrates. Oligo hybridization efficiency and surface density can be modified by varying the oligo-alkylthiol and TEG reagent solution compositions. Enzymatic cleavage of Cy3-labeled DNA was demonstrated to be specific by *Bam*HI. Cleavage of larger targets such as streptavidin and polystyrene beads was not easily accomplished. Based on our results, we believe that oligo hybridization events are affected by surface density and crowding. We hypothesize that enzymatic cleavage of proteins and beads is hindered by sterics. Chemical synapse gaps in the body are approximately 20–40 nm wide [30]. The maximum gap between streptavidin and SAM based on the ds-oligo length is 88 Å, an order of magnitude difference. Studies to increase enzyme-cuting events on these larger biotargets would include the addition of macromolecular exclusion agents such as poly(ethylene glycol) or BSA, extended enzyme incubation times, and variances in buffer ionic strength. I envision the next experiments to perform would be to generate SAMs with longer oligos (50 bp, 100 bp, 200 bp) and to modify the number and position of restriction enzyme sites.

# Bibliography

[1] U. Maskos, E. Southern, *Nucleic Acid Research* **20**, 1679 (1992).

[2] M. Margulies, et al., *Nature* **437**(7057), 376 (2005).

[3] S. Mocellin, et al., *Annals of Surgery* **241**(1), 16 (2005).

[4] M. Bulyk, E. Gentalen, D. Lockhart, G. Church, *Nature Biotech.* **17**, 573 (1999).

[5] T. Herne, M. Tarlov, *J. Am. Chem. Soc.* **119**, 8916 (1997).

[6] A. Csaki, M. R., W. Straube, J. Kohler, W. Fritzsche, *Nucleic Acid Research* **29**(16) (2001).

[7] J. Kim, et al., *Journal of Biotechnology* **96**, 213 (2002).

[8] G. Sasnauskas, S. Halford, V. Siksnys, *PNAS* **100**(11), 6410 (2003).

[9] J. Schumaker-Parry, M. Zareie, R. Aebersold, C. Campbell, *Anal. Chem.* **76**, 918 (2004).

[10] H. Tsubery, M. Mrksich, *Langmuir* **24**(10), 5433 (2008).

[11] D. Peelen, L. Smith, *Langmuir* **21**, 266 (2005).

[12] C. Lee, P. Nguyen, D. Grainger, L. Gamble, D. Castner, *Anal. Chem.* **79**, 4390 (2007).

[13] T. Ishida, et al., *Japn. J. Appl. Phys.* **35**(12), L1710 (1996).

[14] K. Tamada, M. Hara, H. Sasabe, W. Knoll, *Langmuir* **13**, 1558 (1997).

[15] R. DeBono, G. Loucks, D. Manna, U. Krull, *Can. J. Chem.* **74**, 677 (1996).

[16] E. Devor, M. Behlke, 'Strategies for attaching oligonucleotides to solid supports', Integrated DNA Techologies (2005).

[17] M. Pirrung, *Chem. Rev.* **97**, 473 (1997).

[18] M. Heller, E. Tu, A. Holmsen, R. Sosnowski, J. O'Connell, *DNA Microarrays: A practical approach*. Oxford Press (1999).

[19] P. Gilles, D. Wu, C. Foster, P. Dillon, S. Chanock, *Nature Biotech.* **17**, 365 (1999).

[20] M. Heller, A. Forster, E. Tu, *Electrophoresis* **21**, 157 (2000).

[21] C. Boozer, et al., *Anal. Chem.* **76**, 6967 (2004).

[22] C. Boozer, J. Ladd, S. Chen, S. Jiang, *Anal. Chem.* **78**, 1515 (2006).

[23] P. Peluso, et al., *Anal. Biochemistry* **312**(2), 113 (2003).

[24] R. Bailey, G. Kwong, O. Radu, C.G. ad Witte, J. Heath, *J. Am. Chem. Soc.* **129**(7), 1959 (2007).

[25] A. W. Peterson, R. Heaton, R. Georgiadis, *Nucleic Acid Research* **29**(24), 5163 (2001).

[26] K. Peterlinz, R. Georgiadis, *Langmuir* **12**, 4731 (1996).

[27] K. Peterlinz, R. Georgiadis, *Opt. Commun.* **130**, 260 (1996).

[28] M. Newman, T. Strzelecka, L. F. Dorner, I. Schildkraut, A. K. Aggarwal, *Science* **269**, 656 (1995).

[29] P. Weber, F. Slemme, *Science* **243**, 85 (1989).

[30] S. Hormuzdi, M. Filippov, G. Mitropoulou, H. Monyer, R. Bruzzone, *Biochimica et Biophysica Act (BBA)—Biomembranes* **1662**(1–2), 113 (2004).

# Chapter 5

# Protein-coated SAMs as Substrates for Cell Attachment

## 5.1 Background

In this chapter, we apply SAM-coated substrates towards binding and culturing cells. Utilizing these surfaces, we move towards a new generation of panning devices and substrates amenable for cell culture. Original panning and cell separation methods began with polystyrene plates physisorbed with cell-specific antibodies to fractionate B- and T-lymphocytes from a mixed solution [1]. Panning has been an important technique in immunology for separating and purifying cell populations, as well as identifying high-affinity antibodies [2]. However, this technique utilizes undefined substrates and requires large volumes and sample amounts. A more controlled and defined substrate involves SAMs that present cell-specific antibodies. In Chapter 4, we demonstrated target capture by ligands tethered via oligo-oligo interactions. Here, we show immuno-specific capture of B-cells from a mixture of lymphocytes (Figure 5.1).

Polystyrene plates are the standard for cell culture, but alternative substrates such as gold have been explored. Mrksich et al. have succeeded in culturing adherent cells such as baby hamster kidney cells, 3T3 Swiss fibroblasts, and bovine capillary

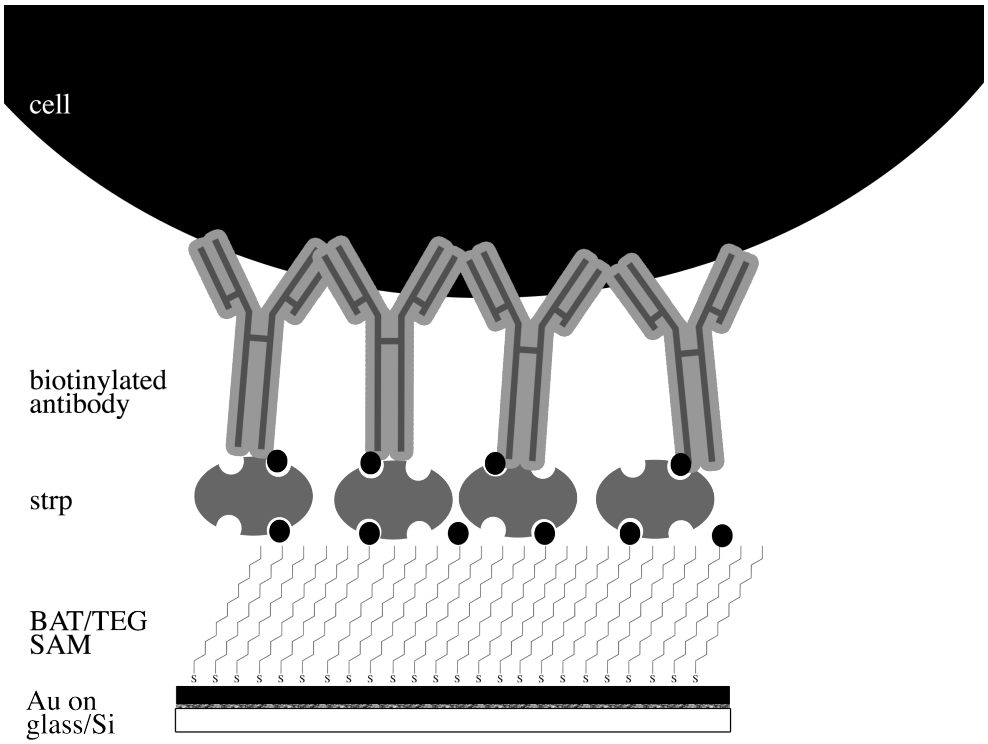


Figure 5.1 **Scheme for immuno-specific cell attachment to SAMs via streptavidin bridge.** Mixed SAMs of BAT and TEG are used to build a streptavidin bridge to bind biotinylated antibodies.

endothelial cells to gold substrates via the self assembly of alkanethiols modified with the small tri-peptide arg-gly-asp (RGD) peptides [3–6]. The RGD motif is found in many extracellular matrix proteins including fibronectin [7–9], vitronectin [10], collagen [11], and fibrinogen [12]. The tri-peptide sequence RGD is the major adhesive ligand that binds integrin receptors such as the $\alpha_5\beta_1$ and $\alpha_{IIb}\beta_3$ receptors [9, 13].

Many other signaling molecules have yet to be explored. One which has received some attention is vascular endothelial growth factor (VEGF). VEGF is a potent mitogen which is expressed as a number of splice variants (121, 145, 165, 189, and 206 amino acids long) encoded by a single gene. These various isoforms may be excreted as soluble proteins, or bound and presented on the extra-cellular matrix. *In vivo* and *in vitro* studies indicate that endothelial cell activation by VEGF may result in changes in cell proliferation, migration, and differentiation [14–16]. In loss-of-function studies on avian embryos, Little et al. demonstrated that VEGF/VEGF receptor signaling can modulate endothelial cell extension and protrusion activity. Their work identifies VEGF as an instructive molecule during de novo blood vessel morphogenesis [14–16]. *In vitro* studies by Lawley et al. demonstrate that exposure of endothelial cells to soluble VEGF exhibited varying levels of morphological changes including tubule formation [17]. Tumor research by Lee et al. indicates that matrix-metalloproteinase-(MMP)-cleaved or soluble VEGF promote capillary dilation of pre-existing vessels with little neovascular response. However, MMP-resistant or surface-bound VEGF supports extensive growth of thin vessels [18].

As cellular mobilization is a precursor to blood vessel formation, *in vitro* studies of surface-bound VEGF may yield insight into receptor signaling and motility of endothelial cells. Endothelial growth factor tethered via star poly(ethylene oxide), a small dendrimer-like structure, on glass causes cultured rat hepatocytes to respond with changes in cell shape and production of DNA [19]. Additionally, advances have been made with the use of photoreactive polymers to pattern and immobilize VEGF

onto glass or polystyrene substrates. Increased cell proliferation of human umbilical vein endothelial cells (HUVEC) on these substrates was determined to be dose dependent on VEGF incorporation into the polymer [16]. In another study, VEGF was physisorbed onto polystyrene dishes in order to promote endothelial cell adhesion, migration, and survival via integrin ligation [15].

Utilizing biotin-streptavidin interactions, SAM can be generated on gold substrates to present VEGF with high fidelity and ease (Figure 5.2). Unlike physisorption techniques, binding of VEGF on gold substrates is easily controlled by varying the composition of the underlying SAM and reduces the risk of protein denaturation. In this way, proteins are presented in a manner which increases the likelihood of ligand-receptor interactions. In this study, varied levels of VEGF are prepared on gold surfaces, and the effects on cell proliferation, morphology, and motility are investigated. The techniques developed here can be transferred to study other cell types in the future.

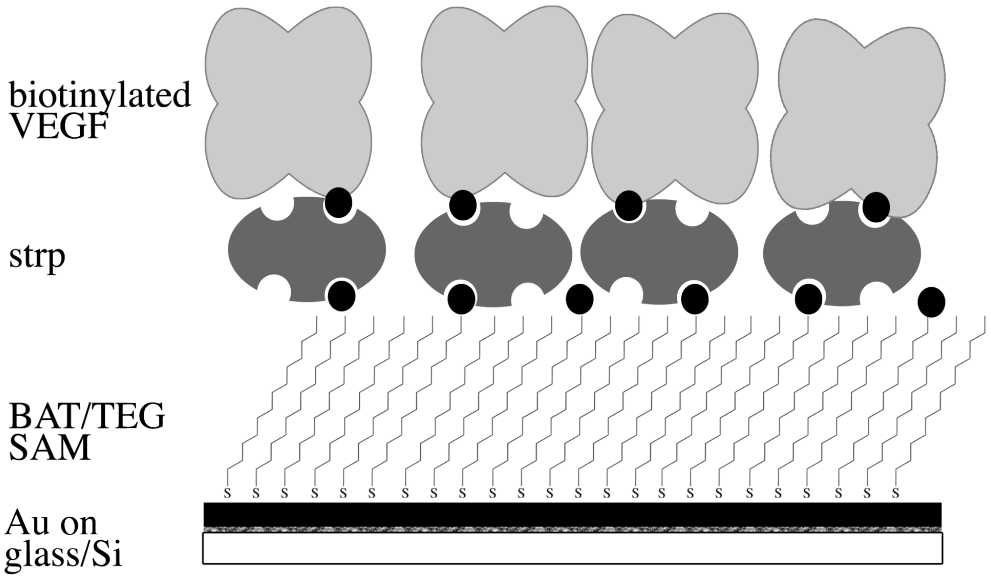


Figure 5.2 **Scheme for VEGF attachment to SAMs on Au.** Mixed SAMs of BAT and TEG are used to build a streptavidin bridge to bind biotinylated VEGF.

## 5.2 Materials and Methods

Silicon wafers were purchased from Wafer World. Chromium was purchased from R.D. Mathis Company and gold shots from Refining Systems, Inc. Cr (30 Å) and Au (1000 Å) were thermally evaporated onto clean silicon wafers under high vacuum. Au/Ti coated glass coverslips were purchased from Platypus Technologies. Reagents BAT and TEG were synthesized as previously described in Chapter 3 or purchased from Platypus Technologies. Tissue culture incubation wells were purchased from Nunc (part no. 155380). Biotinylated murine $\alpha$-B220 IgG and B- and T-cells were provided by Dr. Owen Witte at UCLA. Murine yolk sac endothelial cells were a generous gift from Prof. Charles Littles lab at the University of Kansas Department of Anatomy. Streptavidin was purchased from Zymed, Inc., and biotinylated recombinant human VEGF165 was purchased from R&D Systems.

### Cell Culture

B- and T-cell lymphocytes were cultured in DMEM with 10% FBS (Omega Scientific), 2 mM L-glutamine (Irvine Scientific), HEPES, and penicillin/streptomycin (1080, Gibco/Invitrogen). Cells were cultured at 37 °C in 5% $CO_2$ until 80% confluent. Before the experiments, lymphocytes were washed by centrifugation. Cells were then replated onto Au substrates at approximately 1 x $10^5$ cells $ml^{-1}$ in serum-free media and incubated for 1 hour at 37 °C in 5% $CO_2$.

Murine-yolk-sac-derived endothelial (YSE2) cells were cultured in IMDM (15-016-CV, Fisher Scientific) with 10% FBS, 2 mM L-glutamine and penicillin/streptomycin. YSE2 cells were cultured at 37 °C in 5% $CO_2$ until 80% confluent before passaging. Cells were released from the plates by trypsin-EDTA and washed by centrifugation in serum-free media to remove trace trypsin and serum. YSE2 cells were then replated onto substrates at approximately 1 x $10^5$ cells $ml^{-1}$ in serum-free media and cultured

for 4 hours at 37 °C in 5% $CO_2$.

3T3 fibroblasts were cultured in DMEM (as with lymphocytes) at 37 °C in 5% $CO_2$. Cells were released by trypsin-EDTA and washed by centrifugation in serum free media to remove trace trypsin and serum before replating.

## Cell Panning by SAMs on Au

SAMs were adsorbed onto the gold substrates as an admixture of 10% BAT and 90% TEG (1mM total thiol) in 75% ethanol for 2–12 hours. Substrates were then incubated in streptavidin (60 nM) in PBS for 30 minutes, washed with PBS, and soaked in biotinylated $\alpha$-B220 IgG antibody (20 nM) for 30 minutes. Lymphocytes were plated onto the substrates at 1 x $10^5$ cells $ml^{-1}$ for 60 minutes before gently rinsing in PBS, then imaged.

Images were acquired on an upright Zeiss Axioplan 2 infinity-corrected microscope (Zeiss, Germany) and acquired with a monochrome CCD Zeiss Axiocam HRm camera. Zeiss Plan-Neofluar objectives 10x/0.3, 20x/NA 0.5, and 40x/NA 0.75 were used in conjunction with a Chroma (Rockingham, VT) Cy3 filter set. A mercury arc lamp served as the excitation source. Images were acquired in 8-bit monochrome resolution and 1030 x 1300 pixel resolution.

## Assaying YSE2 Morphology

SAMs were adsorbed on Au from a solution of 10% BAT and 90% TEG (1 mM total thiol) in 75% ethanol for 2–12 hours. Au substrates were then rinsed in water and ethanol, and PBS. Substrates were next soaked in streptavidin (60 nM) in PBS for 30 minutes, washed with PBS, then soaked in bioinylated VEGF (20 nM) for 30 minutes. Substrates were washed again in PBS, placed in a clean falcon plate, and seeded with yolk sac endothelial cells. After 60 minutes, samples were gently washed to remove non-adherent cells. Cells were then fixed and permeabilized for 5 minutes in 4% PFA

and 1% TritonX-100 for 5 minutes, then incubated in rhoadmine-phalloidin at 165 nM in 1% BSA/PBS for 30 minutes. Au samples were imaged using Zeiss upright Axioplan microscope as described above.

## Assaying Cell Motility

Polystyrene Nunc 8-well chambers were affixed to silicone/adhesive gaskets (Gibco) with rubber cement on the silicone side and allowed to cure $>24$ hours. Au-coated glass slides were then affixed with polystyrene chambers by the adhesive side of the silicone gasket. Each chamber well was incubated with alkylthiols (1 mM total thiol) in 75% ethanol for 2–12 hours. Slides were carefully rinsed in PBS, then soaked in 5 ug $\mathrm{ml}^{-1}$ streptavidin in PBS for 30 minutes, then incubated in biointylated VEGF for 30 minutes. YSE2 cells were plated onto Au at 1 x $10^5$ cells $\mathrm{ml}^{-1}$ for 60 minutes in IMDM spiked with bodipy ceramide, and non-adherent cells were gently washed away. The chamber was then imaged on a Zeiss Pascal inverted confocal microscope. An incubation box was built around the microscope, and images were acquired every 5 minutes for 4 hours at 37 °C in supplemented $CO_2$ atmosphere.

LSM acquisition software was used in conjunction with MegaCapture, a macro written by Prof. Sean Megason. This macro allowed us to concurrently collect tiled time lapse images for a $4\times2$ array of Au samples. Tiled images were reconstructed using MegaMontage, also written by Prof. Megason, and analyzed using Imaris software (distributed by Bitplane Scientific Solutions).

## 5.3 Results/Discussion

### 5.3.1 Cell Panning

A mixture of B- and T- cells were incubated over two defined substrates and reviewed for binding efficiency (Figure 5.3). The SAMs generated for this experiment were TEG and a SAM presenting monoclonal $\alpha$-B220 antibodies which are specific to B-cells. After seeding cells and lightly rinsing them, we observed weak, but significant retention of B-cells on the antibody-presenting substrates. On average, we retained 30% of the plated cells after rinsing. We also plated a mixture of B- and T-cells and found that B-cells were retained with T-cell retention at background levels. The dissociation constant $K_D$ for $\alpha$-B220 was not disclosed, but common values are 1 $\mu$M. Researchers, using panning techniques, generated even higher affinity antibodies with $K_D$ values less than 10 pM. Ideally, antibodies with low $K_D$ values are ideal for panning and bioaffinity techniques.

These SAMs were generated without any spatial patterning and were seeded at relatively low cell densities. However, SAMs still provide the ability to control protein presentation on the Au substrate. The panning technique relies on physisorption of antibodies onto a substrate. Undesirable non-specific antigens or ligands may also bind onto the substrate, leading to non-specific cells binding. Au substrates also allow for electrochemical control of the surface. In theory, cells tethered to Au could also be released by applying anodic potentials (Chapter 3). For now, our findings demonstrate feasbility in using SAMs for cell panning. Future work will address optimizing capture efficiency.

### 5.3.2 YSE2 Cell Morphology

In addition to grabbing and panning non-adherent cells via SAMs on Au, we also wanted to explore capturing and culturing adherent cells. Cell morphology is a common indicator of cell health and is easily measured for cells on a variety of SAM substrates. By varying the BAT/TEG alkylthiol ratio, we titrated surface densities of VEGF and TEG. Bare Au substrates served as a control. Like polystyrene plates, bare Au is easily fouled when exposed to tissue culture media. All manner of proteins including vitronectin will denature onto the substrate. Some protein will be inactivated, but many ligands will still be exposed, giving YSE2 cells a good substrate for growth (Figure 5.4). SAMs controlled to present high surface density VEGF will also host YSE2 cells, but they do not spread out to the same extent. Streptavdin contains some RGD domains which may allow for integrin signaling and cell attachment. However, the presence of TEG groups in the SAM likely reduces the levels of cell adhesion and spreading. Compared to Au substrates, cells on VEGF will spread out to 80–85% of the surface area. Cells on intermediate concentrations of VEGF have more variability in cell spread. Some will extend out filapodia and lamellapodia, but it is more typical for these cells to cover 15–80% of the cell surface compared to YSE2 cells on Au. Cells cultured on TEG do not spread out, as expected. Ethylene glycol groups make protein adhesion onto the SAM difficult, and the cells remain as poorly adhered tight balls.

### 5.3.3 YSE2 Cell Migration on SAMs

Cell migration is another process engaged in regularly by adherent cells. VEGF is a known stimulator of endothelial cell migration during angiogenesis and vasculogenesis, so we employed time lapse microscopy to study cell response to our modified substrates. We quantified cell migration with Imaris imaging software. Again, SAM

substrates were prepared presenting varying levels of VEGF, TEG, and FN. For each sample condition, cells from 3 different Au samples were tracked and statistically analyzed. Only cells which stayed in frame the entire time lapse were analyzed. The average cell displacement at time=0 and time=4 hours was calculated for each sample condition. A one-way ANOVA test revealed that cell migration on 1.0 VEGF (substrates treated with 1BAT:0TEG, streptavidin, and biotinylated VEGF) was statistically different than migratory activity on FN, 0.01 VEGF, or 0.25 VEGF. All other comparisons of cell migration were not significantly different (Figure 5.5).

From Chapter 3, we know that 100% BAT SAMs do not form complete monolayers. Some areas of Au are left with pinhole defects. The seqential addition of streptavidin, biotinylated VEGF, and cells in media would yield a surface that presents both VEGF and uncontrolled denatured proteins, some of which presumably promote cell adhesion via integrin signaling, like vitronectin. The 1.0 VEGF sample condition can be considered a "VEGF+other protein" substrate. The combination protein substrate leads to increased cell motility, a phenomenon which has been previously observed [15, 20]. Samples 0.01–0.5 VEGF represent controlled SAM substrates and we believe VEGF and streptavidin are the only proteins presented here. No significant increases in mean cell displacement are calculated here, and in these studies, VEGF alone does not stimulate the same levels of cell migration.

### 5.3.4 YSE2-Specific Response

We also observed that cell response to VEGF was specific to cells with VEGF receptors. YSE2 cells and 3T3 fibroblasts, which lack VEGF receptors were plated on Au and 1.0 VEGF surfaces. The mean cell displacements measured in this experiment show that YSE2 migration on VEGF is statistically greater than displacements measured for 3T3 cells or YSE2 cells on Au (Figure 5.6). In another analysis of this data

set, we measured the cell displacement for individual cells during the time lapse and plot them mean square displacement vs. time (Figure 5.7). Othmer et al. previously modeled cell migration as a 2-D persistent random walk [21].

$$< d^2(t) >= 4\mu[t - P(1 - e^{\frac{-t}{P}})] \tag{5.1}$$

The persistence time $P$ is the time a cell takes between steps, and $\mu$ is the random motility coefficient, formally equivalent to the diffusion coefficient.

We note, however, that the plot's slope for YSE cells on VEGF has a notable break at 110 minutes and cannot be described by Othmer's model equation. Taking a closer look, we plot the individual cell track data as cell square displacement vs. time (Figure 5.8). The final square displacement for cells varies quite a bit, from 1000 $\mu$m$^2$ to 7300 $\mu$m$^2$. Many of the cells do display this same change in speed around time points 60–100 minutes. The implications may point to a time frame in which the cells are processing the VEGF signal before activating a change in cell speed.

## 5.4 Conclusion

In this chapter, we demonstrated SAMs as amenable substrates for cell panning, adhesion, and culture. The ability to control protein presentation on a reactive surface allows us to better understand the effects on individual proteins, molecules, and chemokines on cell behavior. With non-adherent lymphocytes, we demonstrated control in both positive cell selection and repulsion by modifying our SAMs Au substrates with cell-specific antibody and tri(ethylene glycol), respectively. With adherent cells, we use SAMs to affect both cell adhesion and cell response. Time-lapse microscopy allows us to observe changes in cell behavior as a function of surface environment. We detected significant variances in cell migration between cells grown on VEGF and

those grown on fibronectin.

A recent study by Ratner et al. included the generation of VEGF and VEGF/FN gradients on Au SAMs [20]. They report cell displacements from time-lapses taken every 30 minutes on SAMs lacking TEG. I envision future incarnations of this experiment would incorporate TEG groups into the SAM for higher control of the monolayer surface, and higher time-lapse imaging frequency. 30 minutes is too long to reliably track cell migration. Additional explorations would include reducing the surface VEGF density in my monolayers and increasing time-lapse durations. Determination of higher-level endothelial cell structures after long-term culture on VEGF SAMs may provide the framework for studying vascularization.

Our SAM substrates, with the surface control afforded by them, are ideal platforms for identifying the role of individual and combinations of growth factors, adhesion factors, and other proteins on cell biology, migration, repulsion, adhesion, proliferation, differentiation, etc. These substrates could be applied to very delicate systems such as stem cells, and be used as a tool to define minimal media and substrates. A deeper consideration is given for our next steps in Chapter 6.

# Acknowledgements

We thank Mike Filla for sending us YSE2 cells, Dr. Kyunghee Choi at Washington University-St. Louis for supplying the original murine yolk sac endothelial cells, and Dr. Carole Lu for providing fibronectin. C. A. C. thanks Evan Zamir and Cheng Cui for helpful discussions. Lymphocyte experiments were part of a short-lived collaboration with Owen Witte's lab at UCLA.

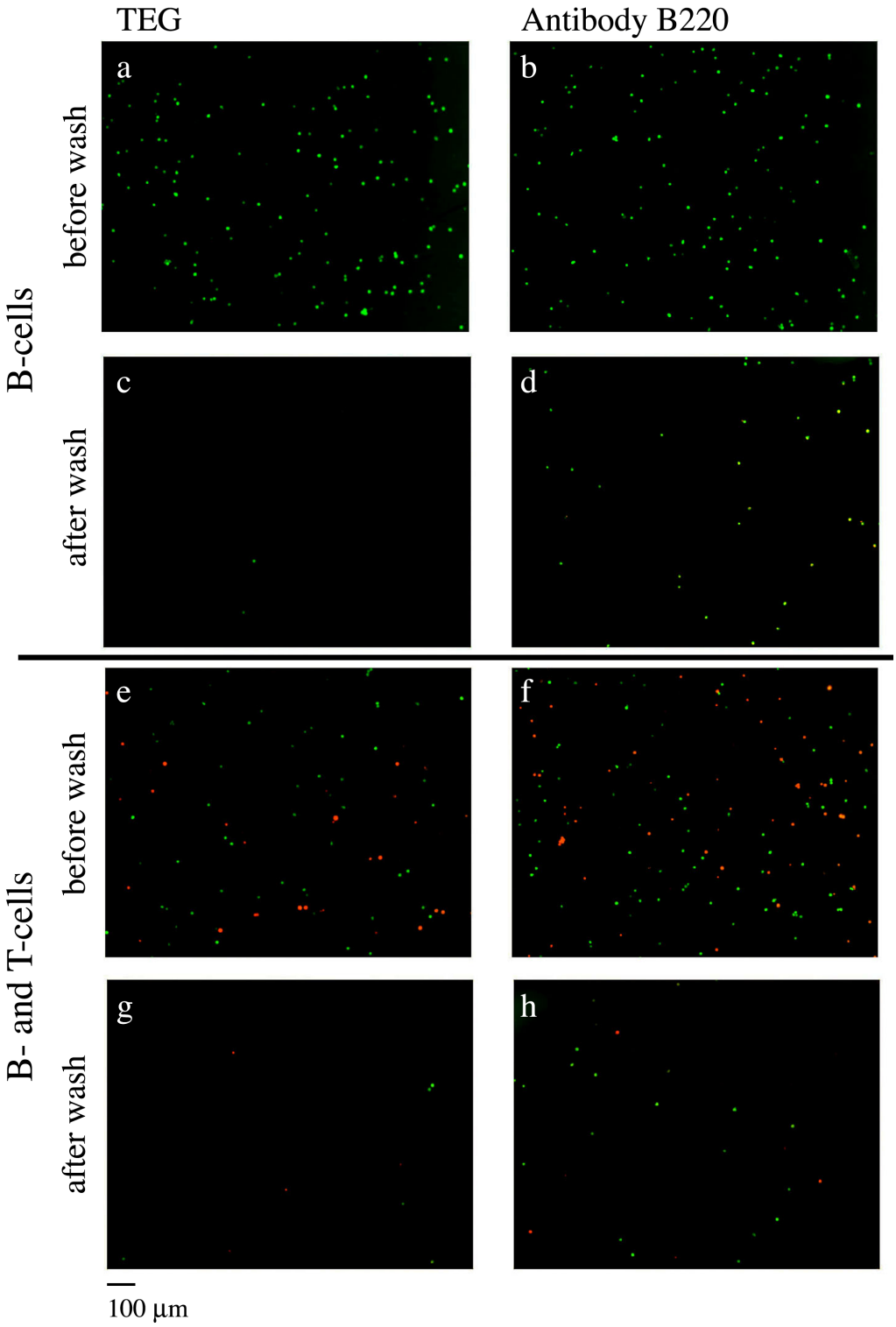


Figure 5.3 **Specific cell capture on Au substrates.** B-cells are labeled in green, and T-cell are labeled in red. a–d) Fluorescent images of Au substrates before and after rinsing plated B-cells on TEG and $\alpha$-B220 SAMs. e–h) Fluorescent images of Au substrates before and after rinsing a plated mixture of B- and T-cells.

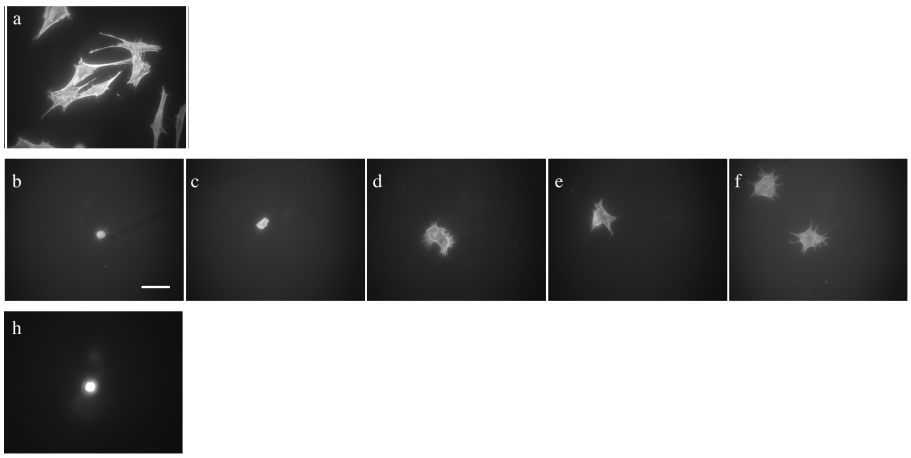


Figure 5.4 **YSE2 cells spreading out on various Au substrates.** a) YSE2 cells plated on Au in tissue culture media spread out very nicely. b–f) Cells on 0.01, 0.1, 0.25, 0.50, and 1.0 VEGF substrates display varying degrees of spreading. g) Cells on TEG substrates do not adhere well and remain as tight balls.

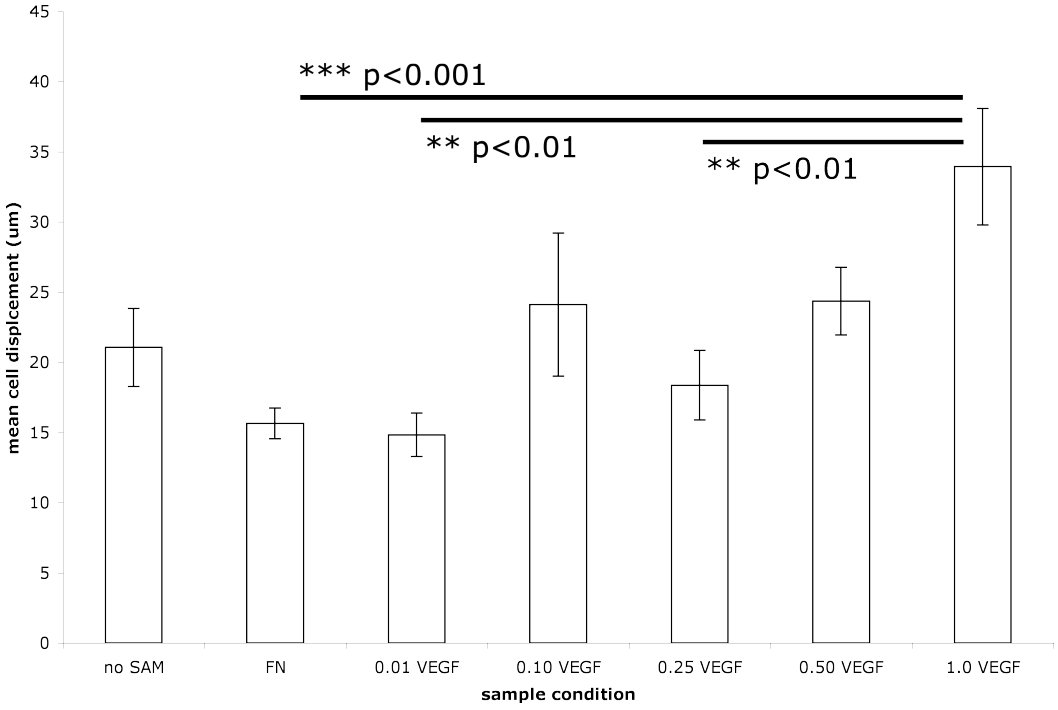


Figure 5.5 **Mean cell displacements for YSE2 cells on modified Au substrates.** SAM conditions for VEGF substrates are described by the molar fraction of BAT/TEG SAM adsorbed, i. e., "0.10 VEGF" is a sample treated with 0.1 mM BAT and 0.9 mM TEG, followed by streptavidin, and the biotinylated VEGF. One-way ANOVA test was applied to the cell displacements. Cell movements on 1.0 VEGF were found to be statistically significant compared to FN, 0.1 VEGF, and 0.25 VEGF substrates.

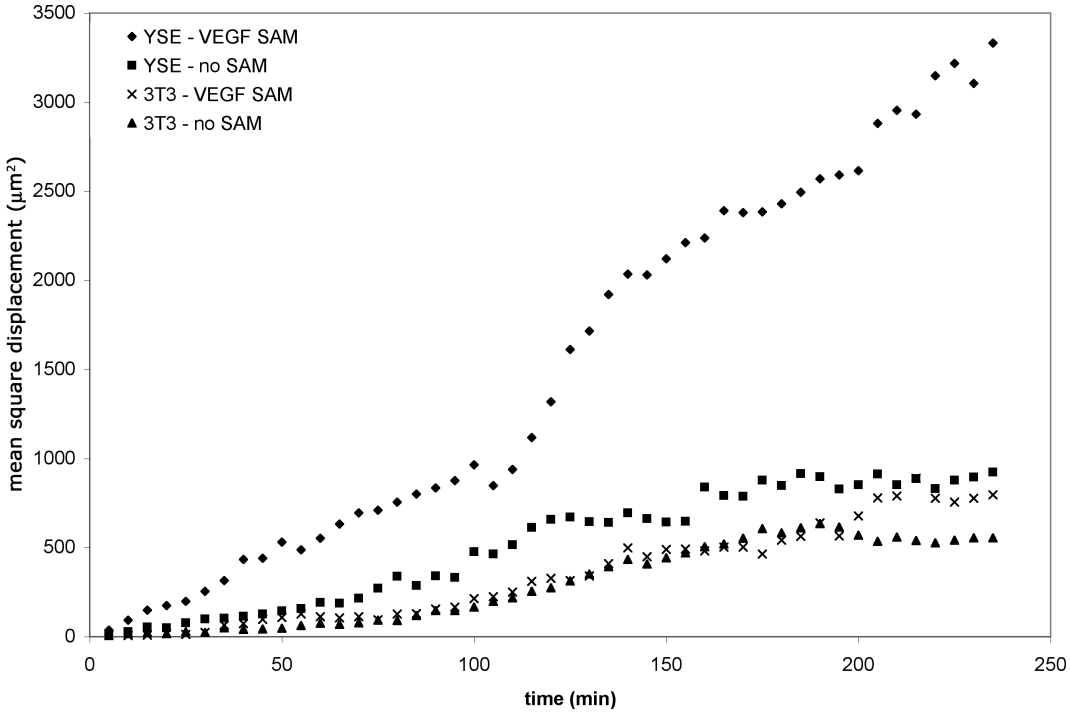


Figure 5.6 **Mean-squared cell displacements for YSE2 and 3T3 cells on modified Au substrates.** One-way ANOVA test reveal that YSE2 cells on VEGF migrate significantly longer distances compared to YSE2 cells on Au or 3T3 cells on the same substrates.

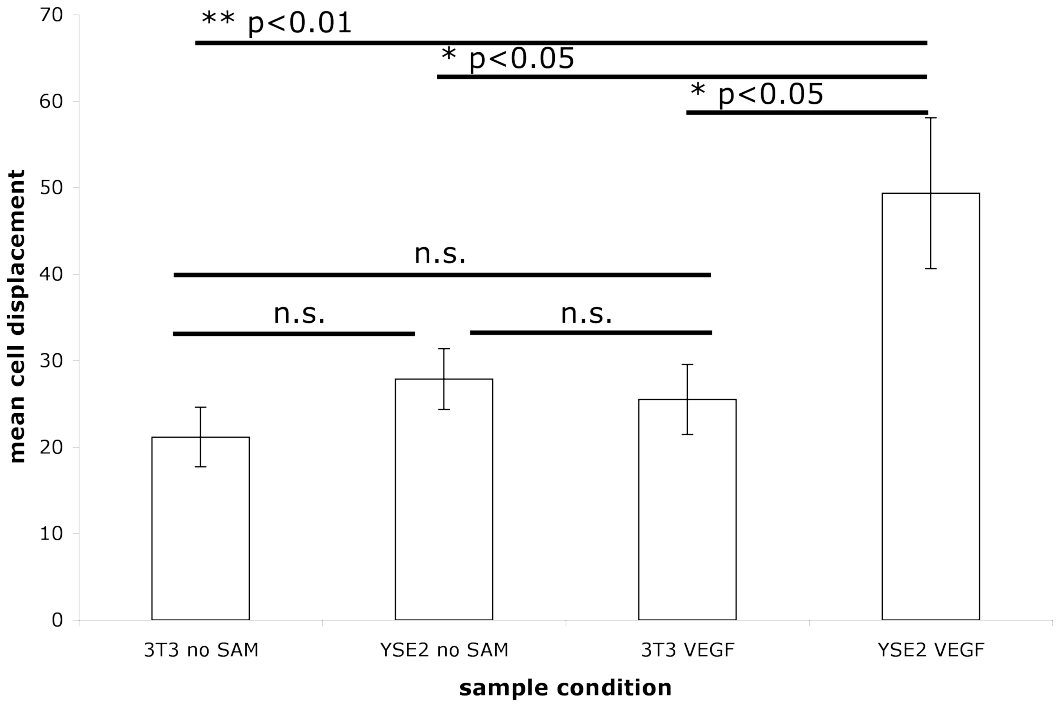


Figure 5.7 **Cell displacements for YSE2 and 3T3 cells on modified Au substrates.** One-way ANOVA statistical test was run on cell displacements for YSE2 and 3T3 cells plated on TEG and plain Au substrates. YSE2 cell migration was significantly greater on VEGF surfaces compared to Au and compared to 3T3 fibroblasts on either substrate. ANOVA indicates that cell displacement between the other samples was non significant.

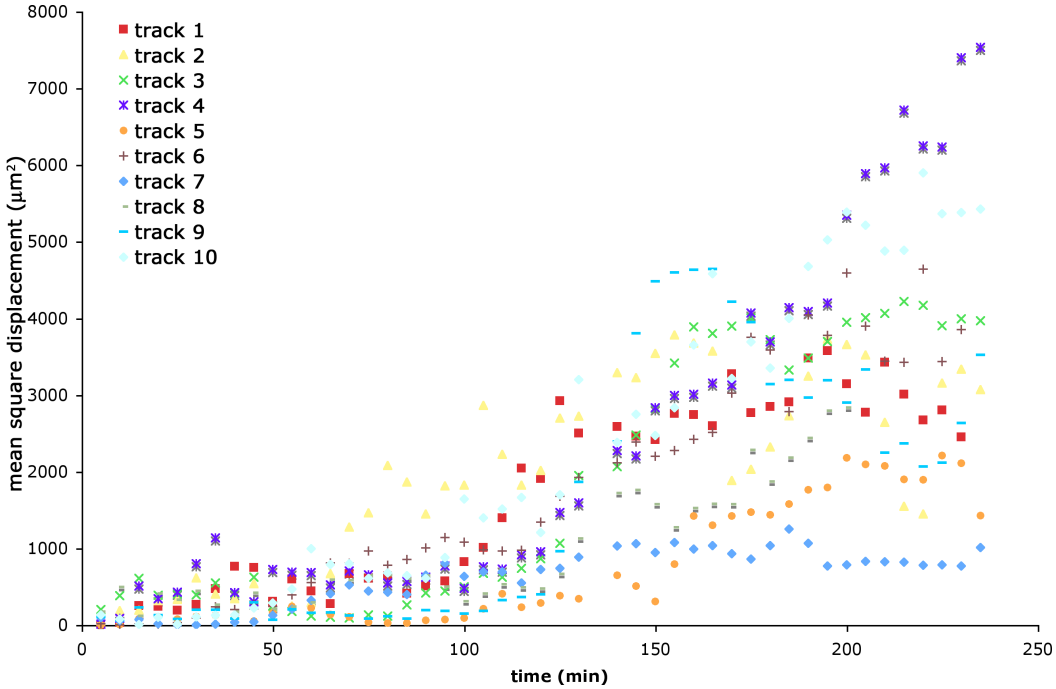


Figure 5.8 **Square displacement vs. time for individual YSE2 cells on VEGF substrates.** A large spread in square cell displacement is observed after imaging migrating cells for 4 hours. Changes in slope are not uniform. After approximately 60 minutes, cells increase their velocity. Cells not exposed to VEGF lack this acceleration.

# Bibliography

[1] L. J. Wysocki, V. L. Sato, *Proc. Nat. Acad. Sci.* **75**(6), 2844 (1978).

[2] D. Lightwood, et al., *J. Immuno. Meth.* **316**(1–2), 133 (2006).

[3] Y. Feng, M. Mrksich, *Biochem.* **43**, 15811 (2004).

[4] B. Houseman, E. Gawalt, M. Mrksich, *Langmuir* **19**, 1522 (2003).

[5] B. Houseman, M. Mrksich, *J. Org. Chem.* **63**, 7552 (1998).

[6] W.-S. Yeo, M. Yousaf, M. Mrksich, *JACS* **125**, 14994 (2003).

[7] E. Ruoslahti, M. Pierschbacher, *Cell* **44**, 517 (1986).

[8] M. Pierschbacher, E. Ruoslahti, P. Sundelin, P. Lind, P. Peterso, *J. Biol. Chem.* **257**, 9593 (1982).

[9] M. Pierschnacher, E. Ruoslahti, *Nature* **309**, 30 (1984).

[10] E. Hayman, M. Pierschbacher, E. Ruoslahti, *J. Cell Bio.* **100**, 1948 (1985).

[11] S. Dedhar, E. Ruoslahti, M. Pierschbacher, *J. Cell Bio.* **104**, 585 (1987).

[12] M. Ginsberg, M. Pierschbacher, E. Ruoslahti, G. Maguerie, E. Plow, *J. Biol. Chem.* **260**(3931) (1985).

[13] E. Ruoslahti, M. Pierschnacher, *Science* **238**, 491 (1987).

[14] C. Drake, A. LaRue, N. Ferrara, C. Little, *Developmental Biology* **224**, 178 (2000).

[15] H. Hutchings, N. Ortega, J. Plouet, *The FASEB Journal* **17**, 1520 (2003).

[16] Y. Ito, H. Hasuda, H. Terai, T. Kitajima, *J Biomed. Mater. Res.* **74A**, 659 (2005).

[17] T. Lawley, Y. Kubota, *J Invest. Dermatol.* **93**, 59S (1989).

[18] S. Lee, S. Jilani, G. Nikolova, D. Carpizo, M. Iruela-Arispe, *Journal of Cell Biology* **189**(4), 681 (2005).

[19] P. Kuhl, L. Griffith-Cima, *Nat. Med.* **2**(9), 1022 (1996).

[20] L. Liu, B. Ratner, E. Sage, S. Jiang, *Langmuir* **23**, 11168 (2007).

[21] H. Othmer, S. Dunbar, W. Alt, *Journal of Mathematical Biology* **26**, 263 (1998).

# Chapter 6

# Conclusions

## 6.1 Summary of Research

Now is an exciting time, when the interplay between science and technology brings together the fields of physics, biology, and chemistry. Researchers at this interface develop new techniques for biological studies and novel lab-on-a-chip tools [1–5]. Work in this thesis focuses on studying monolayer formation, solvent effects, and SAM characterization; all in the vein of building biosensor tools. We found that solvent choice can have profound effects on SAM formation kinetics and composition, and monolayer formation times can be increased 20-fold in aqueous ethanol solvents. Hydrophilic molecules like TEG form quickly. Those with more hydrophobic properties like BAT tend to make SAMs with perturbations. At high density, biotin can fold over in hairpin-like formations, causing disruptions and distortions in the monolayer. TEG inclusion in the SAM raises monolayer stability and quality. The TEG ethylene glycol groups promote BAT ethylene glycol group orientation towards the solvent interface. Monolayers were characterized using electrochemical techniques and found to be free of pinhole defects, as determined by cyclic voltammetry. In addition, we found that monolayers can be oxidatively desorbed using both DC and AC voltage techniques.

This work continued by looking at monolayers which bind DNA. We synthesized

CPG precursors to make oligo-dodecylthiolate SAMs, reagents amenable to making DNA arrays. Oligo-coated substrates were then characterized by fluorescence microscopy for hybridization capabilities. Complement oligo binding was assessed on SAMs with controlled oligo:TEG ratios. Based on fluorescence readings, we found that the optimal density of oligo on substrates were attained with thiol solutions. I apply these substrates to bind not just oligos, but subsequently proteins and cells. Through these studies, we probed binding conditions and their effects on hybridization. The reversible binding nature of DNA and restriction enzymes allowed us to release tethered proteins and target molecules. Coupled with microfluidics or automated systems, cells might be captured and released at a later time for further analyses using these oligo-mediated methods.

In addition, we also explored non-oligo SAMs for the presentation of proteins and cells. Biotin-streptavidin multilayers were demonstrated to specifically bind lymphocytes out of solution. Biotinylated antibodies specific to B-cells were bound to streptavidin-coated SAMs and successfully panned B-cells out of a mixed solution of lymphocytes. These are important first steps towards building analytical tools for studying cell affinity, cell response, and cell quantitation. We continued exploring the application of SAMs for cell culture study. Biotinylated VEGF was bound to streptavidin coated SAMs and endothelial cells were cultured upon these substrates. VEGF, a chemokine, is a known stimulator for endothelial cell migration during angiogenesis and vasculogenesis events. We controlled the VEGF surface density by varying the BAT/TEG composition of the underlying SAMs and observed an increase in cell motility as VEGF surface density increased. 3T3 fibroblasts, which lack VEGF receptors, were not induced to increase motility.

In summary, this work utilized SAMs to generate surfaces which elicit specific responses from cells. In the next experiments, cells isolated on SAMs can be further studied for biological responses.

## 6.2 Outstanding Issues

### Increasing enzymatic release of oligo-tethered biotargets

This work has already shown that small molecules and proteins bound to oligo-SAMs can be released by restriction enzymes. While we readily observe enzymatic release of small molecules (Cy3), larger targets such as cells and beads are released with low efficiency. The next experiments I envision require generating longer (50 bp and 100 bp) ss-oligo probes on Au. Enzymatic release of tethered biological target will then be carried out on these modified substrates.

Unfortunately, the synthesizer at Caltech will not produce oligos at these lengths. One possible solution would be to collaborate with a commercial oligo synthesis group to custom-make the desired oligos with my DMT-modified CPG reagent. Alternatively, elongation of immobilized ds-oligos Au may be performed wtih T4 ligase [6]. In addition to having longer ds-oligos, multiple restriction enzyme sites can be incorporated to increase the probability of cleaving tethered biotargets.

## 6.3 Next Steps

As has been discussed in this thesis, SAMs can be manipulated to present small molecules, carbohydrates, and proteins. My work aims to better understand monolayer formation and create substrates for biological targets. In particular, stem cell research is an important topic for study. Stem cells are pluripotent: capable of developing into any cell in the adult body. They have the potential to treat degenerative, malignant, or genetic diseases.

With the recent advances in stem cell technology, new studies in stem cell biology are possible. Successful proliferation of stem cells in culture is currently achieved using poorly controlled substrates and ill-defined media. Human stem cells are grown

on mouse embryonic fibroblasts and in animal sera, which are a huge source of cross-species antigens. Continued development towards minimal media [7] and substrates [8–10] will be a great improvement. In the recent paper by Watanabe et al., researchers report a new technique for dissociating stem cell colonies *in vitro* by applying a Rho-associated kinase (ROCK) inhibitor which greatly increases cell viability after trypsinization [11]. These cells also retain pluripotency markers E-cadherin, Oct3/4, and SSEA4. The alternative passaging technique involves mechanical slicing hES colonies on mouse embryonic fibroblasts (MEFs) and replating them onto fresh MEF feeder layers. Watanabe's new method would allow cells within a heterogeneous colony—perhaps one undergoing differentiation—to be separated and purified. The ability to gently and effectively screen and separate stem cells is still lacking in the stem cell arena. Current fluorescent activated cell sorting (FACS) methods allow researchers to separate cells, but at the detriment of their health and survival.

Many of the tools generated within my thesis could be applied towards stem cell separation and purification. To incorporate stem cell research, I would enlist the help of Dr. Martin Pera's lab at USC. They have developed an antibody against undifferentiated hES cells, Tg30 (CD9) [12]. In preliminary studies, I have successfully labeled the Fc region of Tg30 with ss-oligo and verified the functional labeling with Cy3-labeled complement strands. A proposed experiment is outlined below.

1. Apply retinoic acid to induce differentiation of pluripotent stem cell colonies into neuronal cells [13].

2. Treat hES colony with ROCK and trypsin and dissociate into single-cell suspension [11].

3. Incubate cell suspension with oligo-labeled antibody against undifferentiated hES cells [12].

4. Create oligo-SAM on Au.

5. Apply stem cell:antibody-oligo complex onto oligo-SAM surface. Undifferentiated cells are panned onto Au and differentiated cells are recovered for continued culture or study.

6. Release panned (undifferentiated) cells with enzyme to harvest and replate.

In parallel, high-throughput platforms could allow researchers to assess which proteins and reagents stimulate stem cell activity, or identify those which allow cells to continue growing undifferentiated. These studies may or may not incorporate Au substrates, but microscopy techniques and time lapse experiments similar to those produced in this thesis could be employed and designed to study stem cell growth, health, and activity.

# Bibliography

[1] H. Craighead, *Nature Insight Review* **442**, 387 (2006).

[2] R. Daw, J. Finkelstein, *Nature Insight Review* **442**(7101), 367 (2006).

[3] A. deMello, *Nature Insight Review* **442**, 394 (2006).

[4] J. El-Ali, P. Sorger, K. Jensen, *Nature Insight Review* **442**, 403 (2006).

[5] G. Whitesides, *Nature Insight Review* **442**, 368 (2006).

[6] J. Kim, et al., *Journal of Biotechnology* **96**, 213 (2002).

[7] M. Amit, C. Shariki, V. Margulets, J. Itskovitz-Eldor, *Biology of Reproduction* **70**, 837 (2004).

[8] C. Xu, M. Inokuma, J. Denham, K. Golds, P. Kundu, *Nature Biotech.* **19**, 971 (2001).

[9] M. Amit, V. Margulets, H. Segev, K. Shariki, I. Laevsky, *Biology of Reproduction* **68**, 2150 (2003).

[10] I. Klimanskaya, Y. Chung, L. Meisner, J. Johnson, *The Lancet* **365**, 1636 (2005).

[11] K. Watanabe, et al., *Nat Biotechnol* **25**(6), 681 (2007).

[12] M. Pera, M. Blasco-Lafita, S. Cooper, M. Mason, J. Mills, *Differentiation* **39**(2), 139 (1988).

[13] K. Guan, H. Chang, A. Rolletschek, A. ad Wobus, *Cell Tissue Res.* **305**(2), 171 (2001).